RRCAT

RAJA RAMANNA CENTRE FOR ADVANCED TECHNOLOGY, INDORE

NEWSLETTER

Volume 21 Issue 1 of 2008

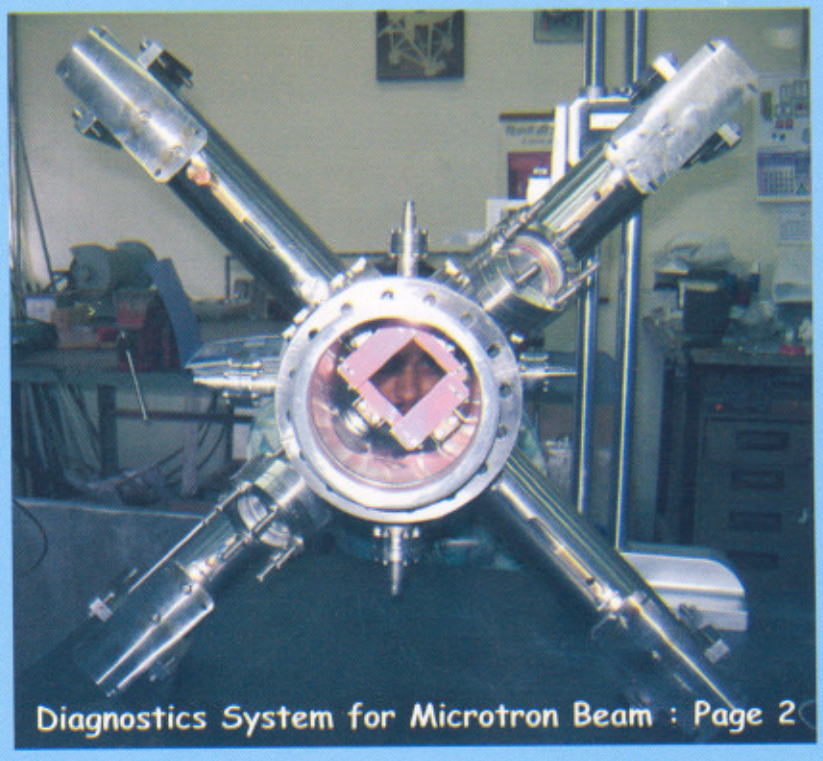

Diagnostics System for Microtron Beam : Page 2

200 kV Capillary Discharge System : Page 12

Shri Diptikant Pathy Comp. Centre IT Building

From the Director's Desk

I am glad to see that Issue 1 of RRCAT Newsletter for 2008 is ready. Editorial Board has done very well to compile a good account of many recent achievements of the Centre.

Over the past 6 months operation of Indus-2 has improved and we are now at the threshold of starting a user programme with 2 or 3 beam lines nearly ready to produce data. In parallel, we have developed some beam diagnostic devices that will help us track the electron beam as it passes through the Indus accelerator structures and the transport lines. This issue contains a glimpse of these activities, as well as some other accelerator component development useful for upcoming programmes in the XI plan. In the area of materials the progress made on study of magneto-caloric materials, nano-particles and quantum well structures have been reported upon.

In the field of lasers, activities related to the development of laser marker systems, capillary discharge based x-ray sources, laser wake field based electron acceleration experiments and other laser plasma related studies are covered in this issue. Infrastructure developments linked to computers, networking and major facilities, like, vacuum brazing furnace (which will be used for making accelerator components) are also discussed. The three theme articles cover the Bose-Einstein condensation (on which activities have been going on in this Centre for some time), modification of metallic surfaces with high power CO_2 laser, where our Centre has been a pioneer, and radiation protection issues in high energy electron accelerators. As usual, other news items and events have been also added.

I wish to compliment the Editorial Board Members for their dedicated efforts in bringing out this issue so speedily. I hope this pace will be continued in future also.

V.C.Sahni
February 25, 2008

From the Editorial Board

The editorial board is happy to be able to bring out the first issue of the Newsletter of 2008 in the first quarter of the year itself. This trend can certainly be sustained, and we will strive to achieve it through the continuous involvement, active participation and support of the scientific community of RRCAT.

This issue contains many interesting news items covering various areas of Laser and Accelerator Programme of RRCAT. It is heart warming to see continuation of this Centre as a cradle where exciting developments take place regularly. Since the flow of information is a prerequisite for progress of any society, in our view, this Newsletter is a vital element in the dissemination of information pertaining to the scientific and technological developments in the Centre. The editorial board believes that if the contributions to the Newsletter are backed up by intensive scientific seminars on the developments, then the information exchange could be even more effective.

The theme articles in the present issue cover two interesting areas of our activities, namely, "Bose-Einstein condensation in a dilute atomic gas" and "Modification of metallic surfaces with high power CO_2 laser". Dr. G. Haridas has contributed to the Young Scientists Forum of this issue with an article on "Radiation physics studies at Indus-1 synchrotron radiation source". The editorial board is quite pleased to see that the younger members of the RRCAT community are enthusiastically contributing to the Newsletter. Such enthusiasm is quite essential for the betterment of the Newsletter.

Last but not the least, the editorial board would like to express its gratitude to all the members of RRCAT community and Director, RRCAT, for their kind help and support.

Editorial Board
March 2008

A.1 Development and installation of multi-functional beam diagnostic device in TL-1 of Indus

A beam slit cum profile monitor has been installed in transfer line 1 (TL-1) of Indus. It is a multifunction diagnostic device. While it can be used as a slit with adjustable aperture to define the beam (similar to a beam scraper), it can also be used to determine the horizontal and vertical beam profile by measuring the current captured by the slit blade as it scans the beam in transverse direction. A fluorescent screen (Cr doped alumina) is mounted on each blade of the slit (Fig.A.1.1) which enables it to act like a conventional fluorescent screen for visually observing the beam profile by stopping the beam on one blade. As an adjustable "Hole" monitor, it allows a portion of the beam to pass through, while one can view the beam edges falling on the blades.

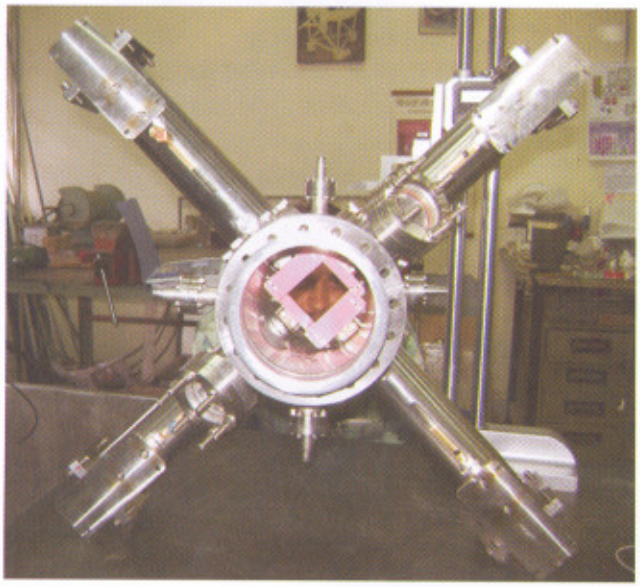

Fig.A.1.1: See through view of the monitor. The four blade movement mechanisms as well as the window for CCD camera placement are seen.

The device has four independent blades, two blades moving in opposing horizontal direction and the remaining two moving in vertical directions. The vertical blades have a linear stroke of 60 mm, and the horizontal blades 40 mm. This arrangement allows for positioning of the hole (and slit) in a field of 60 mm x 40 mm around the theoretical beam centre line. All the parts near the beam line are made of vacuum compatible, non-magnetic materials. The device operates under a vacuum of 10^{-7} mbar. The movement mechanism has a guiding arrangement to precisely maintain the orientation of the blades. It also has an anti-collision arrangement for the blades. The operation is done remotely. The work involved precision machining and welding. Its manufacturing, integration, testing and qualification were done in RRCAT.

Control system for TL-1 beam slit

A remote control for the blade movement is developed (see Fig.A.1.2). A VME based system with serial interface to PC was realized to control and position the blades. The system consists of a clock generator board, a de-multiplexer board, a relay output board, an opto input board, and a 12-bit ADC board. Eight opto-isolated clock signals are given to the stepper motor driver for clock-wise / anticlock-wise motor rotation. For each motor, two clock signals are required. The position of each blade is read from linear pot through ADC board.

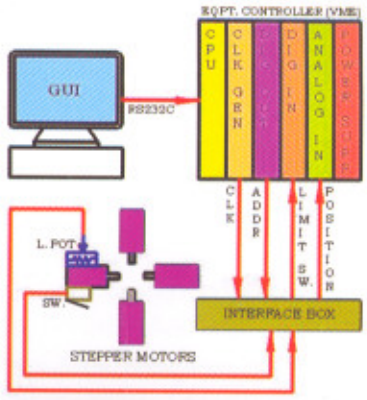

Fig.A.1.2: Block diagram of the slit control system.

Interface

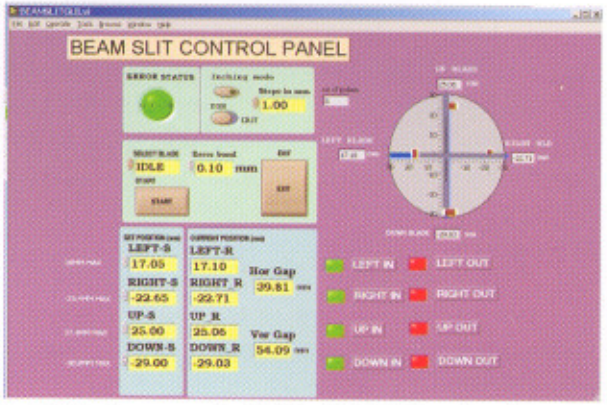

Fig.A.1.3: A screen-shot of the PC display showing control system GUI.

The interface box consists of stepper motor drivers, interlocks, and signal conditioning for position sensors. It provides 20 ppm stable reference to position sensors for long-term repeatability. In the

interface box, hardwired logic was developed for providing safety interlocks to beam slit assembly. A GUI was developed in LabVIEW for remote control of the blade positions, display of the positions, and avoiding collision. Fig.A.1.3 shows a screen-shot of the PC display showing the GUI. The blades can be positioned in automatic or manual modes.

Qualification

The system was qualified for the movement range and smooth operation under actual conditions of use. It was also tested for its overall accuracy which is better than 0.1 mm. The system was also operated for large number of cycles to test the robustness of the design. The overall calibration factors (for converting positions into voltage and vice versa) for each blade were included in the system.

Installation

The Beam slit cum profile monitor, along with its control system, was installed in TL-1 in the first half of November 2007 (Fig.A.1.4) and it is being successfully used since then for its various functions, from the Indus control room.

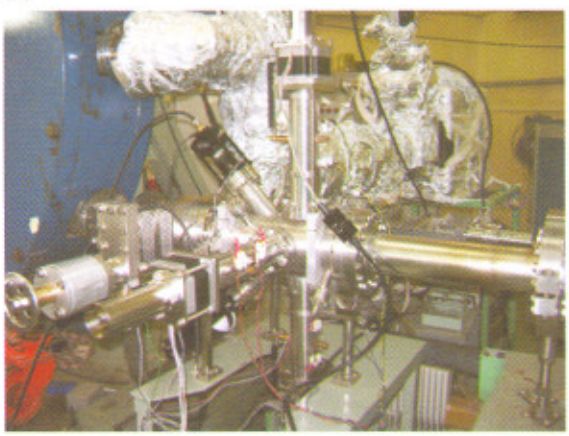

Fig.A.1.4: The monitor integrated in the TL-1. The microtron (blue) is seen on the left.

Utilization

An initial experiment was conducted to measure the horizontal beam profile. Right hand side blade of the slit was moved towards the beam in steps of 0.5 mm in the range of 6 mm to +2 mm keeping other three blades in OUT condition. Fig.A.1.5 shows the plot of signal level of blade current and two fast current transformers (FCT1 and FCT2) located downstream of slit in transfer line1 (TL-1) as a function of the blade position. Fig.A.1.6 shows the beam profile obtained by differentiating blade signal curve with respect to blade position.

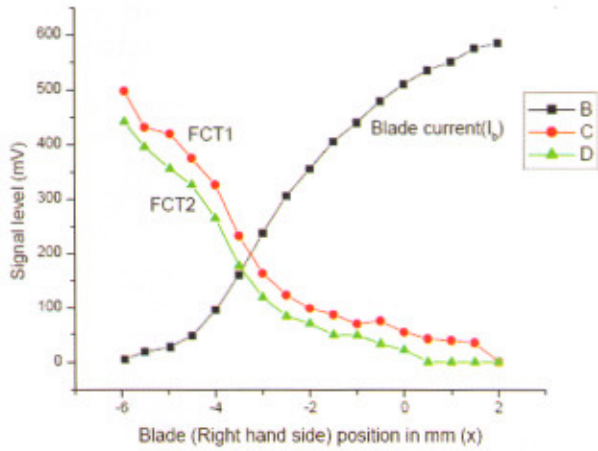

Fig.A.1.5: Variation of the slit blade current (B), FCT1 (C) and FCT2 (D) signals as a function of the blade position.

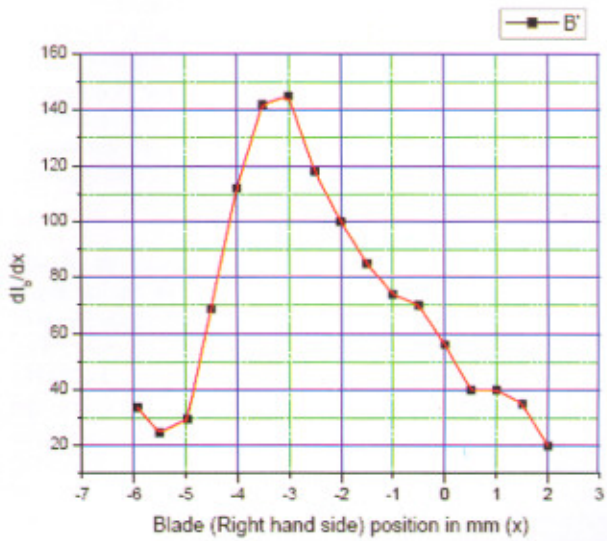

Fig.A.1.6: Horizontal beam profile obtained by differentiating the blade current signal curve with respect to the blade position.

The development and installation of this device was done by a team of engineers from Industrial & Medical Accelerators Section, Beam Diagnostics Section, RF Systems & Controls Division and its manufacturing was done by the Accelerator Component Engineering & Fabrication Division of RRCAT. The ceramic fluorescent screen was precision cut using Nd:YAG Laser in Solid State Laser Division of RRCAT.

Contributed by:
R..S. Sandha, S.G. Goswami,
J. Dwivedi (jishnu@cat.ernet.in),
A.C. Holikatti, T.A. Puntambekar. A. M. Gupta,
and K. Saifee

A.2 Indus-2 beam line front end control system : Design, development & commissioning

Indus-2 is a third generation synchrotron light source with 27 beam lines planned for utilization of the synchrotron light. The equipment assembly called beam line front end (BLFE) is used to interface the beam lines with the Indus-2 ring. The BLFE fulfils the following important requirements:

1. Provides protections consequent to vacuum failure on either side (Machine or beam line).
2. Provides interlocks for the safety of sensitive front end devices.
3. Provides radiation safety interlock.
4. Provides the photon beam conditioning for beam lines.

In order to facilitate and co-ordinate the operation and control of the BLFE from the main control room, a control system has been built by the Controls Laboratory. The BLFE control system is based on the three-layer architecture of Indus-2 control system. The lowermost layer (Equipment Control (EC) layer) interfaces the signals from field devices; the middle layer (Supervisory Layer) collects all the signals and passes it to the uppermost layer, the operator interface layer.

The EC layer caters to approx. 600 signals, in all (400 status signals, 100 digital controls and 100 analog input signals). Beam Energy and Beam Current information can be provided to all the beam-lines from this system. The Supervisory Control And Data Acquisition (SCADA) software at the operator interface layer provides the graphical user interface (GUI), which shows the signals both in tabular as well as in a synoptic form. This software is designed on a client server model. The GUI server communicates with the middle layer using PVSS API manager over Ethernet and collects the data and computes system state variables. The API manager interacts with the hardware (layer-2 server) to get the data and set the physical devices. This periodically polls the L2 server to get current parameter values and set them in the PVSS database (DB). Engineering data value to physical signal value conversion and scaling is done in the API manager. When user wants to set /control any parameter, the corresponding value change is given to API which sends them immediately to L2. GUI server synthesizes present system state according to the system pre-selectable configuration and previous state variables of the system. Accordingly events are generated which trigger automatic actions and alarms.

All events and actions (either automatic or user initiated) are logged along with user name. All user actions need authentication. There are three levels of authentication, the first level provides the operation rights, second level provides the configuration change rights on vacuum limits and third level is the administrator level. Alarms on device malfunction are displayed in the main Indus alarm panel as well as on the BLFE GUI panel with the device blinking to highlight the erroneous device. Presently few beam line controls are functional and others will be coming up in near future. The software is designed to allow the stepwise addition of the new upcoming beam lines with minimal configuration changes.

The control system provides the vacuum interlock by monitoring the vacuum level on both sides of the front end. It withdraws the open permission on gate valve GV1 connecting the front end to the ring periphery to protect vacuum in case pressure increases beyond the set limit. There are separate limits for alarm generation and automatic action, which are user changeable. This is done with proper user authentication.

Radiation safety is assured by interlocking the safety shutter (SS) open permission with electron beam injection. When the electron beam is stored and ramped to the desired level the operator can give SS open permission to the beam line users after proper authentication. The radiation level is continuously monitored and software withdraws the SS open permission in the case of radiation exceeding the safe limits. The operation limits of SS for alarm generation and automatic action are provided to operator with authentication.

Various devices are protected against damage by continuously monitoring the system state and in case of system entering undesired state the software initiates the beam dump. The GUI panel and mimic for the BLFE are shown in Fig.A.2.1, A.2.2.

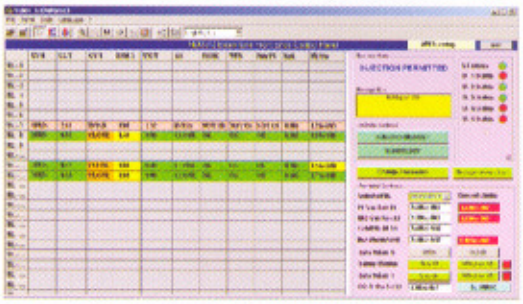

Fig.A.2.1: Main GUI Panel for BLFE control.

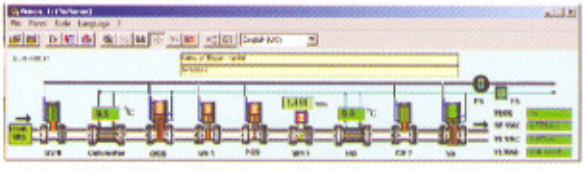

Fig.A.2.2: Synoptic view of a Beam Line Front End.

Contributed by:
P. Fatnani (fatnani@cat.ernet.in)

A.3 Physics design and modeling of H^- ion source

Power Supply Division of RRCAT has initiated the development of an arc discharge driven cesiated H^- ion source for the high current, high energy (50 keV) H^- injector for a spallation neutron source. Both surface and volume production of H^- ions will be used to increase the yield.

The plasma will be produced by arc discharge with multiple filaments and confined by multi-cusp magnetic field configuration. The design of this magnetic field and heat removal system for the H^- ion source plasma chamber has been carried out through mathematical modeling using finite element analysis. A cylindrical plasma chamber of 12 cm inner diameter and 12 cm length has been considered. The magnetic field is assumed to be produced by equal strength permanent bar magnets of dimension 12 x 2.5 x 2.5 cm, of coercivity (H_c) 5.7 x10^5 A/m and remanence of 0.8 T. The results (Fig.A.3.1) indicate that the magnetic field near the chamber wall is 0.23 T, which is desirable for the plasma confinement in the ion source. The field free region ($|B| < 10$ G) with 12 bar magnets is about 50 mm diameter surrounding the chamber axis. Considering a duty factor of ion source = 10% and peak power dumped in the chamber not exceeding 60 kW, the cooling system parameters have been worked out both for SS and OFHC Cu plasma chamber.

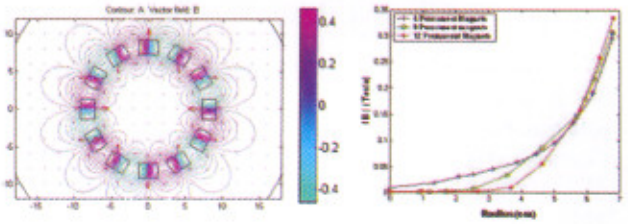

Fig.A.3.1: (a) Multi-cusp magnetic field lines with 12 permanent magnets placed along the cylinder length. (b) Magnetic field intensity variation along a radius that passes through the cusp for different combinations of magnets.

Computer simulations have also been performed using fluid model considering sheath formation near the boundary wall of the plasma chamber under electro-negative plasma equilibrium conditions to get an estimate of the spatial density variation of different species in the H^- plasma. The average cross-sections for various reactions responsible for H^- ion formation and their destruction have been taken into account. The total power requirement for the ion source has been computed using energy and particle balance (Fig. A.3.2). Finally various parameters of the arc discharge and RF discharge have been computed by modeling the plasma generation mechanism through arc and RF discharge. The required plasma density is found to be ~10^{19} m^{-3}.

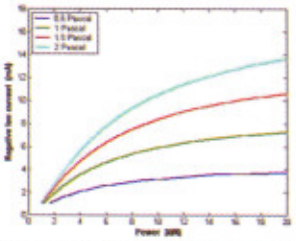

Fig.A.3.2: Variation of RF power absorption in the H^- ion source plasma with H^- ion current at different gas pressure in the plasma chamber.

A Particle-In-Cell (PIC) Monte Carlo Computation (MCC) code has been developed to take into account numerous reactions taking place inside the plasma chamber. The PIC code incorporates elementary module of the MCC algorithm. The extraction code is functioning and has been tested for H^- ions as shown in the Fig.A.3.3 A fast Fourier transform (FFT) based Poisson solver has been used coupled with capacitance matrix to incorporate any arbitrary electrode geometry. In order to overcome the limitations of the FFT solver, a matrix decomposition based Poisson solver has been developed.

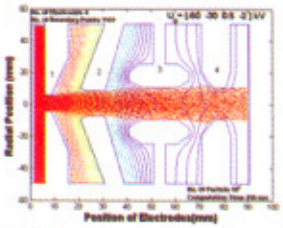

Fig.A.3.3: Extraction of negative ions, through tetrode geometry is shown. The red dot represents the H^- ions and 1, 2, 3 and 4 represent plasma, extractor, accelerator and screening electrode respectively.

Further, the extraction and optimization of H^- ions through various electrode geometries from an ion source has been studied using the IGUN software. The extraction setup shown in Fig.A.3.4 gives an rms emittance of 0.182 cm-mrad and an angular divergence of 6.2 mrad. Sharp corners and steep inclined edges are avoided in the high potential drop region between the puller electrode and the ground electrode to reduce the possibility of electrical breakdown. This study also helps in the understanding of H^- ion extraction.

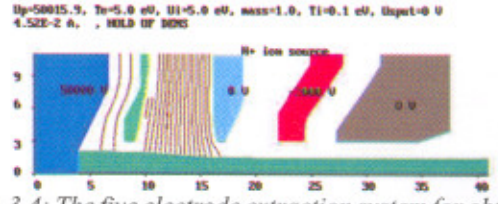

Fig.A.3.4: The five electrode extraction system for obtaining high quality ion beam using the IGUN code.

Contributed by:
V.K. Senecha (senecha@cat.ernet.in)

A.4 Large magnetocaloric effect in the Heusler alloy $Ni_{50}Mn_{34}In_{16}$

Among the various off-stoichiometric Heusler alloys studied in the Magnetic and Superconducting Materials Section (MSMS) of MAASCD, RRCAT, the $Ni_{50}Mn_{50-x}In_x$ system has shown much promise. The high temperature (T) Austenite phase of these alloys undergoes a first order transition into a Martensite phase with the lowering of T and the transition could be induced by both T and magnetic field (H). Very large magnetoresistance and magnetocaloric effect (MCE) has recently been observed across this phase transition in $Ni_{50}Mn_{34}In_{16}$ alloy [V. K. Sharma et. al. Appl. Phys. Lett. **89**, 222509 (2006); J. Phys.: Condens. Matter **19**, 496207 (2007); J. Phys. D: Appl. Phys. **40**, 1869 (2007)].

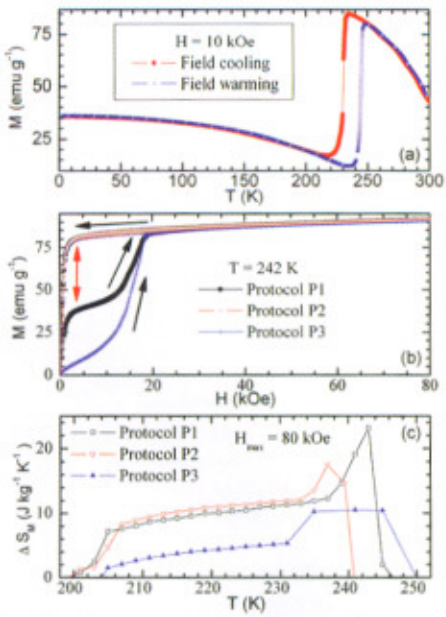

Fig.A.4.1: (a). Temperature dependence of magnetization of $Ni_{50}Mn_{34}In_{16}$, (b) Isothermal field dependence of magnetization of $Ni_{50}Mn_{34}In_{16}$ obtained in different experimental protocols. (c) Temperature dependence of isothermal entropy change of $Ni_{50}Mn_{34}In_{16}$ because of applied magnetic field.

Recently the MCE of $Ni_{50}Mn_{34}In_{16}$ in the Austenite-Martensite phase transition region has been studied in MSMS with different experimental protocols to reach this T-regime. Fig.A.4.1(a) depicts the magnetization (M) vs. T characteristics of $Ni_{50}Mn_{34}In_{16}$ for $H = 10$ kOe. The sharp drop in the $M(T)$ curve below 250 K marks the Austenite-Martensite phase transition in this alloy, and the associated thermal hysteresis confirms the first order nature of this transition. Fig.A.4.1(b) shows the isothermal $M(H)$ characteristics of $Ni_{50}Mn_{34}In_{16}$ obtained at 242 K after reaching the temperature in three different protocols P1, P2, and P3. In P1, the sample is first cooled in zero field from 305 K to 150 K and then gradually warmed up to 242 K while doing isothermal M vs. H experiments at increasing temperatures. In P2, the sample is cooled in zero field directly from 305 K to 242 K. In P3, the sample is cooled in zero field to 30 K, and then warmed up to 242 K before switching on the measuring field. Isothermal $M(H)$ curves were obtained in 4 K temperature interval in the T-regime 150-280 K in the three protocols described above. The $M(H)$ response was found to depend strongly on the protocol used to reach the target temperature.

The isothermal entropy change ΔS_M due to an applied field is a measure of the MCE in a material. The ΔS_M for $Ni_{50}Mn_{34}In_{16}$ was estimated from $M(H)$ isotherms using the Maxwell's relation:

$$\left(\frac{\partial S_M(T,H)}{\partial H}\right)_T = \left(\frac{\partial M(T,H)}{\partial T}\right)_H$$

Fig.A.4.1(c) shows that $\Delta S_M(T)$ is significantly influenced by the experimental protocol, though all the three protocols lead to very high values of ΔS_M. To judge the effectiveness of a potential magnetic refrigerant, the material needs to be characterized in terms of refrigerant capacity (RC) and field hysteresis losses. RC is the heat transferred between the hot and cold reservoirs in an ideal thermodynamic refrigeration cycle. It is defined as:

$$RC = \int_{T_{cold}}^{T_{hot}} [\Delta S_M(T)]_{\Delta H}\, dT$$

The magnetic hysteresis losses in the T-regime 150-280 K is calculated from the area enclosed within the isothermal $M(H)$ loops. The average hysteresis loss ($LOSS$) is subtracted from RC to get the effective refrigerant capacity (RC_{EFF}). The results of these calculations are summarized in Table1.

TABLE 1: $Ni_{50}Mn_{34}In_{16}$ as a magnetic refrigerant.

Protocol	T_{cold} (K)	T_{hot} (K)	RC (J/kg)	$LOSS$ (J/kg)	RC_{EFF} (J/kg)
P1	233.6	244.1	163	103	60
P2	208.6	240.0	367	141	226
P3	230.7	247.4	156	119	37

It is concluded that $Ni_{50}Mn_{34}In_{16}$ is most effective as a magnetic refrigerant, when the working temperature is reached by unidirectional cooling in zero magnetic field; and in this mode, it is comparable to that of the well recognized giant MCE material $Gd_5Ge_2Si_2$. [For details see, M. K. Chattopadhyay, V. K. Sharma and S. B. Roy Appl. Phys. Lett. **92**, 022503 (2008)]

Contributed by:
M. K. Chattopadhyay (maulindu@cat.ernet.in) and V. K. Sharma

A.5 Development of efficiently cooled drift-tubes for high energy SFDTL RF cavities

The drift tubes are very important components of a typical SFDTL type of accelerating structure, as the beam passes through the center of the drift tube and the beam accelerates between the gaps of two drift tubes. The drift tube receives the maximum heat flux; hence development of efficient cooling schemes for drift tubes needs a combined approach of thermal design and fabrication feasibility. Different types of hydraulic channels for increasing over all heat transfer coefficient were studied at Advanced Accelerator Module Development Division of RRCAT. A six cooling channel drift tube was fabricated using hydrogen brazing and subsequently vacuum brazed and tested for UHV compatibility. The brazing of such drift tube is difficult because of six precision components are to be joined simultaneously to meet UHV requirement. Fig.A.5.1 shows cut section of the optimized design for six channels cooling in one brazing step fabrication.

Fig.A.5.1 Cut view of the six-channeled drift-tube.

Contributed by:
V. Jain (vikas@cat.ernet.in), P.K. Kulshreshtha, and A. Kak

A.6 Experimental setup for RF characterization of pillbox cavity

Most cavity resonators used in electron and proton accelerators are derived from the simple cylindrical or pillbox cavity. Comparison of the results for RF frequencies and other parameter are done between numerical techniques and experiments at Advanced Accelerator Module Development Division of RRCAT. Further, a piston tuner arrangement as shown in Fig.A.6.1 is attached to this cavity through vertical port. This tuner system has 50 mm diameter piston attached to the stepper motor. This arrangement can give 25 micron movement in one step. Total stroke length is 70 mm. Here 50 mm inward and 20 mm outward movement is set. Results of fundamental frequency perturbation and theoretical magnetic field calculations are shown in Fig.A.6.2.

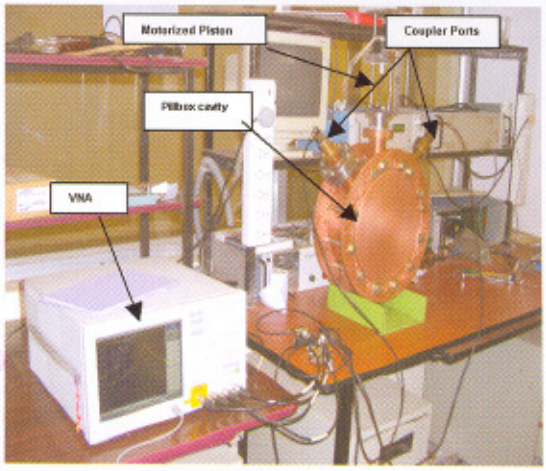

Fig.A.6.1: Experimental setup of Pillbox cavity RF testing.

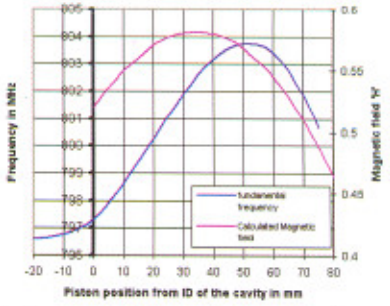

Fig.A.6.2: Displacement of piston tuner vs. fundamental frequency in pillbox cavity compared with calculated magnetic field inside the cavity.

Contributed by:
V. Jain (vikas@cat.ernt.in) and G. Mundra

A.7 Prototype compound motion compact precision jacks

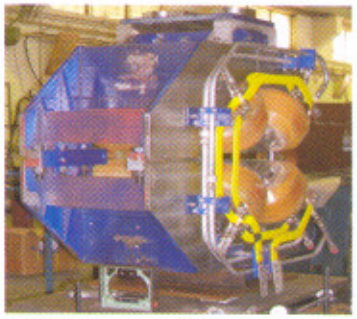

Fig.A.7.1: Performance testing of prototype precision movement compact jack system, mounted below a quadrupole magnet.

Prototype compound motion compact precision jacks (each of capacity 500 kg) have been developed at Advanced Accelerator Module Development Division of RRCAT, for

positioning and alignment of small accelerator components such as quadrupole and sextupole magnets, SFDTL tanks etc. These jacks can be anchored below the components and positioned (its magnetic axis and mid plane) precisely with typical accelerator alignment tolerances of 0.1 mm in linear and 0.2 mrads in rotational position w.r.t their true position in the ring. The designed movement system uses combination of three identical compound motion precision jacks similar to the support system of main dipole magnets of Indus-2. Fig.A.7.1 shows the performance testing of precision movement jack system, mounted below the quadrupole magnet

Contributed by:
K. Sreeramulu (sreeram@cat.ernet.in)
and P.K. Kulshreshtha

A.8 Design and prototype fabrication of an eccentric wheels based motorized alignment mechanism for accelerator components

A remote alignment/ or alignment correction becomes essential for proton LINAC components of medium and high energy, as they become source of radiation because of residual radioactivity and hence become inaccessible. Very high order of alignment accuracy is required to meet the stringent requirement of beam loss. An eccentric wheel mechanism based alignment system has been fabricated at Advanced Accelerator Module Development Division of RRCAT as shown in Fig. A.8.1.

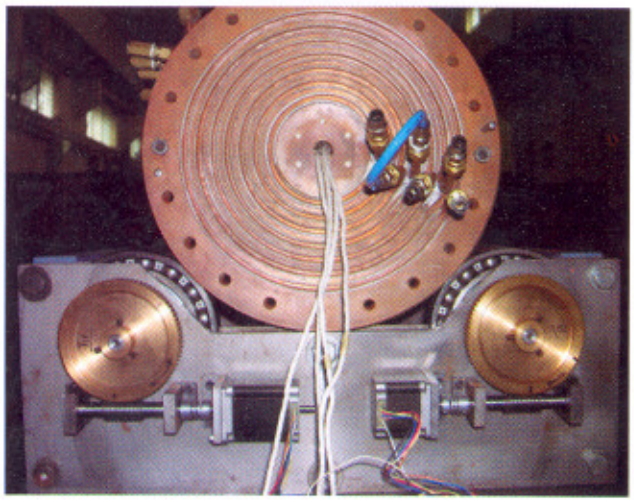

Fig.A.8.1: SFDTL supported on eccentric wheel base alignment system.

The mechanism consists of two sets of two eccentric wheels, one at each end. With the combination of the movements of these wheels it is possible to have very precise movement in a small area in front and in the back plane. With the combination of these movements, two linear (X-Y) and two rotary (pitch and yaw) degrees of freedom is achieved, which is highly suitable for such applications. The eccentric wheels are moved by stepper motor through precision worm and wheel to achieve high resolution of movement. If we operate the eccentric wheels within the range of 43.26 degree to 223.26 degree (in this combination/ design), the direction of force on the worm-wheel does not change and hence the backlash effect can be avoided.

Contributed by:
G. Mundra (mundra@cat.ernet.in) and L. Singh

A.9 Stranded water-cooled cables for rapid cycling magnet coils

The presence of eddy currents in low frequency (~100 Hz) rapid cycling magnets is a source of technical difficulties and the key issue is the reduction of eddy current loss. In order to keep the magnet coil losses at reasonable levels, it is generally necessary to use a special water-cooled stranded cable for operating frequencies above 10 Hz as the macroscopic eddy current losses are proportional to the square of the frequency and the square of the magnetic field. The magnetic field inhomogeneity resulting due to eddy current loss is less and also low operating costs of magnets with stranded coils. Few prototype 6 meters length stranded water-cooled cables using bare / enameled aluminum strands for testing have been indigenously developed at Advanced Accelerator Module Development Division of RRCAT. Fig.A.9.1 shows the details of water-cooled stranded cable showing aluminum strands in various layers. The development of 50 meters continuous length water-cooled aluminum stranded cable is in progress.

Fig.A.9.1: Water-cooled stranded cable, showing strands in various layers.

Contributed by:
K. Sreeramulu (sreeram@cat.ernet.in)
and P.K. Kulshreshtha

L.1 Diode-end-pumped Nd:YVO_4 laser marker system

Laser marking is a non-contact, permanent and indelible marking process. It is highly flexible compared to any other marking process. It can mark alphanumeric, 2D matrix codes, bar codes, logos, serial numbers and any pictures and images. Solid State Laser Division of RRCAT has developed a compact laser marker system using a Q-switched Nd:YVO_4 laser, in collaboration with the Laser Electronics Support Section of RRCAT. The maximum average and peak power is 5 W and 40 kW respectively. The scanning of the laser beam has been done by galvanometric x-y scan mirror assembly with a flat field objective of 163 mm focal length having marking field of 110x110 mm^2. The focussed spot size is around 50 µm and the marking speed close to 2.5 m/s can be achieved. The pulse parameter of this laser is ideal for ablation marking, and precipitation marking such as surface etching and surface annealing.

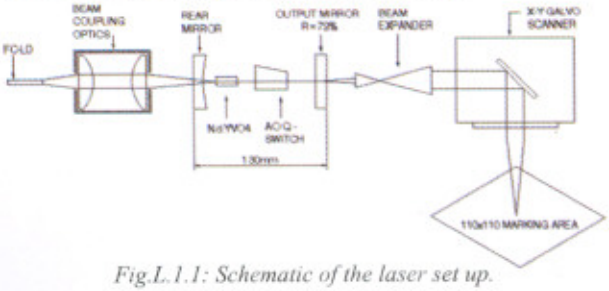

Fig.L.1.1: Schematic of the laser set up.

The system consists of an acousto-optically Q-switched laser and control electronics. The laser gain medium is a rectangular Nd:YVO_4 crystal doped with 0.5% Nd (atomic). The pump source is an 808 nm, 30 W fiber coupled laser operating at 25°C. The pump beam is collimated and focussed by two plano-convex lenses on the crystal to a spot size ~ 400 µm. The resonator is formed by high reflecting rear mirror and 80% plane output coupler. The cavity length is 130 mm. Fig.L.1.1 shows the schematic of the laser set-up. The active Q-switching is accomplished by a high efficiency acousto-optic Q-switch operating at a carrier frequency of 41 MHz. The maximum diffraction efficiency produced by the Q-switch is > 70% for the RF power of 5 W. Such high performance Q-switches are essential for laser system with high gain crystal like Nd:YVO_4. For the extraction of maximum power in TEM_{00} mode, the ratio of the cavity spot size to pump spot size is set to be 0.8. An 8x beam expander was used to reduce the divergence of the beam before the scanner. The typical repetition range for marking application varies from 15 kHz to 40 kHz depending upon the material to be marked.

The control electronics consists of a micro-controller based control module interfaced to PC through RS-232 serial port. The control module has an 'Application Specific Integrated Circuit' (ASIC) based interface to XY scanning head. It also controls the laser On/Off while marking through the acousto-optic Q-switch. A Labview based drawing editor is developed to create a combination of text, bitmap images, geometrical shapes etc. for marking. The editor is specially designed to map the screen drawing pad area to the marker co-ordinate system. It visually indicates the graphic cursor position directly in the marker co-ordinates for editing. The editor provides an intuitive user friendly GUI with horizontal and vertical scales along the drawing pad. All the graphic editing features such as object selection, moving within the drawing area, scaling and MS-Windows™ supported text, fonts, styles, sizes, etc, are available for the user. The editor accepts all the standard image file formats e.g. BMP, TIFF, JPG, etc and internally converts them to bi-level images after suitable image processing. The user can save the drawing for later use in proprietary marker file format.

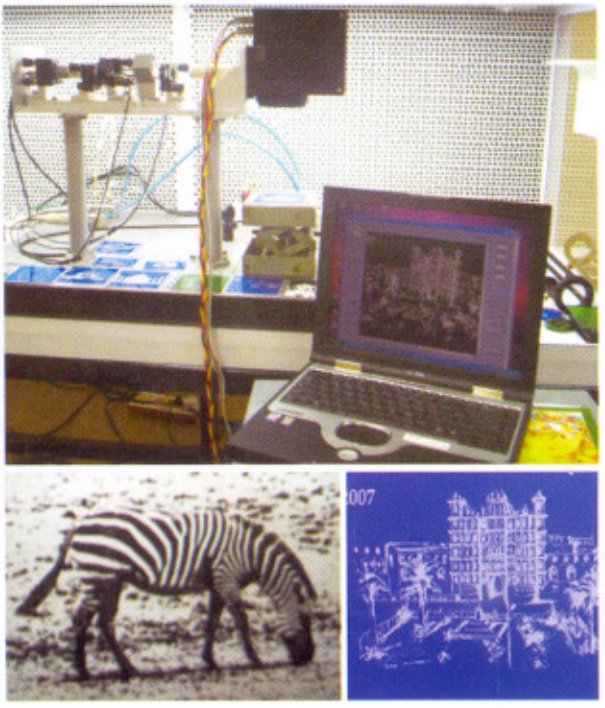

Fig.L.1.2: Photograph of the system and some of the marked samples.

High quality pictures were marked on anodized Al-plates using raster scanning technique. Fig.L.1.2 shows some of the marked samples. In order to make this a compact and portable system, several improvements are being carried out. The overall size and power consumption of the system is around 230 mm x 260 mm x 485 mm and 300 W respectively.

Contributed by:
K. Ranganathan (ranga@cat.ernet.in),
P.P. Deshpande (ppd@cat.ernet.in), and S.M. Oak

L.2 Generation of flattened Gaussian beams from Gaussian mirror resonator

Laser beams of flat top spatial intensity profiles, are attractive for many applications like non-linear optics, holography, lithography, material processing, optical data storage and spectroscopy etc. Several techniques to generate flat top or uniform intensity beam profiles external to the cavity are reported in the literatures. However, in this case there is a substantial loss of energy compared to the original beam energy. In an active resonator configuration, super Gaussian beams (SGB) of flat top intensity profile can be generated by using super Gaussian mirrors. Flattened Gaussian beams (FGB) are another class of beams, which also exhibit uniform intensity profile. Though SGB and FGB look alike and are experimentally difficult to distinguish, mathematically they are quite different. Theory for FGB was first proposed in 1994, and the beams with such profiles were demonstrated external to the cavity. Practical realization of FGB in an intra-cavity setup was not reported. Generation of FGB in an active resonator configuration using a variable reflectivity mirror (VRM) with Gaussian reflectivity profile has been recently demonstrated at the Solid State Laser Division of RRCAT. The system was an electro-optically Q-switched Nd:YAG laser in positive branch unstable resonator configuration.

Generally VRMs are fabricated based on three important parameters. These are : Gaussian order, peak reflectivity and coating spot size. Once these parameters are decided then the resonator magnification is fixed to yield a Gaussian output profile. Therefore such a VRM mirror can be used only in a particular resonator. The transmission profile of such a VRM is given by

$$I_{out}(r) = \left\{1 - R_0 \exp\left[-2(M^2-1)\left(\frac{r}{\omega_i}\right)^2\right]\right\} I_0 \exp\left[-2\left(\frac{r}{\omega_i}\right)^2\right]$$

where M is resonator magnification and r is the radial co-ordinate, w_i the incident spot size and n the Gaussian order. In the present case n = 2 (Gaussian). R_0 is the peak reflectivity. From the above equation one can see that, the output profile will be flattened when the resonator magnification M value is changed from the designed value calculated for a Gaussian profile. This is shown in the Fig.L.2.1.

Experiments were conducted using a 2m convex VRM mirror with Gaussian reflectivity profile coating. The spot size of the coating was 1.8 mm and peak reflectivity of 30%. The rear mirror was 3 m concave and separation between the mirrors was 0.5 m. This results in a resonator magnification of 1.5 for which the output is of Gaussian spatial profile, which is shown in (Fig.L.2.2). The resonator magnification was changed by changing the mirror curvature and resonator length. Output spatial profiles were generated for magnifications 1.5, 1.8 and 2. Generated profiles were fitted with FGB equation [See for details: R.Sundar, K.Ranganathan, and S.M.Oak Applied Optics 47, 2, 147, 2008]. FGBs of order 3 and 4 were generated by changing the resonator magnification as shown in Fig.L.2.3. The output energy had a marginal drop as the reflectivity and hence output coupling was not optimum for different resonator configurations. However, the pulse width did not change appreciably. This technique has an advantage of generating various spatial profiles which include Gaussian, flat Gaussian of different orders and annular like profiles using a single VRM Gaussian mirror.

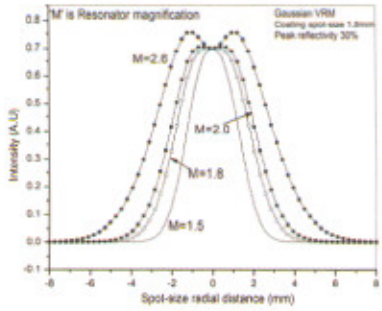

Fig.L.2.1: Theoretical transmitted profile from Gaussian mirror for various resonator magnifications.

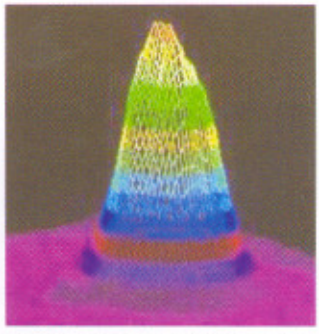

Fig.L.2.2: Gaussian output spatial profile generated from resonator magnification M = 1.5.

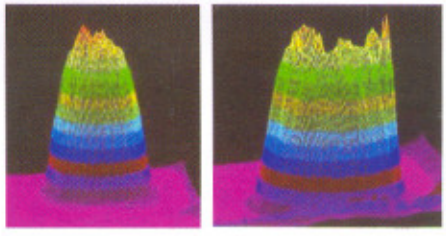

Fig.L.2.3: Output spatial profile of FGB order 3 generated from resonator magnification M = 1.8 and FGB order 4 for magnification M = 2 respectively.

Contributed by:
R.Sundar (sundhu@cat.ernet.in), K.Ranganathan, and S.M.Oak

L.3 Carrier dynamics in surface quantum wells

GaAsP/AlGaAs quantum wells are utilized in diode lasers, detectors and modulators. We have probed the room temperature carrier dynamics in GaAsP/AlGaAs single quantum wells by transient reflectivity measurements. The quantum wells were grown by SLS, RRCAT. A single, 13 nm $GaAs_{0.9}P_{0.1}$ well was grown with a capping layer of $Al_{0.7}Ga_{0.3}As$ (Fig.L.3.1). For sample A this layer thickness (t) is 50 nm whereas for the sample B it is reduced to 5 nm. The ee1-hh1 transition for the quantum well is at 1.58 eV. Surface photo voltage (SPV) measurements of the two samples show significant difference in the energy range 1.53-1.58 eV, which comes from the different contribution of surface states in the two samples. The laser wavelength was set to 1.56 eV, which is slightly below the quantum well ee1-hh1 transition. Pump-probe reflectivity measurements were done by splitting the output of a 100fs, 82 MHz Ti: Saphhire laser into a strong pump and a weak probe and impinging them on the sample with a variable delay between them. The photo-induced carriers generated by the pump pulse cause a change of absorption due to effects like band filling, band gap renormalization, screening and free-carrier absorption. The change in absorption causes a change of refractive index which gives rise to reflectivity change. The magnitude, sign and the decay of this transient reflectivity change depend on the relative contribution of the above processes. This, in turn, depends on various factors like the material properties including transport, lattice temperature, excitation and detection wavelengths and the excitation power.

The reflectivity dynamics for the two quantum well samples is shown in Fig.L.3.2. For sample A the reflectivity change was positive. There is a fast decay (~0.5 ps) followed by a slower rise which lasts which lasts for more than 50 ps. For sample B, on the other hand, the reflectivity change is negative though it also shows a fast and a slow component. As the wavelength is just below the quantum well ee1-hh1 transition but above the GaAs band gap, we expect the AlGaAs/GaAs interface will also contribute to the signal along with the quantum well states, GaAsP/AlGaAs interface states and surface states. Therefore measurements were also done on GaAs as well as an AlGaAs film deposited on GaAs. GaAs showed a positive reflectivity change (Fig.L.3.3a), which decayed exponentially with a time constant varying between 1-2 ps, depending on the pump energy. This matches with earlier reports. The AlGaAs/GaAs thin film, however, showed a slow rise (1-2 ps) followed by a much slower decay (Fig.L.3.3b). For semiconductors, carrier cooling and carrier decay govern the transient reflectivity behaviour. Carrier cooling can lead to a reflectivity rise time much slower than the excitation pulse width. The sign of the reflectivity change at a given excitation wavelength and pump energy is governed mainly by the relative contributions from band filling, band gap renormalization and free carrier absorption. The interface also plays a significant role in heterojunctions. For example, the AlGaAs/GaAs heterojunction has been shown to possess a high mobility two-dimensional electron gas and therefore a transient reflectivity dynamics very different from bulk GaAs. From these observations it is apparent that in our quantum well samples all the interfaces need to be considered along with the quantum well states to explain the carrier dynamics in these quantum wells. Theoretical analysis and further work is in progress.

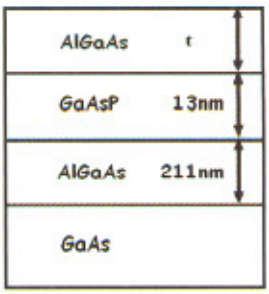

Fig.L.3.1: The quantum well structure.The thickness, t, is 50 nm (sample A) or 5 nm (sample B).

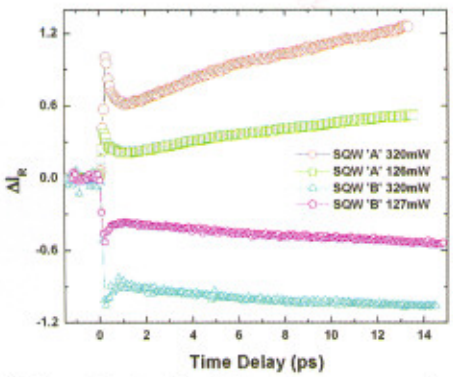

Fig.L.3.2: Transient reflectivity changes as a function of delay between the pump and probe pulses.

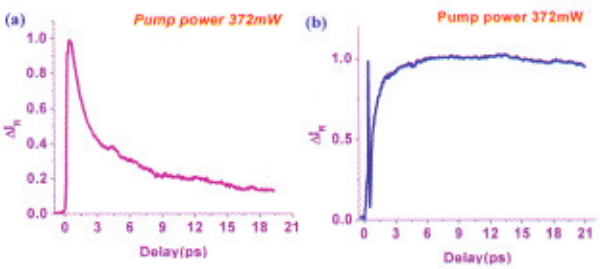

Fig.L.3.3: Transient reflectivity for a) GaAs and b) AlGaAs/GaAs.

Contributed by:
S. Khan, J.Jayabalan, and R..Chari (chari@cat.ernet.in)

L.4 Development of high current fast capillary discharge plasma setup

Discharge created plasma systems are very attractive as gain medium for coherent amplification of XUV-soft x-ray radiation. In particular fast capillary discharge plasmas have been used in setting up table-top soft x-ray lasers. A high current fast capillary discharge plasma device has been set up for pursuing R&D work in soft x-ray lasing at Laser Plasma Division and Laser Electronics Support Section.

Fig.L.4.1: Photograph of the capillary discharge system.

Main components in capillary discharge setup are 400 kV, 750 J Marx generator, a water capacitor, a SF_6 spark gap, a pre-pulse power supply and a capillary. A photograph of the full system is shown in Fig.L.4.1 and the schematic diagram of the set-up is shown in Fig.L.4.2. The Marx generator is made of 10 stages, with each stage consisting of a 60 nF capacitor, spark gap and two 6 kΩ charging resistors. All the capacitors can be charged up to 50 kV by means of a dc power supply. The controller sets charging voltage of the Marx capacitors and gives trigger pulse. A water line capacitor is used because water has a high dielectric constant of 81. This reduces the dimensions of the capacitor for a given capacity, and its equivalent inductance becomes small. A pre-pulse generator is connected to the electrode of the spark gap at the capillary end, through a 1 kΩ liquid resistor fed into the chamber. This resistor is made of a Delrin cylinder filled with copper sulphate solution, and fitted with copper electrodes at both the ends. Pre-pulse generator consists of a dc charging power supply of 20 kV, which charges a capacitor bank of 400 nF which is discharged into the capillary through an inductance of 120 μH and $CuSO_4$ resistor of 1 kΩ.This generates a current pulse of around 20 A for a duration of 100μs. The capillary is filled with argon gas and its pressure is kept in the range of 0.2-0.5 mbar. The setup also includes a $CuSO_4$ voltage divider and a Rogowski coil for voltage and current measurements respectively.

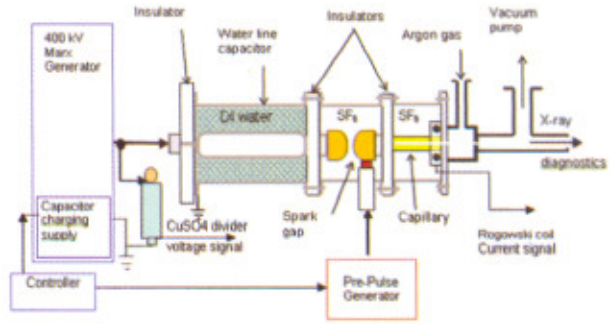

Fig.L.4.2: Schematic diagram of the capillary discharge plasma setup.

The pre-pulse supply is triggered to create pre-plasma in the capillary for few microseconds before the Marx generator is fired. Marx generator in turn charges water capacitor up to self breakdown voltage of SF_6 spark gap. Due to breaking of spark gap, the water capacitor discharges into capillary and generates peak current required for capillary discharge plasma experiments.

This setup has been assembled and tested in our laboratory up to 250 kV (with 25 kV /stage of charging voltage of the 10-stage Marx generator). The pre-pulse generator is being coupled to the setup. Voltage and current pulses recorded with the Marx bank charged to 18 kV /stage are shown in Fig.L.4.3.

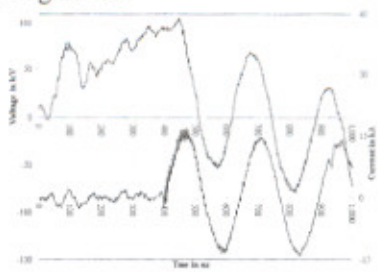

Fig.L.4.3: Voltage from a divider at Marx generator (upper trace) and the current through the capillary (lower trace).

Contributed by:
S. Nigam (snigam@cat.ernet.in), Y.B.S.R Prasad, and C. P. Navathe

L.5 Aggregation and de-aggregation of metal nanoparticle colloidal solutions

Nanoparticles start aggregating when the volume faction of nanoparticles in a nanocolloidal solution is high. In case of spherical nanoparticles, this aggregation has been reported to lead to the appearance of a new surface plasmon peak and increase in background extinction at the red end of the spectrum. We report for the first time a study of optical properties of aggregates of nanoplatelets carried out at the Laser Physics Applications Division of RRCAT. The stability of the aggregated sample against laser irradiation was also studied.

A colloidal solution of silver nanoplatelets was produced by salt-reduction method followed by photo-induced conversion using a 532 nm laser. This solution was kept in the dark for a few months. After this aging time the sample showed evidence of aggregation. Figures L.5.1 a and b show the extinction spectra of the initial (solid line) and aggregated colloid (dashed line). For the nanoplatelets, the strong peaks at 596 nm and 445 nm are from the in-plane dipole and in-plane quadruple resonance while the weak peak at 336 nm is due to the out-of-plane quadruple resonance. Comparing the extinction spectrum of the aggregated colloid with this we find that the overall extinction at the red end of the sample has increased, which is an indication of presence of random aggregations. All the SPR peaks were broadened. The out-of-plane quadruple resonance at 336 nm has blue-shifted by 4 nm, while the SPR peak at 596 nm has shifted by about 69 nm.

To understand effect of aggregation on the extinction spectra of nanoparticles we have done some preliminary calculations and compared extinction spectra of single and double truncated triangular-shaped platelets. In a colloidal solution the nanoplatelets can get attached to each other in any possible orientations. The calculations were done for few of such possible orientations of two interacting platelets. Though the amounts of shifts in various possible orientations are different, all of them show large red shift of in-plane dipole resonance and small blue shift of out-of-plane quadrupole resonance. This shows that the observed changes in the extinction spectrum are caused by aggregation. Fig.L.5.1(c) shows the TEM of the aggregated colloid.

The aggregate sample was again exposed to 532 nm, 250 ns, 7 kHz laser pulses. The average laser power was 50 W/cm^2. Fig.L.5.2 shows the transmission spectra of the sample during the exposure. During the initial stage the peak at 665 nm reduced in strength and also shifts to blue side of the spectrum. On further exposure the peak further blue shifts to 596 nm. The TEM of the sample at this stage is shown in Fig.L.5.3. Almost all of the nanoplatelets have separated.

Both the extinction spectrum results and the TEM show that nanoplatelets have been de-aggregated. It is interesting to note that at similar irradiation levels aggregates of silver nanospheres were unaffected. This shows that, in colloids, the aggregation of nanoplatelets is weaker as compared to nanospheres. Therefore in case of undesired aggregation, laser irradiation of suitable power can be used for de-aggregation.

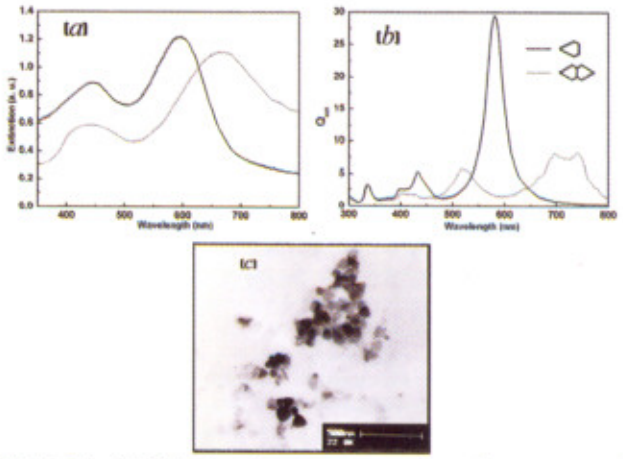

Fig.L.5.1: (a) Calculated extinction spectra of two separated (solid line) and joined (dashed line) nanotriangles. (b) Measured extinction spectra of a nanotriangle colloid (solid line) and aggregated nanotriangles (dashed line). (c) TEM pictures of aggregated nanotriangles.

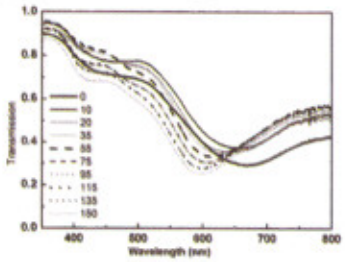

Fig.L.5.2: The transmission of the nanoplatelet sample at various times during exposed to high power nanosecond laser. The values shown are exposure time in minutes.

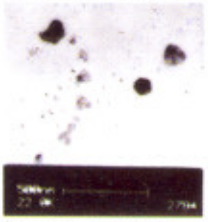

Fig.L.5.3: TEM of the nanoplatelets after exposure to high power laser. There were very few particles that are close to each other.

Contributed by:
J.Jayabalan (jjaya@cat.ernet.in),
A. Singh, and R.Chari

L.6 Sorting and guiding of micro- objects with evanescent optical field

Optical micromanipulation can provide a non invasive means for sorting of microscopic objects for further evaluation and analysis. One approach used for such sorting involves the use of multiple optical traps arranged in linear or three dimensional arrays. Objects of different size or composition, flowing past such trap array get sorted out due to a difference in the magnitude of optical gradient forces on these. Other recent approach uses the evanescent field generated at the surface of the Y-shaped optical waveguide. By adjusting the relative power distribution in the two branches of the waveguide, the particles could be selectively guided down the desired branch. Laser Biomedical Applications and Instrumentation Division of RRCAT has shown that microscopic objects can be sorted in a much simpler and efficient manner by use of the gradient of optical evanescent field at refractive index interfaces. The approach exploits the fact that heavier particles reside closer to the interface compared to lighter particles and therefore interact strongly with the evanescent field to experience larger optical forces.

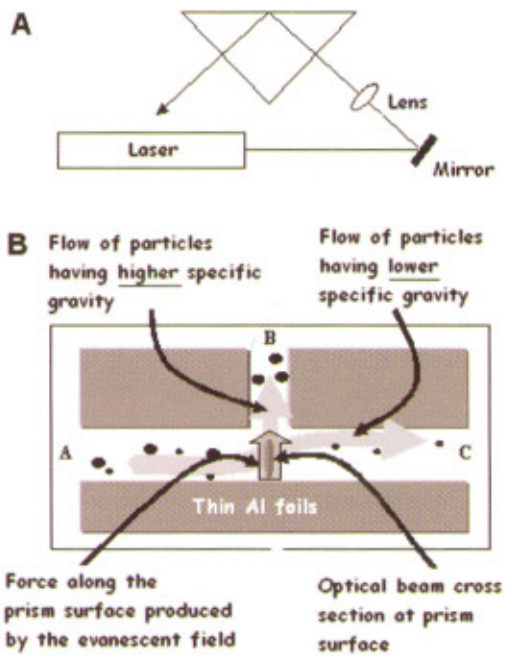

Fig.L.6.1: Experimental set-up.

The experimental set-up is shown in Fig.L.6.1. The output from a 1064 nm, cw laser was made to undergo total internal reflection at the boundary between glass (refractive index 1.51) and water (refractive index 1.33) atop a right-angle crown glass prism (Fig.L.6.1a). To construct the microfluidic channels, strips of thin (~20 μm) aluminium foils were used as spacers between the top surface of the prism and a glass cover slip. The gaps between the aluminium strips were adjusted to form a T-shaped junction as shown in Fig.L.6.1b. Typical widths of such channels were measured to be ~ 30μm. Due to oblique incidence, the cross section of the evanescent wave on the prism interface was elliptical and should result in a force along the surface as shown by the straight upward arrow. A 40X objective lens and a CCD camera were used to monitor the suspended microscopic objects in the aqueous medium flowing inside the channels. The bright field illumination was obtained using a 50W, fiber light guide illuminator placed below the prism.

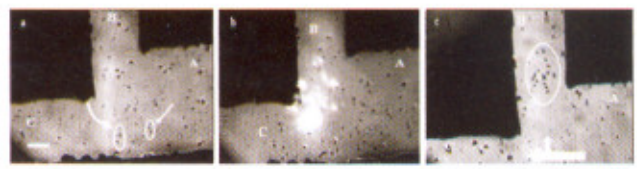

Fig.L.6.2: Sorting of 2 μm diameter polystyrene micro-spheres from a ~50:50 mixture of 1 and 2 μm diameter microspheres. a) 2 μm microspheres are shown by curved arrow and 1 μm microspheres by straight arrow. b) The bright spots are coming from the scattered evanescent field by the microspheres. c) Sorting of 2 μm microspheres into the upward channel by the action of the evanescent field. Increased population of these microspheres can be seen in the encircled region. Scale bar, ~15 μm.

In Fig.L.6.2 we show sorting of 2 μm polystyrene microspheres out of a 50:50 mixture of 1 and 2 μm diameter microspheres When a small volume of micro-particles suspension was injected into the input channel (A), heavier particles due to their interaction with stronger field got deviated by larger angles and thus got directed into the upward output channel (B). The light particles, suffering small deflection, continue to flow to the output channel (C). The power of the optical beam used for the results shown in Fig.L.6.2 was ~ 300 mW. The sorted 2 μm microspheres could be further guided along the channel B by translating the evanescent field. The population of 2 μm microspheres in channel B could be increased from ~50% to ~ 80%. The use of this method for separating red blood cells (RBCs) from white blood cells (WBCs) was also investigated. The RBCs are much heavier (specific gravity (~1.08)) than the different type of WBCs and platelets (specific gravity (~1.07-1.03)). Therefore, a larger optical force is expected on RBCs under the influence of evanescent field. It was found that at an incident power level of ~ 400 mW (1064 nm), the WBCs were observed to be nearly unmoved whereas the velocity for RBCs was ~ 6 μm/s. Therefore RBCs could be preferentially directed in the channel B.

Contributed by:
R. Dasgupta, S. Ahlawat (rsunita@cat.ernet.in), A. Uppal, and P. K. Gupta

L.7 Dependance of high order harmonics intensity on laser focal spot position in pre-formed plasma plumes

High order harmonic generation using ultra-short pulse lasers is an attractive method of generating coherent radiation in the XUV region, as an alternative to soft x-ray lasers, and to achieve attosecond duration soft x-ray radiation. For practical applications, it is desirable to have high conversion efficiency from the driving laser beam to the harmonic radiation. While most studies have been performed using gas jets, pre-formed plasma plumes have been used recently to generate high order harmonics. The use of plasma plumes is attractive for resonance intensity enhancement. However, it may adversely affect the conversion efficiency due to phase-mismatch problem. Since the plasma refractive index depends on the electron density, which in turn is governed by the laser beam intensity, the amount of phase mismatch would depend on the laser intensity, the length of the plasma plume, and the plasma refractive index profile. The laser focussing conditions may therefore play an important role in governing the efficiency of harmonic generation. Hence it is important to optimize the focussing conditions of the laser beam w. r. to the location of the plasma plume to obtain maximum intensity of the harmonic radiation.

At Laser Plasma Division, an experimental study of the dependence of harmonic intensity on the laser focus position w. r. to the plasma plume has been carried out in pre-formed plasma plumes. The laser used in this study was a Ti:sapphire laser system operating at 10 Hz rep-rate. A part of the uncompressed laser radiation (energy : 30 mJ, τ=300 ps) was split from the main beam by a beam splitter. This beam was focussed at normal incidence by a 500 mm focal length spherical lens on a planar silver strip of 2 mm width, kept in a vacuum chamber evacuated to 10^{-5} mbar. This beam (pre-pulse beam) created a plasma plume to serve as the medium for harmonic generation. The laser intensity on the target was ~3×10^{10} W/cm^2. After a time delay of 60 ns, the main laser pulse, compressed to 48 fs (energy: 120 mJ), was focussed in the above pre-formed plasma plume from a direction parallel to the target surface at a distance of ~ 100 μm, using a spherical lens of 500 mm focal length. The peak intensity at the best focus position was ~10^{18} W/cm^2. The high-order harmonics were analyzed by a home-made flat-field grazing-incidence XUV spectrograph based on a variable line spacing grating. The spectrum was recorded on a multi-channel plate detector, the output of which was imaged onto a 12 bit digital CCD camera connected to a PC. The best focus position was varied from -7 mm to +9 mm from the plume centre by moving the focussing lens. The femtosecond laser intensity at the centre of the plasma plume for different locations of the best focus varied from ~10^{15} W/cm^2 to ~10^{18} W/cm^2.

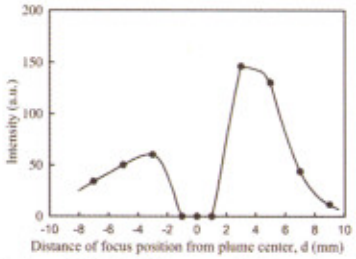

Fig.L.7.1: Variation of the 23rd harmonic intensity with the change in focus position of the femtosecond laser beam w. r. t. the centre of the plasma plume.

The harmonic intensity nearly vanished when the laser beam was focussed at the centre of the plume (see Fig.L.7.1). Further, the harmonic intensity showed peak when the best focus was located on either side of the plume centre. The peak harmonic intensity was higher when the laser beam was focussed after the plasma plume as compared to the opposite case, and this difference decreased for higher harmonic orders. Moreover, the distance of the best focus position corresponding to the peak harmonic intensity increased for higher harmonic orders. The results have been explained in terms of variation in coherence length for harmonic generation, relativistic drift of electrons, and defocussing of the harmonic radiation due to the radial ionization gradient in the plasma for different positions of the laser focal spot. [For more details, please see *H. Singhal et al, J. Appl. Phys. 103,013107 (2008)*]. The study can be useful in optimizing laser focus position for achieving maximum intensity for various harmonic orders.

Contributed by:
H. Singhal (himanshu@cat.ernet.in) and P.A. Naik

L.8 Spatial profile of laser wake-field accelerated electron beam

Conventional accelerators are large size systems because the accelerating electric field has to be kept below ~50 MV/m to avoid electrical breakdown in the accelerating structures. On the other hand, laser wake-field generated inside a plasma can give extremely high accelerating field ~100 GV/m, and this may pave way for developing very compact accelerators in future. Laser Plasma Division of RRCAT has recently initiated experimental investigations in laser wake-field electron acceleration, in collaboration with scientists from KEK, Japan. Initially, a scintillator (NE102) photo-multiplier tube combination was used to detect the high-energy electrons [RRCAT Newsletter 20, 1, p.10, 2007]. Now, the spatial profile of the electron beam has been measured using DRZ

phosphor and CCD camera combination.

Fig.L.8.1 shows a schematic of the experimental setup used to measure the electron beam profile. At a gas jet pressure of 37 bar and laser intensity of ~2 x 10^{18} W/cm^2, a collimated beam of electrons with a low-divergence (~10 mrad), with few tens of MeV energy was observed. A typical electron beam profile recorded on DRZ phosphor screen is shown in Fig.L.8.2.

The experiments were carried out using the 10 TW Ti:sapphire laser facility at RRCAT. This provides laser pulses of maximum energy of about 450 mJ in 45 fs pulses. The laser beam was focussed on a helium gas jet using a 40 cm focal length gold coated off-axis parabolic mirror. The gas jet was produced by a shock wave-free slit type (10 mm x 1.2 mm) supersonic Laval nozzle. Helium gas was puffed using a fast solenoid valve and its density was varied by changing the backing pressure of the gas. The Ti:Sapphire laser beam was focussed at the entrance edge of the gas jet, about 1.5 mm above the nozzle entrance. The focal spot diameter of the beam was 18μm (FWHM).

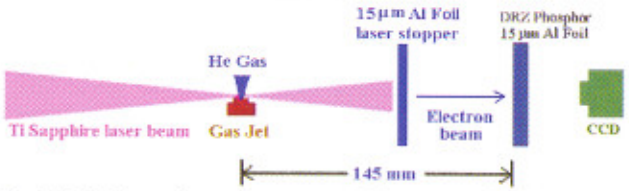

Fig.L.8.1: Set-up for measurement of beam profile of the laser accelerated electrons.

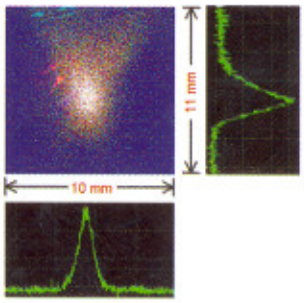

Fig.L.8.2: Electron beam profile recorded using DRZ phosphor, on a CCD camera.

Contributed by:
P.A. Naik (panaik@cat.ernet.in) and A. Moorti

L.9 Improving performance of porous silica sol-gel anti-reflection coated optics for high power Nd: glass laser

Porous silica sol-gel coated optics is used in high power laser systems because it has high laser induced damage threshold (LIDT) and has high spatial uniformity over large diameters. High power laser systems have MOPA (master oscillator power amplifier) architecture and use sequential optical relaying using vacuum spatial filters to overcome laser wavefront distortions caused by self-focusing of the laser at high intensities. In order to use the sol-gel AR coated optics in spatial filters, the degradation of optical performance and LIDT of the coatings at the laser wavelength upon exposure to the vacuum oil vapours is an important consideration. Laser Plasma Division of RRCAT has developed a technique using hexamethyl-disilazane (HMDS) vapour treatment of the coatings to overcome the degradation of optical performance [R. Pareek et al Optical Engineering (in press)] of sol-gel AR coatings. The degradation in the optical quality of the coatings occurs mainly due to the adhesion of contaminant vapours to the polar silica nano-particles in the coatings. The polar nature of the silica coatings can be reduced if the coatings are exposed to HMDS vapours. This may prevent the degradation of the coatings upon exposure to contaminant vacuum oil vapours.

Two sets of single layer AR coatings, namely silica and ammonia and HMDS treated porous silica were prepared and exposed to rotary pump oil vapours in a vacuum chamber. Fig.L.9.1 shows the reflection spectra of a) porous silica coating, and b) the same coating exposed to oil vapours. It is seen that for the silica coating not exposed to oil vapours, the spectrum has a minimum of its reflectivity spectrum at λ_{min} = 1054 nm (lasing wavelength) with a reflectivity of R = 0.26%. It is also observed from Fig.L.9.1b that the minimum of reflectivity shifts to a higher wavelength by 122 nm as compared to the minima of the coating not exposed to oil vapours. A substantial degradation of the reflectivity occurs for vapour exposed silica coating giving a reflectivity of 2.1% at 1054 nm in comparison to the 0.26% reflectivity of the coating not exposed to oil vapours.

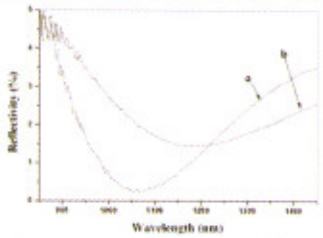

Fig.L.9.1: Reflection spectra of a) porous silica coating and b) the same coating after exposure to oil vapour.

Figure L.9.2 shows reflection spectra of a) a porous silica coatings treated with ammonia and HMDS, and b) the same coating exposed to oil vapours. It can be seen that there is only a marginal shift of ~20 nm of the λ_{min} value between the oil vapour exposed and un-exposed coatings that were treated with ammonia and HMDS. The shift in the minima of the spectra of treated coatings is much smaller than that of

untreated coatings in Fig.L.9.1. The change in reflectivity of the oil vapour exposed and unexposed HMDS treated coatings is small (~0.01). It was also observed that the ammonia and HMDS treated coatings have a higher LIDT at the lasing wavelength in comparison to untreated coatings after exposure to the oil vapour. This finding agree well with the measurements of imaginary part of refractive index at 1054 nm.

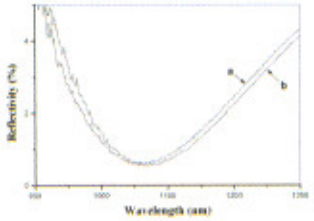

Fig.L.9.2: Reflection spectra of a) porous silica coating treated with ammonia and HMDS and b) the same coating after exposure to oil vapour.

Contributed by:
R. Pareek (rpareek@cat.ernet.in) and A. S. Joshi

L.10 High voltage programmable ramp generator for high speed streak camera

Streak camera is a high speed recording instrument, used as a diagnostic tool for studying very fast events, especially in the field of intense laser-matter interaction. Streak camera consists of a streak tube which has a photocathode, deflecting plates and a phosphor screen. When the light from the event is incident on photocathode, it generates photoelectrons, which are deflected by deflecting plates and an image is generated on the screen. For this reason, streak camera requires a high voltage and fast ramp generator of amplitude of +/- 500 V and rise time of 1 ns. However, it is also necessary to vary the slope of this ramp so that the event can be analyzed properly. In this article, we have presented a high voltage ramp generator with programmable slope and microprocessor based control, developed for this purpose. The ramp generator consists of a high voltage step generator, followed by an integrator. The components of the integrator are designed such that they can be varied by a microcontroller. The unit generates two bipolar ramp voltages with fastest speed of < 1ns and provides continuous slope variation from 6 ns to 30 ns for a ramp voltage of 500 V. This is developed by Laser Electronics Support Section, RRCAT as a part of automation of streak camera.

The step voltage is generated by two stacks of avalanche transistors connected in series to minimize the jitter. The stacks are biased by applying positive ramp bias at one end of the first stack and negative ramp bias at the other end of the second stack. Both the stacks are triggered through a pulse transformer having one primary and two secondary windings (1:1:1). The outputs thus generated are connected to two integrator units through two high voltage dc relays. By activating these relays, the step voltages can be connected to the integrator units, thus getting slower slope of ramp voltages decided by the value of R, L, and C.

Variable and high voltage capacitor and inductor required for this unit and which can be controlled by microprocessor were developed in-house. For variable C, a gang capacitor with two identical capacitors variable from 47 pF to 253 pF was used. The shaft of the same is rotated by a stepper motor. For variable L, two solenoid coils are used and the inductances are varied by moving the ferrite cores by another stepper motor. The inductances vary between 3 μH to 15 μH. A resistor of 110 Ω is used for all the values of L and C as it provides overall satisfactory performance. A photograph of the variable slope ramp generator module showing its constructional features is shown in Fig.L.10.1. Fig.L.10.2 shows the ramp output waveforms with variable L and C.

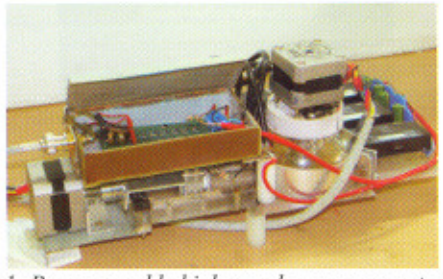

Fig.L.10.1: Programmable high speed ramp generator module.

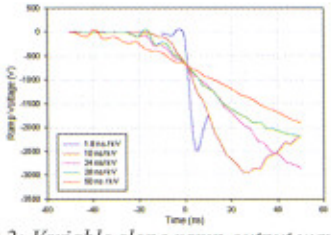

Fig.L.10.2: Variable slope ramp output wave forms.

For controlling various operations of the ramp generator, a micro controller ADμC831 (Analog Devices) is used. This microcontroller is programmed to drive both stepper motors described above and is interfaced to the PC using RS232 link. A LABVIEW based graphical user interface (GUI) is developed in personal computer for operation of the instrument.

In fastest mode, two step voltages with < 1ns rise time are generated. The rise time is calculated for a variation of 500 V in linear part of the ramp. The ramp speed can be adjusted to any desired value within the range 6 ns to 30 ns by changing L and C, with the help of stepper motors.

Contributed by:
J. Upadhyay (janky@cat.ernet.in) and C.P. Navathe

I.1 Computing and information management developments at RRCAT

A) Commissioning of 16 nodes (32 processors) Xeon based HPC cluster Aryabhatta:

Sixteen nodes (32 processors) Intel Xeon based High Performance Computing (HPC) cluster named as 'Aryabhatta', is commissioned for computing applications. HPL (High Performance Linpack) benchmark for this cluster resulted in 262 gigaflops peak computing power. The cluster is configured with 64 bit Red Hat Enterprise Linux AS4 operating system, resource manager 'Torque' and job scheduler 'Maui'. Each node contains two dual core Xeon processors @ 3.73 GHz with 4 MB L2 cache per processor, 4 GB memory and Gigabit network interface. The total number of processors on this cluster is 32 and each processor is dual core with hyper threading. All the nodes are HP DL 380 G5 series servers.

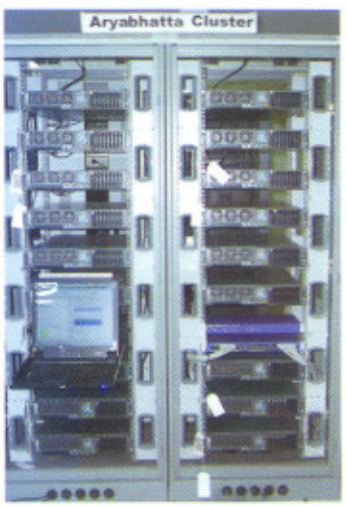

Fig.I.1.1: 16-nodes HPC cluster-Aryabhatta.

Intel Fortran compiler (ifort), GNU Fortran 77 compiler (g77), GNU Fortran 90/95 compiler (gfortran), Intel C Compiler (icc), GNU C & C++ compiler (gcc & g++) are installed on this cluster. Parallel processing libraries installed on this cluster are mpich2-1.0.5 for g77, gfortran & ifort and mpich-1.2.7 for g77, gfortran & ifort. In addition to these compilers and parallel processing libraries, parallel numerical libraries including Intel Math Kernel Library, LAPACK, CBLAS, f77BLAS, ATLAS are also installed on the cluster.

As per the user requirements, parallel applications WIEN97 [computation of electronic structure of solids within density functional using Linearized Augmented Plane Wave (LAPW) method] and CPMD (Car-Parrinello Molecular Dynamics - Electronic Structure and Molecular Dynamics Program) are successfully ported and running on 'Aryabhatta'.

B) Commissioning of HPC clusters as part of DAEGrid:

Two cluster have been installed and made operational as part of DAEGrid. The operating system is Scientific Linux version 4.4 on both the clusters. Intel Fortran V 9.0, gcc, gfortran compilers, Math Kernal library v 8.0, parallel processing library mpich-1.2.7 are installed on both the clusters. Genius based grid-portal on Scientific Linux has been installed on these clusters. Users from RRCAT can submit their parallel and sequential applications on the resources available under DAEGrid, using grid-portal made operational in User Hall of Computer Centre.

Daksha: Eight node cluster named "Daksha" has been installed and made operational as part of DAEGrid. Each node contains Intel dual core Xeon processor @ 3.60 GHz with 2 MB cache, 4 GB memory and gigabit network interface.

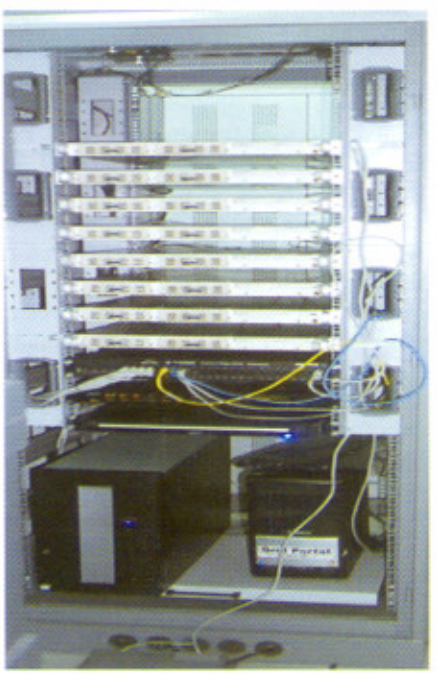

Fig.I.1.2: 8-nodes HPC cluster - Daksha.

Ramanujam: Sixteen nodes (32 processors) high performance computing cluster "Ramanujam" has been installed and added to the DAEGrid. Each node comprises of two dual core Xeon processors @ 3.73GHz, 4 MB L2 cache per processor, 4 GB memory and Gigabit network interface. The total number of processors on this cluster is 32 and each processor is dual core with hyper threading. All the nodes are HP DL 380 G5 series servers.

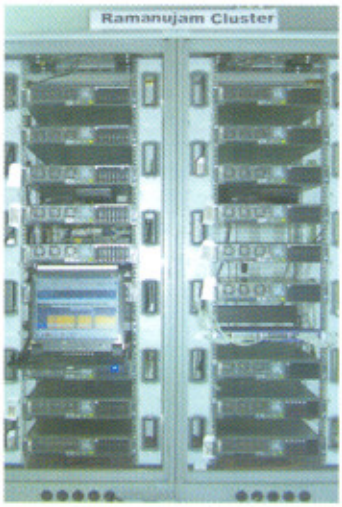

Fig.I.1.3: 16-nodes HPC cluster-Ramanujam.

C) Configuration of MRTG on all computing servers:

Multi Router Traffic Grapher (MRTG), an open source web based software has been configured for all computing servers to monitor the load of CPU, memory usage, hard disk usage and network traffic. The data is stored in round-robin database, so that system storage footprint remains constant over time. The software records the data in a log on the client along with previously recorded data and creates the HTML document detailing the traffic for the devices such as CPU, memory and network in graphical form.

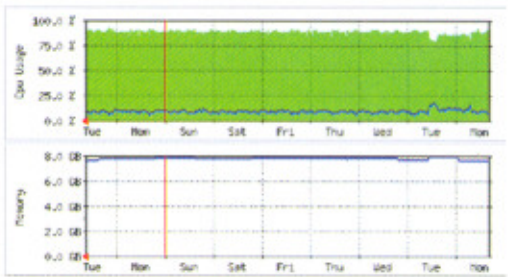

Fig.I.1.4: CPU and Memory usage of chi (HP Alpha ES45) server.

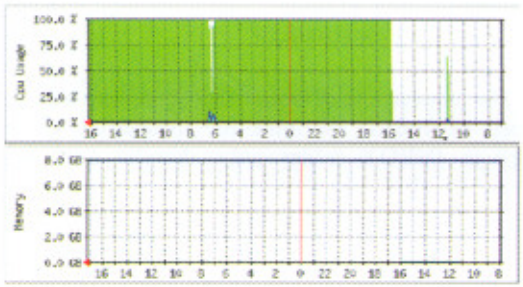

Fig.I.1.5: CPU and Memory usage of epsilon (Intel Itanium 1.6 GHz) server.

D) Migration of existing client / server based Information Systems to web / n-tier based architecture :

Various information management systems for RRCAT Administration, Accounts, and IRPSU are developed and maintained by Computer Centre. These systems were working on client/ server (two-tier) architecture. These days zero client deployment concept (web based platform using n-tier architecture) is being used world-wide, as it provides a platform which is simpler to implement, administer and accessible to wider user base.

Hardware infrastructure required for migration to n-tier architecture was procured and commissioned. Two Xeon @ 3.4 GHz with 4 GB RAM as Oracle 10g Database Servers, two Xeon @ 3.4 GHz with 4 GB RAM as Application Servers and one Xeon @ 3.2 GHz with 2 GB RAM for Identity & Access Management were installed. Software products including Oracle Standard Database 10g (10.1.2) for backend database, Oracle Developer Suite 10g (10.1.2) for development and Oracle Application Server 10g (10.1.2) for deployment were procured. The planning related to deployment topologies, which included application deployment, central services and administration, unified login across information management system of Oracle 10g infrastructure and mid-tier was done. Migration of data of purchase information system from Oracle 7.3 database to Oracle 10g SE database was done as proof of concept. Then migration strategy for successful web-deployment using Oracle platform was finalized.

Migration of forms and reports, application deployment, central services and administration, unified login across information management system of Oracle 10g infrastructure and mid-tier were completed. Migration and re-engineering of all applications related to Administration, Integrated Purchase-Stores-Audit and Integrated Accounting System to Oracle 10g platform was completed with single sign-on functionality. Single sign-on feature was implemented using Oracle Identity Management which provides the infrastructure to centrally manage user and application identities, their authorizations and other policy decision points. Data was migrated from Oracle 7.3 to Oracle 10g database and Oracle Internet Directory was configured for authentication.

Comprehensive training to all the users was provided and now the information management systems of Administration, Accounts and IRPSU are successfully running on Oracle 10g platform. The whole exercise has resulted in sustainable information systems compliant with international standards.

E) Enhancements to RRCATInfonet:

Authenticated module for Project Monitoring has been released on RRCATInfonet, which provides various reports for monitoring the procurement status of XI Plan projects. The online information is made available from the Integrated Purchase-Stores-Audit System and Integrated Accounting Software. The access is authenticated and only the authorized persons will be able to access the information related to their respective projects.

Modules for logging network related complaints and viewing complaint status, have also been added to RRCAT Infonet. Changes were carried out on RRCAT Infonet server to incorporate connection pooling feature for connectivity to Oracle 10g database. This has resulted in increased number of concurrent users for the services provided by RRCATInfonet.

F) Enhancements to RRCAT Website:

RRCAT website has been enhanced with new look and feel. The web pages have been re-designed and re-arranged with updated contents. The look and feel has been changed using pull down menus and cascading style sheets. The contents for RRCAT Newsletters from the year 1988 to 2007 are provided in electronic form by conversion from paper copy. The contents of divisional pages have been re-arranged as per the changes in organizational structure.

G) Deployment of APAC-07 Proceedings:

Proceedings of APAC-07 (Asian Particle Accelerator Conference 07) were generated electronically and deployed on http://jacow.org website. Contributions to the conference were classified into different groups based on invited papers, contributed papers, and poster presentations. Proceedings of conference can be viewed based on Session, Classification, Author, Keyword or Institute. All the contributions are available in PDF format.

H) Deployment of JAS-08 Website:

A website for Joint Accelerator School 2008 has been developed and deployed on http://jas08.cat.ernet.in. This site contains information related to Programme schedule, Registration details, Committee details and Contents of the delivered talks, in PDF format.

Contributed by:
A. Rajan (alpana@cat.ernet.in) and A. Rawat

I.2 Development in networking and communication at RRCAT

A) RRCATNet planning, expansion and upgradation:

Under phase IV of network expansion, internal - CAT5E based - networking of few buildings namely, Laser R&D H - Block, Fire Station, AECS, TSH, and Old Production building was completed. In all, 200 nodes were added to RRCATNet. All the above mentioned buildings have been connected to the RRCATNet using DSLAM links and CAT6 cables. The commissioning of optical fiber backbones to various buildings under phase IV is underway and is expected to be completed in few months time.

B) Enhancements to RRCAT Data Centre:

The data centre at RRCAT, houses all the shared computing and IT resources of our centre. Due to addition of more number of such resource over the past few months, the electrical and AC facilities of the data centre had to be augmented. Necessary augmentation was carried out to support the requirements and thereby ensure smooth operations of the data centre.

User data on the email servers at our centre is increasing day by day, hence the backup related setup has to be constantly revamped. Backup of the various email server related log files and user data is currently being performed on network attached storage using the ethernet connectivity. The backup is performed using the tar and gzip utility over the network, with a full backup being performed on Sunday morning and incremental backups on other week days. Enhancements were made to the backup setup, for reducing the backup window from the previous duration of more than 24 hours to about 9 hours at present in full backup mode and to 2 hours in incremental mode. This has resulted in faster access of email services during working hours.

C) Email and Internet access setup enhancements:

Designing of a new email setup, utilizing fast and high capacity SAN based disk storage systems in cluster mode was completed and necessary hardware and software has been processed for procurement.

The current email setup at our centre was further enhanced to include facilities for forwarding of emails received in INBOX folder only, thereby excluding all unwanted DETECTED_SPAM folder emails from being forwarded, thus increasing our usable internet bandwidth.

Various unified threat management products were evaluated for incorporation in our network, to provide clean virus free traffic flow from and into our network. The

selected solution is now under implementation.

D) Anunet and DAEGrid Setup:

DAEGrid network was secured from external networks by the commissioning of a firewall based on unified threat management product from Fortinet Inc.. This implementation has allowed us to build customised firewall for using various applications with varied security requirements on the DAEGrid setup, thus enhancing the security of the setup on the whole.

E) Inter DAE Video Conferencing setup:

Promotion interviews were successfully conducted for the first time ever in RRCAT, using the video conferencing facilities, commissioned at RRCAT and BARC. The process involved setting up a video conference between BARC and RRCAT with an interview committee attending the video conference at BARC and the candidate and his DR attending the video conference at RRCAT. In all, 14 candidates were successfully interviewed.

F) Expansion of the telecommunication network:

Telecommunication facilities were extended to the new Laser R&D block H and Alignment Lab buildings. Mobile access facilities were enabled on 20 extensions and 80 new telephone connections were installed inside RRCAT campus. To take care of near future requirements, two number of 400 pair cables were terminated at laboratory area exchange. Revamping of 40 number of TDPs was carried out to strengthen the telephone cabling network in our campus, thus increasing the uptime of the telephone network.

G) Workshop on Unix operating system:

Unix is a preferred operating system in any R&D organization. Two weeks workshop on Unix was organized by Computer Centre during 9-20 July 2007 at User Hall. workshop was aimed at providing basic understanding of the Unix operating system and user level commands, useful to perform day to day operations on the Unix systems. workshop was attended by 24 candidates nominated from various Divisions/ Sections in RRCAT.

H) ANSYS training programme:

The resources in User Hall were utilized by engineers of our centre to conduct ANSYS training programme to get updated about the latest features available in this software package. About 30 participants from various Divisions/ Sections of RRCAT benefited from this training.

Contributed by:
S. S. Tomar (tomar@cat.ernet.in) and A. Rawat

I.3 Development of vacuum brazing furnace

Fig.I.3.1: Photograph of the vacuum brazing furnace.

In joining of components, where welding process is not possible, brazing processes are employed. Value added components, high quality RF systems, UHV components of high energy accelerators, carbide tools etc. are produced using different types of brazing methods. Furnace brazing under vacuum atmosphere is the most popular and well accepted method for production of the above mentioned components and systems. For carrying out vacuum brazing successfully it is essential to have a vacuum brazing furnace with latest features of modern vacuum brazing technology.

A vacuum brazing furnace has been developed and installed at Accelerator Components Engineering & Fabrication Division, RRCAT, for carrying out brazing of components of copper, stainless steel and components made of dissimilar metals/materials. The above furnace has been designed to accommodate jobs of 700 mm diameter x 2000 mm long sizes with job weight of 500 kgs up to a maximum temperature of 1250°C at a vacuum of $5x10^{-5}$ Torr. Oil diffusion pumping system with a combination of rotary and mechanical booster pump have been employed for obtaining vacuum. However, this pumping system will be replaced with a dry vacuum pumping system in the near future for

better and clean brazed components. Molybdenum heating elements, radiation shield of molybdenum and stainless steel - 304 have been used. The above furnace is computer controlled with manual over ride facility. PLC and Pentium PC are integrated together to maneuver steps of operation and safety interlocks of the system. Close loop water supply provides cooling to the system.

Many components have been vacuum brazed successfully including vacuum brazing joints of copper to copper and stainless steel to copper components. Main components vacuum brazed include : safety shutter, fixed mask, collimator etc. These are components of the front end of beam line. Test cup assembly of LINAC with six joints of copper to copper is also vacuum brazed. Vacuum brazing of Ceramic-to-metal is under progress. After vacuum brazing, these components are leak tested up to 5×10^{-10} mbar L/s. The above facility has further augmented the development and manufacturing capability of RR CAT.

Contributed by:
R.V. Singh (rvsingh@cat.ernet.in),
K. Yedle, and A. K. Jain

I.4 Automization of management of receipt and distribution of water using SCADA in RRCAT

RRCAT receives water from two water sources viz Narmada authority and some tube wells located in and around colony area. The water from these sources is collected into under ground water sumps located in colony area and another set of sumps near guard house. This stored water is then pumped to 15 m high overhead tanks located in the colony area as well as in the laboratory area. There are two pumping stations : one in the colony area and other near the Guard House. Overhead tanks are at three locations : 1) near Indus building, 2) opposite Community Centre and 3) one at the new efficiency apartment complex. The water collected in overhead tanks is distributed to the users in colony and laboratory areas by gravity flow. The distribution to each segment is carried out by operating number of distribution valves installed at various locations in the premises. In order to efficiently carry out management of receipt and distribution of water, number of operators are required to work round the clock in the shifts and physically move to all locations wherever valves, pumps etc exist at discrete locations.

In view of non availability of requisite staff; engineers from Construction and Services Division and Laser Electronics Support Section of RRCAT have successfully commissioned a water automation system by which entire operations related to management of receipt and distribution of water are now performed from main control room located in colony pump house area. At this control room, a Supervisory Control And Data Acquisition (SCADA) system has been installed using PLCs to automate the entire operation. Now any pump or valve located in the laboratory area or in colony area can be operated by click of a mouse. Water level in the sumps as well as overhead tank is constantly monitored and updated on PC panel. To make it convenient for operator, the control system has a graphic user interface and a Hindi panel. Apart from this, water which is received from the Narmada Authority is now metered using an electronic flow meter and data is logged on daily basis. The system has manual, semi automatic and fully automatic modes so that one can select a mode depending on the situational demand. This system is operational since November 2007 and operators have been trained. A layout of the automated water distribution system in the colony area is shown in Fig.I.4.1. Presently new colony area comprising of new efficiency apartment complex is not covered under automation.

Computer Centre, RRCAT has provided required telephone connections and allowed the use of existing telephone cables in the above set-up.

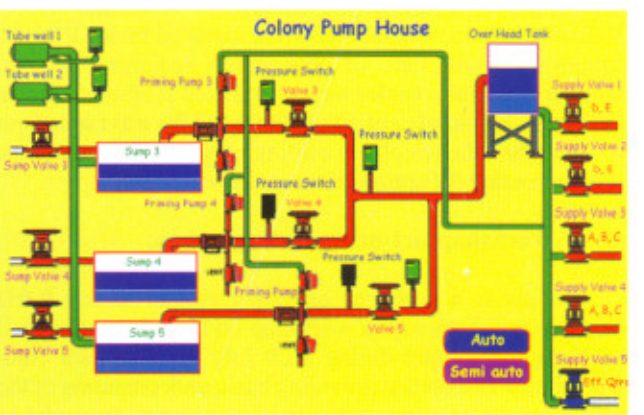

Fig.I.4.1: A layout of the automated water distribution system in the colony area.

Contributed by:
L. Jain and S. Farkya (sunilfarkya@cat.ernet.in)

T.1: Bose-Einstein condensation in a dilute atomic gas

S. R. Mishra (srm@cat.ernet.in), S. P. Ram, and S. K. Tiwari

1. Introduction

Since the first observation of Bose-Einstein condensation (BEC) in a dilute atomic gas of ^{87}Rb at JILA (Colourado, USA) in 1995 [1], the research in this field has exploded in several directions and is providing deeper insight in atomic physics, coherent matter waves, atom optics, many-body physics, ultra-cold collisions, degenerate fermions etc. Besides the basic research, the implications to future devices such as atom laser, atom-gyroscope, precision measurements etc. have also received a considerable thrust.

In Laser Physics Applications Division at RRCAT, we have developed a set-up for achieving BEC of ^{87}Rb atoms to learn the technology as well as to explore its applications such as an Atom Laser. The work is at an advanced stage. In this article, we discuss briefly about the process of Bose-Einstein condensation, and then describe some details of our experimental set-up such as the experimental scheme, milestones achieved, and direction and efforts in progress to complete the remaining task.

2. Bose-Einstein Condensation

Though the experiments in 1995 on alkali atoms should be considered as a milestone in the history of BEC [1,2], the experimental and theoretical research on this unique phenomenon predicted by Einstein (1924, 1925) using Bose statistics (1924) for particles with integer spin has attracted attention of researchers for a long time. In particular, super-fluidity in helium was considered by London (1938) as a possible manifestation of BEC. Similarly, narrow line-width emission observed from excitons in semiconductors has also been attributed to BEC of excitons in the ground state. A striking difference between BEC observed in 1995 in samples of dilute atomic gases and that in others is due to weak interactions in dilute atomic gases. The BEC thus observed in these gases can be considered as a purely quantum statistical process as predicted by theory of Bose and Einstein. Since the first observation of BEC in an alkali vapour sample (^{87}Rb) in 1995 at JILA, many groups have succeeded in achieving BEC in atomic gases of different elements such as ^{23}Na, ^{7}Li, ^{85}Rb, ^{41}K, H, He, ^{133}Cs, Cr along with BEC-BCS transitions in fermionic systems of ^{6}Li, ^{40}K, and Yb.

In a sample of indistinguishable particles having integer spin, i.e. bosons, BEC occurs when thermal de Broglie wavelength ($=h/(2\pi mkT)^{1/2}$) becomes comparable to the inter-particle separation. This essentially requires that temperature should be so low that kinetic motion diminishes to the extent that all particles are in the ground state of the system. Mathematically, it is expressed in terms of phase-space density as $n\lambda^3>2.61$, where 'n' is number density of bosons. The phenomenon of BEC is a purely quantum statistical effect, and is specific to the indistinguishability and bosonic nature of the particles under consideration. In real systems such as a gas of atoms, because of finite interactions, observation of BEC is difficult due to requirement of very low temperature (typically T~100-500 nK at density $n\sim10^{13}$-10^{14} cm^{-3} for ^{87}Rb) to reach the above phase-space density condition. Increasing density for sake of a higher temperature, the condensed phase (i.e. solid or liquid) is reached before the BEC phase due to increase in the interaction energy.

With the advent of cooling of atoms using lasers, the path to reach BEC has become much easier than before. Using a laser cooling set-up known as magneto-optical trap (MOT), it is possible to reach temperature typically as low as ~1-10μK in a gas of atoms. Beyond this value, the temperature is lowered by evaporative cooling. In majority cases, to achieve BEC in dilute atomic gases, atoms are initially trapped and cooled in a MOT and then subjected to evaporative cooling in a trap to reach BEC transition. During the evaporation, atoms are trapped either in a magnetic trap formed by an inhomogeneous magnetic field or in a dipole force trap formed by a non-resonant laser beam. To avoid loss of atoms from the trap due to background collisions, evaporative cooling is performed in a UHV chamber at pressure of ~10^{-10} to 10^{-11} Torr. In a magnetic trap, evaporation of atoms is forced by an appropriately designed radio-frequency (RF) field which flips the spin of higher energy atoms selectively and ejects them from the trap. In an optical dipole trap on the other hand, evaporation is executed by lowering the intensity of the trapping laser. Both these methods involve considerable complexity and require an expertise in different areas of physics and engineering.

Since formation of a MOT from vapour needs a larger pressure (~10^{-8} Torr) than that is required in the evaporation chamber (~10^{-10}-10^{-11} Torr), double-MOT systems are built in which atoms are first trapped in a MOT in the vapour chamber and then transferred using a push laser beam to another MOT in a UHV chamber to perform evaporative cooling [3]. Alternatively, now a days, single MOT based BEC systems are also becoming popular, in which a MOT is formed directly in a UHV chamber from the jet of atoms using a Zeeman slower [4]. The Zeeman slower however involves a complex design of magnetic field used in it.

3. BEC set-up at RRCAT

At RRCAT, we have chosen to build a double-MOT system to achieve BEC of ^{87}Rb atoms. A schematic of the system is shown in Fig.T.1.1. In the following we present the details of design, operation of the system and its present status.

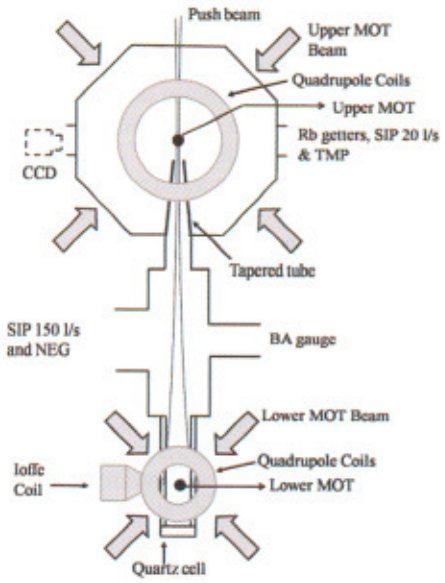

Fig.T.1.1: A schematic of double-MOT set-up developed in our laboratory at RRCAT for BEC of ^{87}Rb atoms.

3.1. Vacuum System

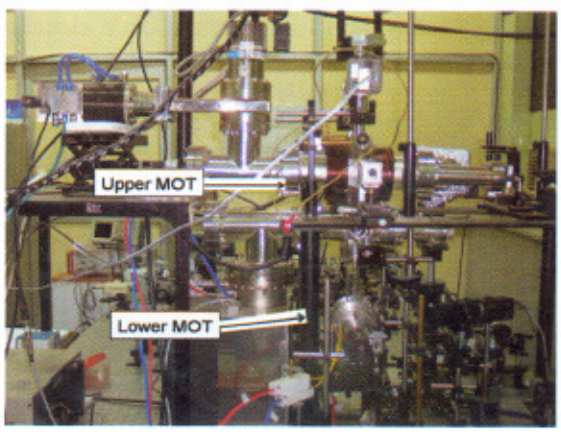

Fig.T.1.2. A photograph of the set-up for BEC.

In our set-up (see photograph in Fig.T.1.2), the vacuum system consists of two parts (upper part and lower part) having different vacuum levels. The upper part is an octagonal chamber of stainless steel (SS) in which upper MOT is formed from the background Rb-vapour at pressure of 2×10^{-8} Torr. The lower part is connected to the upper octagonal chamber by a differential pumping tube which is tapered in shape with inner diameters of 5.0 mm and 12.0 mm at ends and length 70 mm. A chamber in the lower part has connections to a combination pump (a 150 L/s SIP and a NEG module), BA gauge, tapered tube and 25x25x75 mm dimension quartz glass cell (Optiglass, UK). The lower MOT is formed inside this cell after atoms are pushed to the cell from the upper MOT by a push beam. The vacuum chamber was fabricated in Workshop-B of RRCAT.

We use a 70 L/s turbo-molecular pump (TMP) for roughing of the whole vacuum system. A gate-valve is used between the pump and the chamber to isolate the vacuum system from the atmosphere when TMP is off. We have also connected a 20 L/s sputter ion pump for pumping the upper octagonal chamber, in addition to combination pump used in the lower part. The roughing of the vacuum system using TMP was done in presence of mild baking at temperature of 100-150 °C for a prolonged time. Then, at base pressure of 10^{-6} Torr in the system, both the ion pumps were switched-on. After removal of degassing from ion pumps, the gate-valve was closed and TMP was switched-off. With both the ion pumps on, we achieve a pressure of 1×10^{-8} Torr in the upper chamber and 1.2×10^{-9} Torr in the lower chamber without operating the NEG module. When we activated NEG module for about 20 minutes, the vacuum got improved to $\sim1\times10^{-10}$ Torr in the lower chamber.

3.2. Operation of Double-MOT system

In our system, upper MOT is formed in the octagonal chamber having Rb-vapour in the background, and lower MOT is formed in the quartz cell. The upper MOT and lower MOT positions are vertically separated by ~340 mm. For the formation of upper MOT, the Rb-vapour was generated from a getter source (Varian, Italy) which was inserted in the chamber after fixing it on a two-pin feed-through. A DC current of ~3.6 A was supplied to the getter to generate Rb-vapour. With Rb-vapour, the pressure of the upper chamber changes from 1×10^{-8} Torr to 2×10^{-8} Torr.

The cooling laser beams for the upper and the lower MOTs were obtained from two separate grating controlled external-cavity diode lasers (DL-100, TOPTICA, Germany), whereas re-pumping laser beams were obtained by dividing output from a single laser of similar configuration (SACHER, Germany). For each MOT, cooling beam and re-pumping beam were first mixed, and combined beam was then expanded and split into three MOT beams (MB) which entered the chamber. After retro-reflection of each of these three beams from a mirror at exit of the chamber, required six MOT beams for each MOT were obtained.

For the upper MOT, total power in the three MOT beams entering the chamber was ~26 mW (with ~17 mW in cooling part and ~9 mW in re-pumping part). The diameter of each MOT beam for upper MOT was ~10 mm. For the lower MOT, the total power in the three MOT beams entering the cell was ~27 mW (with ~18 mW in cooling part and ~9 mW in re-pumping part). The diameter of each MOT beam for lower MOT was ~7 mm. All the lasers were frequency stabilized and locked using saturated absorption spectroscopy (SAS). The cooling lasers were locked at ~12 MHz to the red of $5S_{1/2}$ F = 2→$5P_{3/2}$ F' = 3 transition of ^{87}Rb, whereas re-pumping laser was locked at peak of its $5S_{1/2}$ F = 1→$5P_{3/2}$ F' =2 transition. The required polarizations of the MOT beams were set using quarter-wave plates. The quadrupole coils (QC) for upper MOT generated the axial magnetic field gradient of ~12 G/cm at DC current of 3.1 A, and those for lower MOT generated the axial magnetic field gradient of ~10 G/cm at current of 2.8 A.

The push beam (PB) was a continuous wave (cw) Gaussian laser beam (~100-200 μW) and resonant to $5S_{1/2}$ F = 1→$5P_{3/2}$ F' =2 transition. It was focused to $1/e^2$ size ~100μm on the upper MOT position, which corresponds to an intensity of ~10^3 mW/cm^2 at the upper MOT and ~13 mW/cm^2 at the lower MOT position for a power of ~150μW.

In absence of the push beam, the upper MOT captures ~1.4×10^6 atoms whereas the lower MOT does not have any measurable number. After applying the push beam, due to the push beam acceleration (~1.1×10^5 m/s^2 at ~160μW), the atoms from the upper MOT are ejected in form of continuous flux, and are captured again in the lower MOT inside the glass cell. The number of atoms in the lower MOT varies with the push beam power, and was found to be maximum for a push beam power of ~160μW. This optimum power can be correlated to the trap depth of upper MOT and capture velocity of the lower MOT.

We have estimated the number of atoms in a MOT by fluorescence imaging technique using a digital CCD camera (PixelFly, PCO, Germany). From the fluorescence image of a MOT cloud, the number of atoms (N) can be obtained using the relation,

$$N = N_c \frac{8\pi\left[1+4\left(\frac{\Delta}{\Gamma}\right)^2+6\frac{I_0}{I_{sat}}\right]}{\Gamma\left(6\frac{I_0}{I_{sat}}\right)\eta\,\Omega\,t_{exp}}$$

where N_c is total number of counts in the image, t_{exp} is CCD exposure time, is quantum efficiency of CCD, I_{sat} is saturation intensity for atomic transition, I_0 is the total intensity of cooling beams in the MOT, Γ=2πx5.9 MHz is the ^{87}Rb natural line-width, Δ is detuning of cooling beam and Ω is solid angle for the collection of fluorescence from atoms on CCD. The number (N) obtained by this method was found comparable to that measured by collecting the fluorescence on a high sensitivity photodiode [5].

In our efforts to improve the number in the lower MOT, we found that a weakly focussed hollow laser beam propagating vertically upward from the lower MOT side to the upper MOT can enhance the number in the lower MOT. This enhancement depends upon the detuning of the hollow beam from $5S_{1/2}$ F = 2→$5P_{3/2}$ F' = 3 transition [6]. Fig.T.1.3 and Fig.T.1.4 show the observed enhancement results for number in lower MOT for different values of hollow beam detuning. The hollow beam was generated using a home-made metal axicon mirror as reported earlier [7].

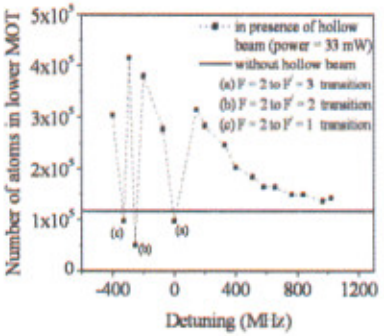

Fig.T.1.3. Measured variation of number of atoms in lower MOT with hollow beam detuning.

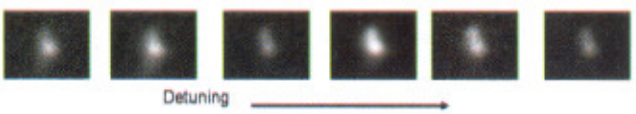

Fig.T.1.4. Images of lower MOT cloud for different hollow beam detuning values (some images showing enhancement in number).

The temperature of the atoms in MOT was measured by free expansion method which was to be ~200-400 μK in both the MOTs. It can be reduced further by applying molasses for some time on the atom cloud.

3.3. QUIC Magnetic Trap

For magnetic trapping and evaporative cooling of atoms trapped in lower MOT, we use a Quadrupole-Ioffe Configuration (QUIC) trap, first proposed and demonstrated by the Esslinger *et al* [8]. This is a simpler magnetic trap than time-averaged orbiting potential (TOP) trap and Ioffe-Pritchard (IP) trap, and operates at lower current than IP trap. A QUIC trap consists of two identical quadrupole coils and one Ioffe coil, which is conical in shape at one end. In a QUIC trap, as current in Ioffe coil is increased, the magnetic field

along the axis of the Ioffe coil (and hence the trapping potential) starts deforming and finally gives a nearly harmonic field distribution with nonzero off-set field to prevent Majorana spin flips.

The schematic of the QUIC trap, which we have developed for our BEC set-up, is shown in Fig.T.1.5. The coils dimensions were fixed by the simulations of magnetic field for the geometry appropriate to our set-up. The quadrupole coils have inner diameter of 34 mm, outer diameter of 69 mm and length of 37.5 mm. The Ioffe coil has a conical section of length 14 mm, minimum diameter of 6 mm (inner) and maximum diameter of 35 mm (outer). The straight section of the Ioffe coil has length of 21 mm with inner diameter of 6 mm and outer diameter of 35 mm. Each quadrupole coil has 184 turns and the Ioffe coil has 214 turns (160 in straight section 54 in conical section). The separation between the quadrupole coils was kept 50 mm. The distance between the end of the Ioffe coil and the symmetry axis of the quadrupole coils was kept 24 mm.

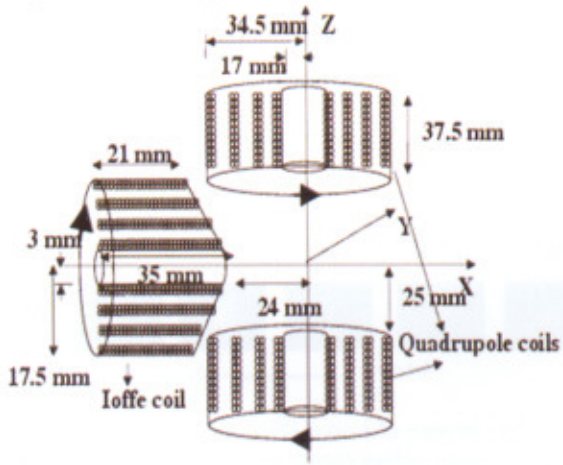

Fig.T.1.5. Schematic of arrangement of coils in QUIC trap for our set-up.

The coils were cooled by chilled water flowing in jackets surrounding them to remove the dissipated heat. The binding of coils was done in such a way that after every two layers, a spacer was positioned to create a gap for flow of water between the layers.

As expected, with increasing current in the Ioffe coil (I_{Ioffe}), the zero of the net magnetic field is shifted towards the Ioffe coil (Fig.T.1.6). The measured magnetic field of the trap for different values of I_{Ioffe} is as shown in Fig.T.1.6. At Ioffe coil current I_{Ioffe}= 29 A and quadrupole coil current I_q =23 A (Fig.T.1.6 b), we observed net field distribution becoming nearly harmonic with ~7 gauss as off-set field at the trap minimum [9]. The continuous curves in Fig.T.1.6 show the results of simulations, and experimental results were found in good agreement with it.

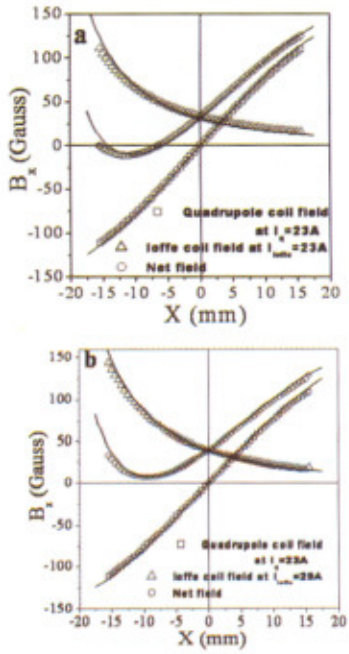

Fig.T.1.6. Variation of magnetic field with distance for a quadrupole coil current I_q =23 A and different values of Ioffe coil current I_{Ioffe}

3.4. Radio frequency (RF) evaporation system

The RF evaporation of atoms in a magnetic trap is a stimulated emission process which can be initiated by RF field of appropriate frequency such that photon energy ($h\nu_{rf}$) matches with the magnetic splitting between sublevels (as shown in Fig.T.1.7).

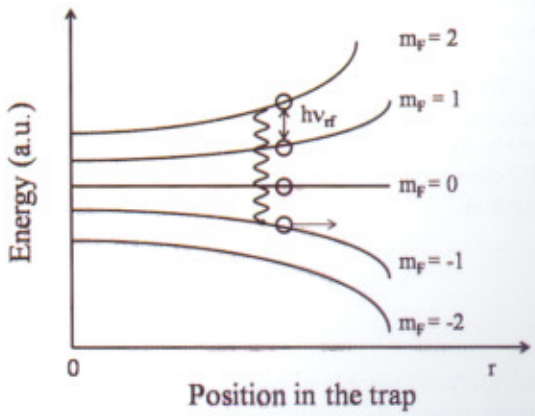

Fig.T.1.7. Schematic of the RF field stimulated transitions leading to ejection of an atom during RF-evaporation process.

To remove more energetic atoms from the trap, the frequency is swept in a calculated range from high to low in a specified time duration. In our RF evaporation system, we have planned to use a commercial RF synthesizer combined with a home-made amplifier system. The synthesizer can be controlled by LabVIEW on a PC to scan RF frequency in the desired range. The amplifier (developed at RF Systems & Control Division, RRCAT) amplifies the synthesizer signal upto ~2W. For our trap, the required scan range of RF is from ~14 MHz to 2 MHz, which is likely to get changed as the trap parameters and the initial temperature of atoms change.

3.5. Control system

Making Bose condensate in laser cooled atomic gases is a involved process which requires the operation of both the MOTs, the magnetic trap, the RF-evaporation, and detection and imaging, in a well controlled sequence of events. Step-wise, we have to perform laser cooling in the upper MOT, transfer the atoms to the lower-MOT, do optical pumping, do magnetic trapping in a QUIC trap, perform RF evaporative cooling, all in sequence, and then do detection and imaging to observe BEC. In order to accomplish the above events in the precise sequence, we need to activate and control several instruments within a short duration. The required precision in their activation time can be as short as few microseconds, which needs the control system to be accurate to that time scale. For this purpose, an electronic controller (18 output channels) compatible with LabVIEW and PC has been developed and programmed (by Laser Electronics Support Section, RRCAT) to provide appropriate switching pulses to activate different instruments and devices. Various devices controlled here include acousto-optic modulators for switching the MOT laser beams, power supplies for current in coils, RF synthesizer, CCD camera etc, to execute the sequence of events from MOT formation to RF-evaporation and imaging. The control system has been tested. Using this system, efforts to operate magnetic trap for atoms are in progress.

4. Conclusion

To conclude, we have developed a double-MOT set-up for BEC of ^{87}Rb atoms and made both the MOTs operational. We have gained expertise in characterization of the cold atoms, designed and tested a QUIC trap for magnetic trapping of the atoms, and got developed and tested control system and RF system. Presently we are in the process of loading atoms in the magnetic trap, a stage just before the RF-evaporation to form BEC.

We are very grateful to many colleagues at RRCAT for their continuous support and help in all this development. Specially, we would like to thank Mrs. L. Jain, Mrs. S. Tiwari, V. Bhanage, P. P. Deshpande, M. A. Ansari, H. R. Bundel and C. P. Navathe, all of Laser Electronics Support Section, RRCAT, for development of control system for the set-up, and M. Lad, P. R. Hannurkar and their colleagues at RF Systems & Control Division, RRCAT, for development of RF amplifier system. We are also thankful to C. Rajan and P. Kumar, LBAID, RRCAT, for development of high current switching circuits, S. Raja, LBAID, RRCAT, for fabrication of the tapered tube used in vacuum chamber, and H. S. Vora, LSED, for his help in CCD image processing. Finally, we thank Dr. S. C. Mehendale for a critical reading of the manuscript.

References:

1. M. H. Anderson, J. R. Ensher, M. R. Mathews, C. E. Wieman, E. A. Cornell, *Science* **269**, 198 (1995).
2. "Bose-Einstein condensation in dilute atomic gases", *Proc. International School of Physics* (Enrico Fermi course CXL), Edited by, M Inguscio, S. Stringari, and C. Wieman (IOS Press Amesterdam, 1999).
3. C. J. Myatt, N. R. Newbury, R. W. Ghrist, S. Loutzenhiser, and C. E. Wieman, *Opt. Lett.* **21**, 290 (1996).
4. W.D. Phillips and H. Metcalf, *Phys. Rev. Lett.* **48**, 596 (1992); T.E. Barret et al, *Phys. Rev. Lett.* **67**, 3483(1991).
5. V. B. Tiwari, S. R. Mishra, H. S. Rawat, S. Singh, S. P. Ram, S. C. Mehendale , *Pramana J. Phys.* **65**, 403 (2005).
6. S. R. Mishra, S. P. Ram, S. K. Tiwari, S. C. Mehendale, Proc. National Laser Symposium NLS-07 (Dec. 2007), Vadodara.
7. S. R. Mishra, S. K. Tiwari, S.P. Ram, S. C. Mehendale, *Opt. Eng.* **46**, 084002 (2007).
8. T. Esslinger, I. Bloch and T. W. Hänsch. *Phys. Rev. A* **58**, R2664 (1998).
9. S. R. Mishra, S. P. Ram, P. P. Dwivedi, S. K. Tiwari and S. C. Mehendale, Proc. Sixth DAE-BRNS National Laser Symposium NLS-06, (Dec 2006), Indore.

T.2 Modification of metallic surfaces with high power CO_2 laser

Rakesh Kaul (rkaul@cat.ernet.in)

Introduction

Many of the life-limiting mechanisms of engineering components originate from associated surfaces. These include corrosion, wear, stress-corrosion cracking, fatigue, corrosion-fatigue etc.. Material's susceptibility to these degradation mechanisms is strongly influenced by surface characteristics including chemical composition, microstructure, hardness, state of stress, roughness, nature of previous processing etc. A suitable modification of the character of the surface, without changing bulk of the material, provides an effective way to modify material's response to these unwanted effects. Surface modification can be in terms of change in composition, microstructure, topography, hardness, state of stress, cleanliness etc. The broad area of surface modification, now popularly known "Surface Engineering", has vast potential for providing cost-effective solution to enhance/extend life of engineering components operating under susceptible conditions. Laser, with its wide range of characteristics (e.g. wavelength and mode of operation - continuous wave/pulsed) and associated flexibility to manipulate with the help of optics, has emerged as a powerful tool to precisely control desired surface effects. Lasers are capable of inducing different kinds of surface effects including thinfilm deposition, solid-state transformation hardening, melting, alloying, cladding, surface cleaning/decontamination, shock peening etc. Compact lasers with the flexibility of transportation through fine optical fibers (e.g. diode, fiber and Nd:YAG lasers) are attractive industrial tools for processing in hostile environments or in the regions with limited access. With the integration of highly automated workstations with lasers, which are cost effective, powerful, reliable and compact, laser material processing (LMP) is set to become tomorrow's processing technology.

Realizing the important role that lasers can play in shaping Indian industry, CO_2 laser program was initiated at RRCAT, with the objective of developing high power industrial CO_2 lasers. Subsequent years witnessed development of high power lasers, ranging from 10 kW to 20 kW. During late-90s, activities were initiated towards material processing with in-house developed CO_2 lasers. For material processing applications, 3.5 kW and 10 kW transverse flow CO_2 lasers were integrated with beam delivery systems and computer numerically controlled 3-axis workstations. Recently, a 5-axes CNC workstation has also been integrated with 3.5 kW laser system for laser rapid manufacturing (LRM). During last couple of years, a variety of laser processing studies have been carried out and forthcoming part of the paper describes a few important laser surface treatment studies performed at Laser Material Processing Division of RRCAT.

1. Laser hardfacing to suppress dilution in Colmonoy deposit on austenitic stainless steel

Nickel-base alloys, "Colmonoy", have been selected as hardfacing material for many austenitic stainless steel (SS) components in 500 MWe Prototype Fast Breeder Reactor (PFBR) at Kalpakkam [1]. Hardfacing is intended to impart enhanced galling resistance to the mating surfaces and to avoid self-welding in the flowing sodium environment at a temperature of about 823 K. A major problem associated with Colmonoy hardfacing of SS components is extensive dilution from the base metal. Due to large difference in the melting temperatures of Colmonoy and SS, Colmonoy deposits pick up significant amount of dilution from SS base metal. C. R. Das et al [2] reported that Colmonoy 6 deposits on type 316LN SS, made by Gas Tungsten Arc Welding (GTAW), carry extensive dilution from the base metal, which significantly influences their microstructure and hardness up to a deposit thickness of 2.5 mm.[2] For overcoming adverse effects of dilution, it is essential to increase thickness of post-machined Colmonoy deposit, which not only adds to the cost of fabrication but also causes greater distortion of the component.

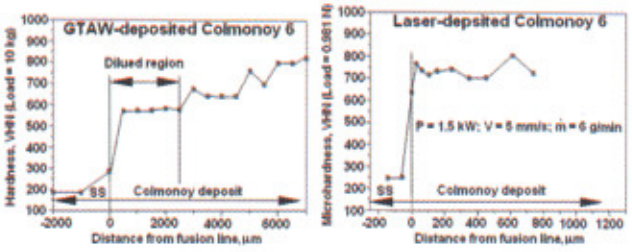

Fig.T.2.1: Comparison of hardness profiles across transverse cross-sections of Colmonoy deposits made by GTAW and laser.

Low heat input characteristics of laser cladding process has been exploited to suppress dilution in Colmonoy 6 deposits on type 316L SS base metal. Very low degree of dilution was achieved in laser-deposited Colmonoy by carefully controlling process parameters. Fig.T.2.1 compares hardness profiles across the cross-sections of Colmonoy 6 hard-faced SS specimens made by GTAW and laser. Crack-free Colmonoy 6 deposits were obtained by keeping the specimens undergoing hardfacing in a specially made sand bath maintained at 673 K and leaving the hard-faced specimens buried under sand for about 15 minutes [3]

2. Laser-assisted graded hard facing of Stellite 6

Co-based alloys "Stellite" are extensively employed as hardfacing material for many engineering applications for enhanced resistance against high temperature wear, oxidation and corrosion. In Fast Breeder Test Reactor (FBTR), there are many applications of Stellite overlay on austenitic SS to obtain enhanced galling resistance at elevated temperatures of about 823 K[4,5]. Large difference in the coefficients of thermal expansion between austenitic SS and Stellite often causes cracking of Stellite hardfaced SS components. Cracking resistance of Stellite 6 clad SS components can be effectively enhanced by providing smooth transition in chemical composition across substrate/clad interface. Present work describes laser-assisted graded deposition of Stellite 6 overlays on type 304 SS.

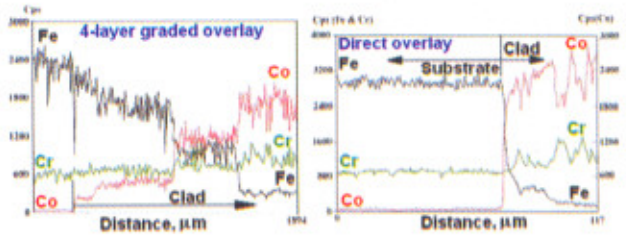

Fig.T.2.2: Comparison of concentrations profiles of Fe, Co and Cr across transverse cross-sections of graded and direct Stellite6 deposited austenitic SS specimens.

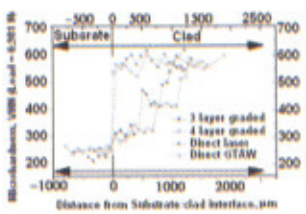

Fig.T.2.3: Comparison of micro-hardness profiles across transverse cross-sections of graded and direct Stellite6 deposited austenitic SS specimens.

The process of laser cladding has been employed to deposit 3 and 4-layered graded Stellite 6 overlays on SS. Multiple clad layers of graded composition were deposited by laser cladding with pre-mixed alloy powders of different compositions. In contrast to abrupt transition in chemical composition and micro-hardness across substrate /clad interface of directly hardfaced SS specimens, graded hardfaced specimens exhibited gradual transition in chemical composition and micro-hardness across substrate/clad interface. Both, the composition and micro-hardness measurements on graded hardfaced specimens exhibited stepped profiles, with each step coinciding with the interface between successive graded layers, as shown in Fig.T.2.2 and T.2.3. Graded overlaid specimen demonstrated higher cracking resistance under thermal cycling conditions than that of directly overlaid specimen [6].

3. Laser surface alloying with Cr, Ni and Mo to enhance pitting resistance of austenitic SS

Austenitic stainless steels are susceptible to localized corrosion in chloride bearing environment [7]. Super austenitic SS, with high concentrations of Cr (≈25%) and Mo (≈6.5 %), exhibits superior corrosion resistance than the popular 18/8 variety of SS. Surface alloying of SS with Cr and Mo, therefore, offers an economical means of enhancing corrosion resistance of relatively cheaper type 18/8 SS. The method of laser surface alloying, achieved by melting of powder-coated substrate, does not result in uniform chemical composition of the modified surface [8,9] In the present study, desired surface alloying was effected by laser cladding type 304L SS substrate with pre-mixed powders of type 316L SS and Cr. For controlling ferrite content in the weld metal, arising out as a result of addition of ferrite stabilizers like Cr and Mo, laser cladding was also performed with pre-mixed powders of type 316L SS, Cr and Ni. The average chemical compositions of resultant (Cr+Mo) and (Cr+Ni+Mo) alloyed surfaces, as found out by Quantitative Energy Dispersive X-ray Fluorescence (EDXRF) (in wt%) were: 24.2 Cr; 9 Ni; 2 Mo; 0.6 Mn and 24.4 Cr; 21.7 Ni; 1.4 Mo; 0.3 Mn, respectively. Potentio-dynamic polarization studies performed in 0.5 M NaCl solution demonstrated that the combined effect of Cr, Mo and Ni alloying in raising pitting resistance was more pronounced than that produced by alloying with Cr and Mo, as shown in Fig.T.2.4. Laser surface alloying with Cr, Mo and Ni brought about more than 3-fold increase in pitting potential over that of the untreated substrate (from 310 mV to 980 mV) whereas pitting potential for Cr and Mo alloyed surface was found to be 780 mV [10].

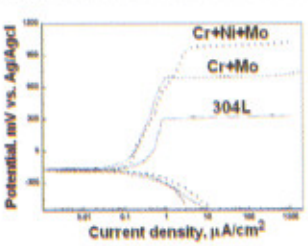

Fig.T.2.4: Potentiodynamic polarization plots of laser surface treated Cr+Mo and Cr+Ni+Mo alloyed and untreated type 304L SS (substrate) specimens in 0.5 M NaCl solution.

4. Laser surface alloying with Si for improved corrosion resistance of type 304L SS

Type 304L SS is a major material of construction in chemical and reprocessing plants involving extensive use of nitric acid (HNO_3). Normally protective Cr_2O_3 film on the surface of SS is rapidly dissolved under aggressive HNO_3

environment or at temperature above 353 K [11]. The stability of Cr_2O_3 film is enhanced by Cr and Ni addition. Si is another important alloying element influencing corrosion resistance of austenitic SS in HNO_3 environment. Si offers excellent corrosion resistance when its concentration is either below 0.2 wt% or above 1.6 wt%. With 0.4 -1 wt% Si content, the alloy suffers excessive inter-granular corrosion (IGC) [12]. ASTM specifications allow upto 1 wt% Si in type 304L SS. Hence, surface enrichment of Si above 1.6 wt% is an effective means of enhancing corrosion resistance of type 304L SS in concentrated boiling HNO_3 environment. Laser surface alloying with Si was achieved by laser cladding type 304L SS substrate with pre-mixed powders of type 304L SS and Si. The results of polarization study performed on Si-alloyed specimens in 6N HNO_3 solution demonstrated that in contrast to untreated substrate, laser surface-alloyed specimens exhibited significant reduction in passive current density from 1μ A/cm^2 to less than 0.1μA/cm^2, as shown in Fig.T.2.5, signifying greater stability of protective film on laser alloyed surface [13].

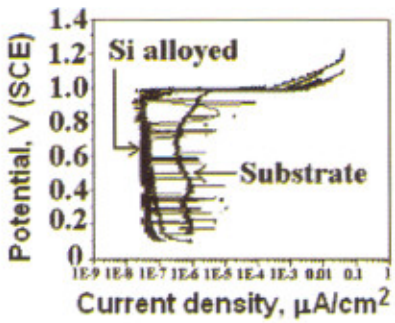

Fig.T.2.5: Potentiodynamic polarization plots of Si-alloyed and untreated type 304L SS (substrate) specimens.

5. Laser surface treatment to enhance inter-granular corrosion resistance of type 304 SS

Austenitic stainless steels, in spite of having good general corrosion resistance, strength, and formability [14-16], are particularly prone to localized corrosion like crevice, pitting, inter-granular corrosion (IGC) and stress corrosion cracking (SCC). In nuclear fuel reprocessing, waste management industries and in many chemical industries, using nitric acid as the process fluid, the main corrosion problem is IGC [17,18]. The basic cause of IGC is sensitization of SS. IGC of austenitic SS arises from inter-granular precipitation of Cr-rich carbides $M_{23}C_6$ during exposure to the temperature regime of 773- 1073 K. Inter-granular carbide precipitation is accompanied by the development of Cr-depleted zones adjacent to grain boundaries. Cr-depleted, zones, being anodic with respect to grain interior, are preferentially attacked in the corrosive environment leading to IGC [14-18]. Sensitization is also a main reason for inter-granular stress corrosion cracking (IGSCC) of SS weldments in certain environments e.g. oxidizing water chemistry in boiling water reactors [19].

Present study demonstrated that laser surface melting (LSM) treatment of type 304 SS brings about significant increase in its resistance against sensitization and IGC during subsequent exposure to susceptible temperature regime [20]. Fig.T.2.6 compares exposed surfaces of base metal and laser treated specimens after undergoing ASTM A262 practice B test. Degree of sensitization (DOS) of laser surface melted specimens remained largely unaffected by exposure to severe sensitization heat treatment at 923 K for 9 hours. In the best conditions, laser melted surface, even after undergoing this heat treatment, exhibited comparable or even lower DOS than the base metal in as-received condition (refer Table-1). Figure T.2.7 compares Double-loop Electrochemical Potentiokinetic Reactivation (DL-EPR) plots of base metal and laser melted specimens after undergoing 9-hour long sensitization heat treatment at 923 K. Enhanced resistance against sensitization of laser-treated surface is attributed to its duplex microstructure (involving austenite and -ferrite) and higher fraction of low angle grain boundaries (refer Table-2). The message of the investigation is that LSM treatment of unstabilized austenitic SS brings about significant reduction in its risk sensitization and IGC, arising out as a result of subsequent exposure to susceptible temperature regime. The technique has also been applied as a pre-welding treatment to suppress sensitization in the heat-affected zone (HAZ) of type 304 SS weldment [21].

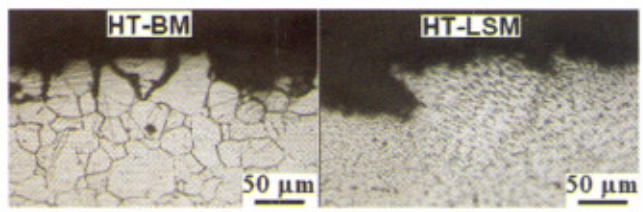

Fig.T.2.6: Transverse cross-sections of heat-treated (923 K for 9 hours) base metal and laser surface melted specimens after undergoing ASTM A262 Practice B test. Clear IGC attack on the exposed base metal surface (left) is in contrast to un-attacked laser treated surface (right).

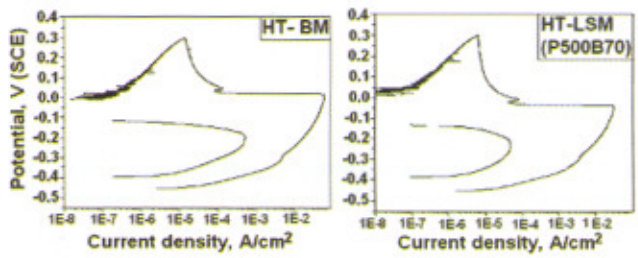

Fig.T.2.7: Comparison of DL-EPR plots of hea treated (923 K for 9 hours) base metal and laser surface melted specimens.

Specimen	Without heat treatment	After heat treatment
Base metal	0.36	4.52
Laser treated 1	0.09	0.107
Laser treated 2	0.24	0.327

Table-1: Effect of heat treatment on degree of sensitization (DOS) of base metal and laser surface melted specimens.

Nature of grain boundaries	Base metal	Laser melted surface
Low angle grain boundaries, $2^{0} < \theta < 5^{0}$	0.042	0.17

Table-2: Grain boundary character distributions, as determined by orientation imaging microscopy, in base metal and on laser treated surface.

6. Laser surface treatment to suppress sensitization in mod. type 316(N) SS weld metal

AISI 316 LN SS with 0.024-0.03% C and 0.06-0.08% N is the primary structural material for 500 MWe PFBR. Welding of this material is being carried out using modified E316-15 electrode with 0.045-0.055% C and 0.06-0.10%N. Welded SS components are subjected to solution annealing heat treatment for achieving full stress-relief and restoration of mechanical properties and corrosion resistance. Higher C content of the filler metal makes the weld metal prone to sensitization during cooling from the solution annealing temperature. It has been shown that in order to avoid sensitization of the weld metal, weldment needs to be cooled at a rate higher than 75 K/h. However, rapid cooling of the weldment carries associated risk of distortion and reintroduction of residual stresses. A study had been taken up to develop a laser surface treatment to evolve a surface microstructure which would be more resistant against sensitization during post weld solution annealing treatment with cooling at a slow rate of 65 K/h

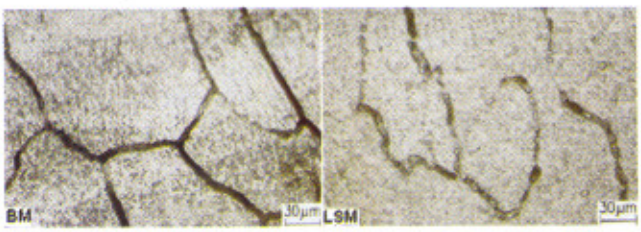

Fig.T.2.8: Comparison of the microstructures of solution annealed as-deposited (BM) and laser surface melted 316(N) weld metal specimens. Discontinuity in inter-granular carbide network in laser-melted specimen reflects its lower susceptibility to IGC.

Experiments involving LSM were carried out with 150 W average power pulsed Nd:YAG laser and 10 kW CO_2 laser, in both continuous wave (CW) and pulse modulated (100 Hz) modes. LSM treatment parameters have been found to have a profound effect on the IGC resistance of the resultant microstructure after subsequent solution annealing treatment. Best results were obtained when LSM was performed with high frequency pulse modulated CO_2 laser beam. Laser treatment of type 316(N) SS weld metal with high repetition rate pulse modulated CO_2 laser successfully induced greater resistance against IGC during solution annealing treatment involving cooling at the rate of 65 K/h Laser treated weld metal remained un-sensitized after solution annealing involving slower rate of cooling at 65 K/h [22]. Figure T.2.8 compares microstructures of untreated and laser treated 316(N) weld metal specimens after undergoing solution annealing treatment. Numerical simulation study performed with ANSYS 7.0 software to understand the physical reason behind difference in sensitization behavior of laser surface melted specimens under CW and high frequency pulse modulated conditions and the predictions were subsequently validated by electron back scattered diffraction (EBSD) analysis. In contrast to formation of long columnar grains growing from the fusion boundary in CW laser surface melted region, LSM with high frequency pulse modulated laser beam resulted in the evolution of fine grains near the fusion boundary region which is believed to be the cause for enhanced resistance against sensitization. The direct implication of these results is that the a laser surface melted type 316LN SS weldments can be cooled at a slower rate during subsequent solution annealing with reduced risk of sensitization and thus minimizing distortion and reintroduction of thermal stresses.

7. Laser beam shaping for improved microstructure during laser surface melting

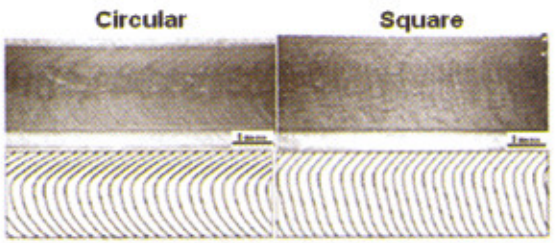

Fig.T.2.9: Comparison of the shapes of solidification fronts produced during LSM with circular and square shaped laser beams. Re-constructed profiles of associated solidification fronts are provided on the bottom of the figure.

Laser surface melting of austenitic SS at high-speed carries the risk of centerline solidification cracking due to the formation of tear-drop shaped melt pool. Laser beam shaping can be effectively employed to engineer surface microstructure of laser-melted region by controlling the

shape of associated melt pool. Results of the present study demonstrated that by using a square laser beam in place of a circular one for LSM, the orientation of the solidification front associated with the resultant melt pool can be made flatter and more steeply oriented with respect to the direction of laser scanning (Fig.T.2.9). Development of this kind of melt-pool during LSM results in the growth of smoothly curved columnar grains with broader region of axial grains at the centre-line of laser surface melted track, as shown in Fig.T.2.10. Surface microstructure generated by LSM treatment with square laser beam should enhance resistance of against centerline solidification cracking (over that obtained with circular laser beam) even at higher processing speed [23].

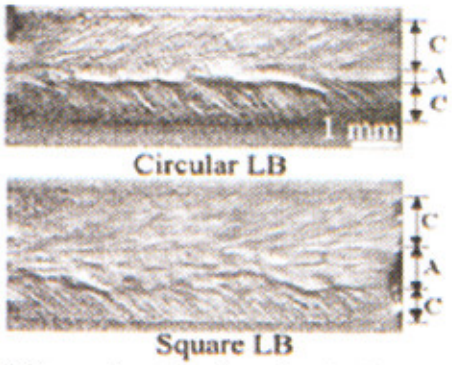

Fig.T.2.10: Comparison of surface microstructures produced by LSM with circular and square shaped laser beams. (A: axial grained region; C: columnar grained region)

8. Laser surface treatment to control end grain corrosion of austenitic stainless steel

Apart from IGC, another form of corrosion to which particularly bar, wire, and tubular products of SS are susceptible to in nitric acid environment, is end-grain corrosion. It takes place on the tubular and forged surfaces that are perpendicular to hot-working direction and occurs as localized pitting like attack that develops along the hot-working direction and finally corrosion occurs as intergranular attack [18, 24-27]. It has been identified as a major form of corrosion in those components in which cross-sectional surfaces are exposed to oxidizing process [25]. In reprocessing plants, using sensitization resistant low carbon grade or nitric acid grade (NAG) stainless steels, end-grain corrosion is shown to be a major degradation mode in components like instrument tubing and tube-to-tube sheet welds. There are also reports of end grain corrosion in forgings and set in pipe branches [24]. Exposure studies carried out in a dissolver in a reprocessing plant (in vapor phase) showed very heavy corrosion rates of 0.2-0.6 mm/year even for NAG grade of SS and this was attributed mainly to end-grain corrosion [24]. Directional nature of end-grain attack has been explained by the dissolution of aligned sulphide inclusions along the hot-working direction [18, 24-27]. Segregation of P, Cr and Si along the flow lines during the fabrication stage is another proposed mechanism for end-grain corrosion [18, 26-28]. The end-grain corrosion of a material is related to the defect in manufacturing and processing stage such as a high-inclusion content in the material or use of an improper solution annealing heat treatment. Instead of discarding these defective materials against end-grain corrosion, some suitable methods can be used to avoid or minimize such type of attack

In the present work LSM treatment was evaluated for its effectiveness to reduce end-grain corrosion in type 304 SS. Laser surface treated specimens of two heats (A and B) were subjected to ASTM A262 practice C to find out the susceptibility of these materials against IGC. LSM brought about significant reduction in the corrosion rates of both the heats with respect to corrosion rates observed for corresponding specimens in as-received conditions (refer Table-3). The reason for improvement in the resistance against end-grain corrosion is brought about by removal / redistribution of elongated MnS inclusions (refer Fig.T.2.11) and elimination of segregation of Cr, Si, and P along the flow lines. Another contributing factor for increase in IGC resistance is the presence of δ-ferrite on the laser treated surface, which makes the austenite grain network discontinuous [29].

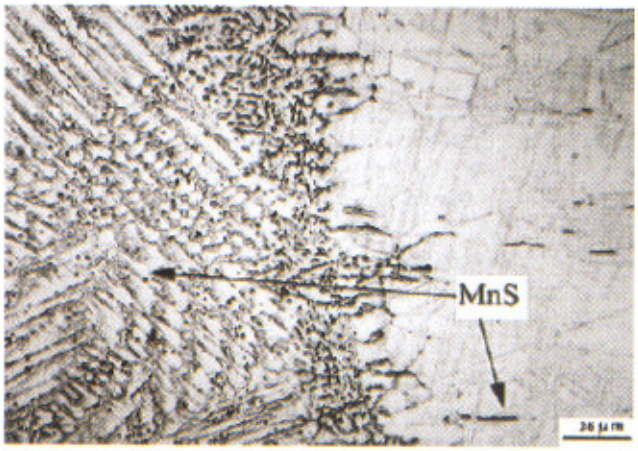

Fig.T.2.11: Transverse cross-section of laser surface melted specimen of heat B. Arrows indicate change in the morphology of MnS inclusions by laser melting. Laser melted region is on the left side of the photomicrograph.

Specimen	As-received	Laser melted surface
Heat A	1.858	0.185
Heat B	3.5763 (after 3 periods)	0.208

Table-3: Corrosion rates (in mm/yr) measured after 5th period of ASTM A262 practice C test for type 304L SS specimens

Conclusions

Laser surface treatment studies performed so far have demonstrated unique capability of laser to exercise control over surface composition and microstructure for yielding enhanced performance characteristics. After building this initial foundation, our present research activity focuses on developing laser surface treatments for enhancing or extending life of engineering components operating under fatigue and corrosive conditions through modification in surface microstructure and state of stress. Efforts are also being made to couple laser with conventional processes to make resultant hybrid process more capable and versatile.

Acknowledgements

Author expresses his sincere thanks to his collaborators in BARC, IGCAR, UGC-DAE CSR and also in different divisions of RRCAT for their valuable contributions in various studies. He thankfully acknowledges constant support received from the team members of Laser Materials Processing Division.

References

1. Hard Facing Task Force: 'Recommended hard facing materials or NSSS components', Report IGC/HTF/05, Indira Gandhi Centre for Atomic Research, Kalpakkam, 2000.
2. C. R. Das, S. K. Albert, V. Ramasubbu, A. K. Bhaduri, C. Sudha, and A. L. E. Terrance, Proc. National Welding Seminar, Chennai, (2002).
3. R. Kaul, P. Ganesh, S. K. Albert, A. Jaiswal, N. P. Lalla, A. Gupta, C. P. Paul and A. K. Nath, Surf. Eng. **19**, 269 (2003).
4. IGC'97 Highlights, Indira Gandhi Centre for Atomic Research, Kalpakkam, India, 87-88.
5. K. Ahmed and J. Krishnan, Trans. Metal Finisher's Assoc. of India **10**, 163 (2001).
6. R. Kaul, P. Ganesh, M. K. Tiwari, A. K. Singh, P. Tripathi, A. Gupta and A. K. Nath, Lasers in Eng. **12**, 207 (2002).
7. U. K. Mudali and M. G. Pujar, Corrosion of Austenitic Stainless Steels, H. S. Khatak and B. Raj (Eds.), Narosa Publishing House, New Delhi, 74 (2002).
8. A. S. Khanna and K. Sridhar, Lasers in Surface Engineering, N. B. Dahotre (Ed.), Surface Engineering Series, vol. 1, ASM International, OH, USA, 413 (1998).
9. K. Sridhar, A. S. Khanna, A. Gasser and M. B. Deshmukh, Lasers in Eng. **6**, 107 (1996).
10. U. K. Mudali, R. Kaul, S. Ningshen, P. Ganesh, A. K Nath, H. S. Khatak and B. Raj, Mat. Sci. Tech. **22**, 1185 (2006).
11. A.J. Sedricks, *Corrosion of Stainless Steels*, John-Wiley and Sons, New York (1979).
12. B. Raj and U. K. Mudali, Proc. 12th Annual Conf. of Indian Nuclear Society, Indore, 93 (2001).
13. R. Jagdheesh, R. Kaul, U. K. Mudali, P. Ganesh, A. K. Nath, D. Sastikumar and H. S. Khatak, Proc. Int. Conf. on Advances in Surface Treatment: Research & Applications, Hyderabad, 385 (2003).
14. A. J. Sedriks, *Corrosion of Stainless Steels*, 2nd edition, John Wiley and Sons, NY, 1996.
15. D. A. Jones, *Principles and Prevention of Corrosion*, 2nd Edition, Prentice Hall (1992).
16. V. Kain, R. C. Prasad, P. K. De, Corrosion NACE 58, 15 (2002).
17. R. L. Cowan, C. S. Tedmon, Intergranular Corrosion of Alloys: Advances in Corrosion Science and Technology, vol. 3, M. G. Fontana and R. W. Staehle (Eds.), NY, Plenum, 293 (1973).
18. V. Kain, P.K. De, Int. J. Nuclear Energy Sci. Tech. **1**, 220 (2005).
19. P. Andresen, M. Morra, W. Catlin, Proc. Corrosion 2004, Houston, USA, Paper No. 04678 (2004).
20. S. Mahajan, V. Kain, P. Ganesh, R. Kaul, A. K. Nath and R.C. Prasad, Proc. CORROSION, Nashville, USA, Paper No. 7191 (2007).
21. R. Kaul, N. Parvathavarthini, P. Ganesh, V. Kain and R. K. Dayal, Proc. Int. Welding Cong., Chennai, Paper No. C011 (2008).
22. N. Parvathavarthini, R. K. Dayal, V. Shanmugam, H. S. Khatak, R. Kaul, P. Ganesh and A. K. Nath, Symp. on Joining of Materials, Tiruchirapalli, Paper No. WPA1 (2004).
23. J. Khare, R. Kaul, P. Ganesh, H. Kumar, R. Jagdheesh and A. K. Nath, J. Laser Applications, **19**, 1 (2007).
24. R. D. Shaw, Corrosion Prevention and Control at Sellafield Nuclear Fuel Processing Plant, Brit. Corr. J. **25**, 97 (1990).
25. V. Kain, P. Sengupta, P. K. De and S. Banerjee, Metall. Mat. Trans. A. **36A**, 1075 (2005).
26. G. O. H. Whillock, B. F. Dunnitt and M. Takeuchi, Corrosion, **61**, 58 (2005).
27. V. Kain, S. S. Couthai and H. S. Gadiyar, Brit. Corr. J. **27**, 59 (1992).
28. J. Stewart and D. E. Williams, Corrosion Sci. **33**, 457 (1992).
29. K. Chandra, V. Kain, and P. Ganesh, J. Mat. Eng. Perf. **17**, 115 (2008).

T.3: Radiation physics studies at Indus-1 synchrotron radiation source for radiation protection in high energy electron accelerators

Haridas. G. (haridas@cat.ernet.in)

1. Introduction

Electron accelerators are widely used world over for various applications in industry, medicine and in basic and applied research. The electron energy used for industrial and medical applications is up to ~10 MeV. For research applications, the energy may extend to very high values (hundreds of MeV, GeV or TeV). High energy accelerators are on the rise as they are powerful tools to search the yet to be seen elementary particles, thereby unraveling the hidden realities of the universe. Livingston in 1962 in his famous "Livingston Plot" predicted a ten-fold increase in particle energy, every six years, which was confirmed by Panosky [1] two decades later who brought out a revised plot, which is shown in Fig.T.3.1.

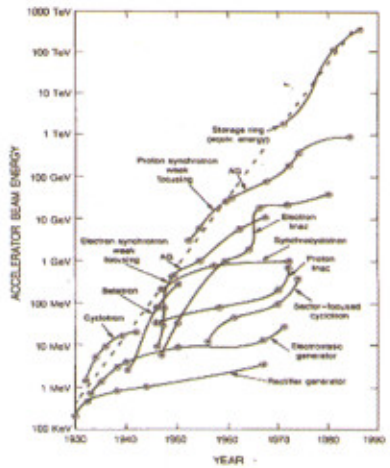

Fig.T.3.1: Livingston Plot: Envelope of the curves suggests a ten-fold increase in particle energy, every 6 years.

High energy electron accelerators are widely used at several laboratories in order to produce intense synchrotron radiation from storage rings [2]. High energy electrons are preferred for the production of synchrotron radiation due to its very low rest mass, in comparison with other fundamental particles and hence they can be accelerated to relativistic velocities easily unlike other charged particles.

When the high energy electrons interact with accelerator structures, residual gas molecules in the vacuum chamber, experimental targets etc, bremsstrahlung x-rays [3,4] are produced [5]. These x-rays have a broad spectrum extending up to the kinetic energy of the electron beam. Bremsstrahlung x-rays are the main radiation hazard in any high energy electron accelerator. These x-rays may further induce photo nuclear reactions within the interacting material and as a result several secondary particulate radiations like neutrons, protons, muons etc. may be generated. Thus the increase in the primary particle energy poses a great challenge in radiation protection due to the complex radiological conditions existing in such accelerators and lack of proper dosimetric systems [6].

Conventionally, radiation dosimetry and shielding aspects had been limited to radiation of few MeV, whose primary sources were mainly, naturally occurring radio-isotopes, nuclear fuel cycle operations like mining, milling, nuclear reactor operation, fuel reprocessing and x-ray generators used in diagnostic radiology and research. With the increase in the electron energy and the subsequent production of high energy bremstrahlung x-rays, the conventional dosimetric and radiation shielding concepts may not provide adequate safety to personnel in such accelerator environment. This is basically due to the difference in the interaction mechanism of this high energy radiation with matter, as compared to low energy radiations, up to few MeV.

When a photon with energy far above the pair production threshold (1.02 MeV) is incident on a medium, an energetic electron and photon are formed, as pair production is the dominant interaction mechanism at high photon energies. Subsequently, the energetic electron and positron radiate out photons and these photons in turn produce further pairs giving rise to a cascade (or shower) of electrons, positrons and photons resulting in an electromagnetic shower [5]. H.J. Bhabha, in his work on theory of cosmic ray showers, calculated the number of particles (electrons and positrons) emerging from a lead plate of 5 cm on 100 GeV electron bombardment to be 1000 or more [6]. An example of a massive shower generated when a 10 GeV electron is incident on a target of tungsten is shown in Fig.T.3.2.

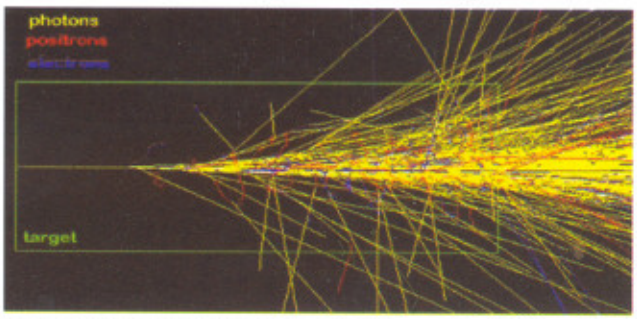

Fig.T.3.2: A massive electromagnetic shower simulated in a block of tungsten target on 10 GeV electron incidence.

As a result of the shower generation, the particle fluence increases with depth of the interacting medium and

their mean energy decreases. Therefore the energy deposition in the medium increases with depth, giving rise to a build up in the radiation absorbed dose (energy absorbed per unit mass of the medium). As the mean energy of photon in the medium reduces to a low value, the pair production and Compton scattering compete at certain depth [7] in the medium, beyond which dose build up dose not take place and hence the dose will fall off almost exponentially owing to Compton and photoelectric effect. The whole process would therefore result in a depth dose curve in the interacting medium with a rising and falling edge. The depth at which the maximum dose (D_{max}) occurs is the shower maximum (X_{max}) of the electro-magnetic shower.

Conventional radiation monitors, usually calibrated in terms of personal dose equivalent, $H_p(10)$ [8] when used to monitor such high energy photon radiation do not indicate the true dose received by the worker as they show only the dose equivalent at a depth of 10 mm in tissue. Thus the absorbed dose and hence the dose equivalent (a quantity used in personnel radiation protection) in a high energy photon field would be higher than the dose equivalent indicated by a conventional radiation survey meter.

Studies were carried out at in the high energy photon radiation field at Indus-1 Synchrotron Radiation Source (SRS) to find out the dose equivalent build up factor experimentally with conventional survey meters and water phantom, simulating a human body. Emphasis has been given to measurements using water phantoms, as human body contains about 62 % water [9], and can be applied for all practical radiation protection purposes. Monte-Carlo simulations were also carried out to simulate the experimentally observed dose build up factors. Dose build up factors as a function of the depth in water phantom was then estimated from which a high energy correction factor for radiation monitors is deduced.

2. Preliminary observations on cascade development around Indus-1

A set of 31 observations on the electro-magnetic cascade development and the subsequent radiation dose build up in different media were made with three different radiation monitors around Indus-1 SRS. The following three radiation monitors were used for the measurement:

1. Victoreen survey meter (Model 450P, USA),
2. Pulsed x-ray monitor (Model WM10, ED, BARC, India) and
3. RADMON survey meter (Model 701, Nucleonix, India).

All these monitors have a tested, near flat energy response from ~60 keV to 1.25 MeV.

In the experiment, a number of observations were made within the shielded enclosures at various locations around the storage ring of Indus-1 during the storage mode of operation. To see the dose build up, various media were interposed between the source (storage ring) and the monitors and the response was noted. The dose rate build up factors were then found out from the response with build up medium to the response from the bare monitor. It has been observed that all the monitors showed dose rate build up with the build up medium in front of the monitors. The measured dose rate build up factors [10] varied in the range 1.9 to 4.5, which are pictorially shown in Fig.T.3.3. These observations refer to various values of stored current on different days and for different build up media like water phantom, tissue phantom, steel of few mm etc. This clearly demonstrated the shower generation within the media and indicated that all the radiation monitors studied are underestimating the radiation dose within the shielded enclosure.

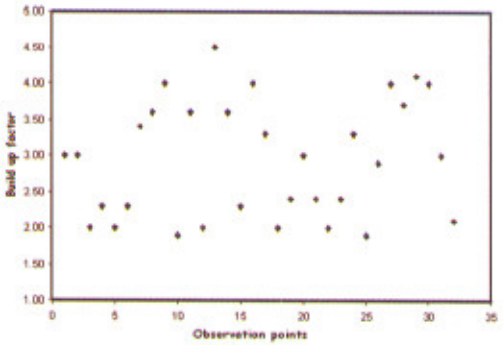

Fig.T.3.3 Dose build up factors observed for 31 observations around Indus-1.

3. Systematic measurements on radiation dose build up

Based on the preliminary observations on the radiation dose build up around the storage ring, systematic measurements were performed at the front-end (the interface between the storage ring and a beam line) exit and near the bending magnet-3 (BM-3) using water phantom and Victoreen survey meter.

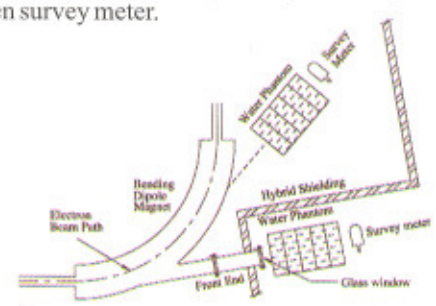

Fig.T.3.4: Schematic diagram of the experimental set-up for depth dose measurements.

The Victoreen survey meter was used to get the depth dose profile in water so as to see how the dose profile varies with depth of a human body when exposed to the photon radiation. Measurements were done at 10 mA of stored current in the ring. The schematic diagram of the experimental set up for studying the depth dose profile is shown in Fig.T.3.4.

In the radiation field near the bending magnet, the survey meter response was noted by varying the thickness of water slab. Since it was difficult to surround or immerse the instruments in water, as it is to be done ideally, water slabs were kept in front of the survey meter. Similar experiment was carried out at the front-end exit. The depth dose profiles obtained near the bending magnet and at the front- end are shown in Fig.T.3.5 [11].

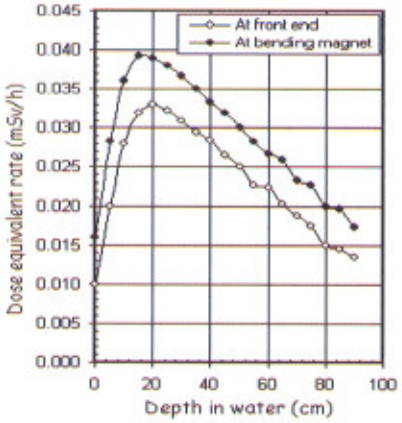

Fig.T.3.5: Depth dose curves measured at bending magnet and front- end (of BM-3) of Indus-1 SRS.

The depth dose profiles indicated that at the bending magnet, the maximum dose equivalent rate occurred at about 15 cm, giving a dose build up factor of 2.5 w.r.t. the bare monitor. At the front-end location, the dose equivalent rate peaked at a depth of 20 cm, with a dose build up factor of 3.3. To confirm the dose build up in another medium and with other type of detectors, measurements were performed with copper as the build up medium and $CaSO_4$(Dy) TLD as the detector, which confirmed the same [12].

4. Monte Carlo Simulations of depth dose around the Storage Ring

Experimental observations discussed above were simulated using the Monte Carlo codes : EGS-4 [13] and EGSnrc [14]. Experimental depth dose curves obtained from the measurements with Victoreen survey meter indicated spectral variations at different locations around the storage ring. Therefore a different approach was adopted to simulate the experimental conditions which enable explain the experimental results.

A pencil beam of 450 MeV electrons is allowed to be incident on different thicknesses of semi-infinite copper target and the emergent bremsstrahlung spectra are scored in air in the forward direction with a central axis scoring radius of 5 mm. Copper is selected because the structural materials in and around the accelerator are of medium atomic number. The bremsstrahlung spectra obtained from 3 mm, 50 mm and 100 mm copper targets are shown in Fig.T.3.6. (Spectra from other thicknesses are not shown due to mix-up of spectral data in the figure).

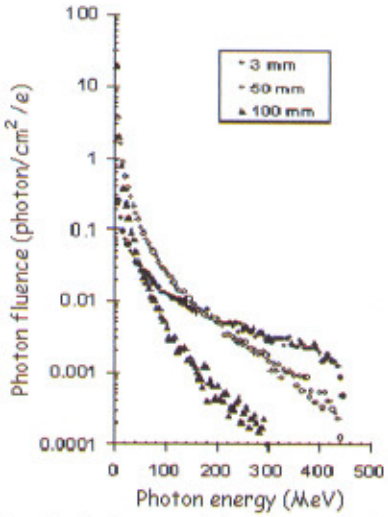

Fig.T.3.6: Simulated bremsstrahlung spectra obtained from different thickness of Cu target on 450 MeV electron incidence (using EGS-4).

It can be seen from Fig.T.3.6 that the spectrum from 3mm Cu (thin target) is more populated on the high energy side compared to the other two. For thick targets, the low energy component dominates due to the spectral degradation on account of interaction within the Cu target itself. These spectra of photons are allowed to be incident as a broad parallel beam on water phantom and the depth dose in water is scored. For the depth dose calculation, total histories of 10 millions are used to have better statistical accuracy. For electron and photon transport, cut-off energies used were 0.521 MeV for electrons and 0.01 MeV for photons. The statistical accuracy obtained in all the simulations was within ±1 %. The simulated depth dose curves obtained is shown in Fig.T.3.7. The top curve corresponds to spectrum from 3 mm Cu and the bottom one is from 100 mm thick Cu.

One can see from the depth dose curves that dose maximum (D_{max}) and the shower maximum (X_{max}) decreases as one moves from a thin target to a thick target. The dose build up factors are calculated as the ratio of D_{max} to the dose at 1 cm depth in water from the simulated depth dose curves. The X_{max} corresponding to D_{max} is also noted in each case. The

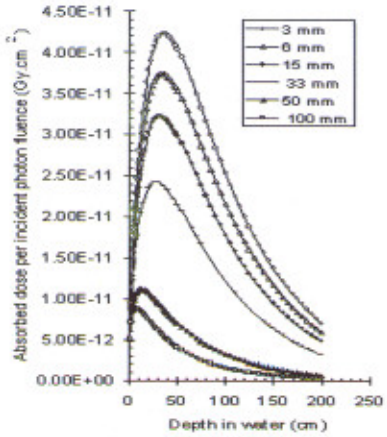

Fig.T.3.7: Simulated depth dose curves in water phantom for different incident bremsstrahlung spectra from Cu targets of different thickness obtained from 450 MeV electron incidence (using EGSnrc).

average energy of the incident photon spectra and the calculated dose build up factors plotted as a function of the shower maximum, X_{max} is shown in Fig. T.3.8.

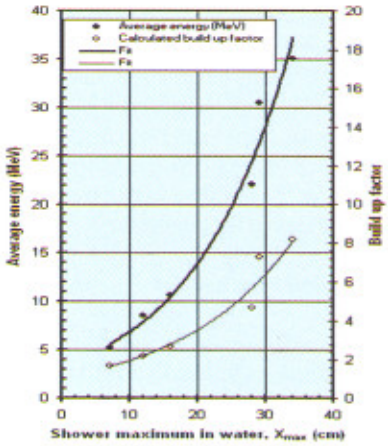

Fig.T.3.8: Calculated dose build up factor & average energy of incident bremsstrahlung spectra as a function of the shower maximum.

5. Results of the simulations and comparison with measurements

From Fig.T.3.8, the shower maximum and the build up factor is seen to increase with the average energy of the incident photon spectrum. Moreover, as the shower maximum increases, the build up factor also is seen to increase. An exponential fit to the average energy as a function of the X_{max} assumes the following form.

$$E_{avg}(MeV) = 3.41e^{0.07 X_{max}} \quad (1)$$

It follows that,

$$X_{max} = \frac{1}{0.07}\ln\left(\frac{E_{avg}}{3.41}\right) \quad (2)$$

The above equation says that at an average energy of 3.41 MeV, $X_{max} = 0$ and hence dose build up in water does not take place below this energy.

Similarly the exponential fit to the build up factor assumes the form,

$$BF = 1.08\exp\left(X_{max}/16.9\right) \quad (3)$$

where X_{max} is the shower maximum in water in cm. The simulated build up factor enables us to compare with the experimental values. Table T.3.1 gives the comparison of the experimental and the simulated build up factors as a function of the shower maximum, X_{max}.

Table.T.3.1: Comparison of dose build up factor from experiments and simulations.

Location	Shower maximum (cm)	Build up factor	
	Measured	Measured*	Simulated**
Bending magnet	15.0	2.5	2.6
Front end	20.0	3.3	3.5

* From Fig. T.3.5 ** From Equation 3

It is seen from the table that the simulated and experimental build up factors are in very good agreement. The difference in the average energy (representing the incident spectrum) explains the different shower maxima and build up factors observed during the measurement. Due to electron interaction within the accelerator structures (thickness of the absorber may vary depending upon the angle of incidence, position of the beam about the closed orbit, beam current etc.), the emerging spectra would be different and hence the depth at which dose maximum occurs will vary. Since the minimum vacuum envelope thickness the electron beam encounters is about a few millimeter, the average energy of the photons is about a few tens of MeV. For instance, from 3 mm Cu, the value is ~33 MeV, which gives a shower maximum beyond 30 cm in water. Therefore at X_{max} = 30 cm in water, the approximate size of a human body, a dose build up factor of 6.4 is obtained from equation 3. This build up factor can be used as a conservative high energy correction (multiplication) factor for the monitor reading in the high energy photon radiation field within the shielded enclosures of Indus-1.

A thought was given to surround the ion chamber detectors used within the shielded enclosures of the monitor by a proper build up material with thickness giving rise to the same build up factor. But it was felt that it could give rise to underestimation in a photon field where the spectrum is softer. Therefore it is safer to correct the instrument response manually with the suggested correction factor.

6. Effectiveness of the correction factor outside the shield

In order to see the applicability of the high energy response correction factor for the radiation monitors outside the shielded enclosures of Indus-1, the energy spectra in the direct and the transmitted photon field were measured using a 2" x 2" BGO (Bismuth Germanate) detector during the storage mode of Indus-1 operation. The direct spectrum was obtained from the storage ring through a hole (~100mm dia) in the shielding and for the transmitted spectrum, a lead block of 80 mm thick was used to block the hole in the shielding. The spectra obtained are presented in Fig.T.3.9 [15]

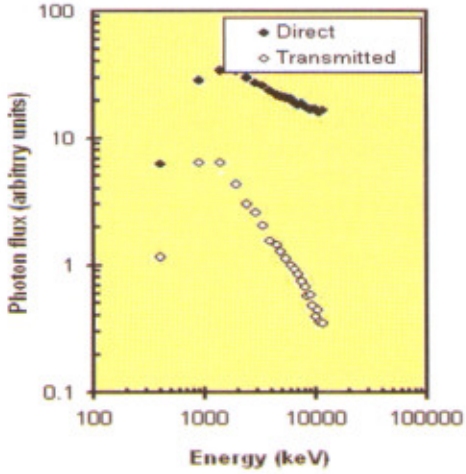

Fig.T.3.9: Measured direct and transmitted bremsstrahlung spectra (through 80 mm Pb) from Indus-1 (BM-1side).

The trend of the direct spectrum indicates that it is extending to very high energies. However, the average energy of the transmitted spectrum was estimated to be 3.3 MeV, which is less than 3.41 MeV, below which no build up takes place in water (from eq.3). Therefore, the correction factor suggested for the monitor response within the shielded enclosures does not apply behind the present hybrid shielding (80 mm lead + 80 mm mild steel) of the storage ring. Bremsstrahlung x-ray energy estimation outside the shield was also carried out using TLD badge, which gave an effective energy of 2.18 MeV [16]

7. Dose build up experiments outside shielding of Indus-1

A set of dose build up study was carried out outside the shielded enclosure of Indus-1 to ensure no dose build up in the transmitted photon field through shield as predicted by eq.3 and the spectrum measurements. For this study, integrating type of dosimeters were used with different build up media for sufficiently large time in order to obtain meaningful results. Table. T.3.2 summaries the results.

Table.T.3.2: Mesured dose build up factors in the direct and transmitted bremsstrahlung photon field at Indus-1.

Field conditions	Dose rate without buildup	Dose rate with buildup / material	Buildup factor
Direct photons in the forward direction from storage ring (BM-1 side)	1.0 mR/h	3.0 mR/h / 5mm iron	3.0
	1.0 mR/h	2.0 mR/h / 100 mm water	2.0
Transmitted photons through 50 cm concrete in the forward direction. (BM-1 side)	0.5 mR/h	0.4 mR/h / 5 mm iron	0.8
	255 mR*	185 mR* / 100 mm water	0.73
	380 mR*	280 mR* / 100 mm water	0.74

*Data from DRD (Integrating type)

It can be seen from the table that the dose build up factor is greater than 1 in the direct photon field, whereas it is less than 1 in the transmitted photon field, through 50 cm concrete. Compared with concrete, the present hybrid shielding comprising of mild steel and lead has higher atomic number and hence energy degradation will be more dominant. Therefore the build up factor would be much more less than what is observed for concrete.

8. Summary and conclusions

The experiments on radiation dose build up in and around Indus-1 storage ring was carried out with different radiation detectors and build up medium. The results show that radiation dose increases in the build up medium up to certain depth and declines thereafter in the radiation field around the storage ring within the shielded enclosure and in the streaming radiation field, in accessible areas. Specific studies with a 30 cm water phantom, simulating a human body in the high energy photon radiation field from Indus-1 suggests that conventional radiation monitors when used for radiation dose measurements in high energy bremsstrahlung radiation field, the dose received by the radiation worker is underestimated many fold than $H_p(10)$, the personnel dose equivalent measured by the conventional monitors. The build up of radiation dose was attributed to the generation of electro-magnetic shower within the build up medium, usually initiated when a high energy photon or electron far above the pair-production threshold is incident on the medium. Based on the dose build up experiments and Monte-Carlo calculations, a high energy correction factor of 6.4 was obtained for the radiation monitors within the shielded

enclosures and in the streaming high energy field. This correction is only for application in personnel radiation protection as the factor is deduced based on dose measurements and simulations in water phantom. Applicability of the correction factor was checked outside the shielding by spectrum measurements and dose build up measurements. It is found that no correction needs to be applied for radiation monitors outside the shielded enclosure except at streaming bremsstrahlung photon field. It is concluded from the study that

1. Conventional radiation monitors and dosimeters underestimate dose in high energy photon radiation environment near high energy electron accelerators by many factors.
2. Proper correction needs to be applied to the monitor reading when measured within the shielded enclosure or in the streaming radiation field in order to estimate the dose equivalent correctly.
3. Since radiation dose build up takes place in a material medium when high energy photons are incident, shielding should be sufficiently greater than the shower maximum (X_{max}) in the shield material. Otherwise, high energy photons contribute to the radiation field significantly in accessible areas, which is not desirable.
4. Any non-uniformity or gaps in the shielding structure around the ring can result in streaming of high energy photons to accessible areas.
5. The present study suggests that the presence of high energy photons in accessible areas can be detected by observing radiation dose build up in radiation detectors with proper build up media thereby adequate control measures can be enforced.

ACKNOWLEDGEMENT

The encouragement and fruitful technical discussions by Dr. D.N. Sharma, Head, RSSD, BARC and Dr. P.K. Sarkar, Head, ARSS, BARC on the work are acknowledged. The author acknowledges with gratitude Shri. Gurnam Singh, Head, IOAPDD, RRCAT and his entire team including the acceleration operation crew for providing the accelerator facilities to carry out experiments. The co-operation and enormous technical discussions by members of Health Physics Unit, RRCAT are hereby remembered. Thanks are due to Dr. R.V. Nandedkar, former Head, Synchrotron Utilisation Division for his guidance and discussions.

References

[1] Panosky.W.K.H, *Phys. Today* **33**, 24 (1980).
[2] Herman, W, Synchrotron Radiation Sources A primer, World Scientific Publishing (1994).
[3] Swanson.W.P, Radiological Safety aspects of the operation of electron linear accelerators, *IAEA Tech.Rep.188* (1979).
[4] Radiation protection for particle accelerator facilities, National Council on Radiation Protection & Measurements, *NCRP 144* (2003).
[5] H.J.Bhabha and W.Heitler, *Proc. Royal Soc. of London,* **159**, 432 (1937).
[6] Basic aspects of high energy particle interactions and radiation dosimetry *ICRU Report 28,* International Commission on Radiation Units and Measurements *(1978).*
[7] Swanson.W.P, Dosimetry at high energy particle accelerators, In *Dosimetry of ionizing radiation* Edited by Kase.KR.et.al (1990).
[8] International Commission on Radiation Units and Measurements. Determination of Dose Equivalents Resulting from External Radiation Sources. *ICRU Report 39 International Commission on Radiation Units and Measurements* (1985).
[9] Herman Cember, *Introduction to Health Physics*, 3rd Edition, McGraw-Hill (1996).
[10] Haridas.G, Thakkar.K.K, Pradhan.S.D, Nayak.A.R and Bhagwat.A.M, Response of monitoring instruments to high energy photon radiation, *Nuclear Instrumentation and Methods in Physics Research* **A449**, 624, (2000).
[11] Haridas.G, Nayak.M.K, Dev V., Thakkar.K.K, P.K.Sarkar and Sharma.D.N, *Radiation Protection Dosimetry*, **118**, 233 (2006).
[12] Haridas.G, Bremsstrahlung X-ray dosimetry studies at high energy electron accelerators for personnel protection *Ph.D Thesis* Devi Ahilya Viswa Vidyalaya, Indore(2006).
[13] Nelson..W.R, Hideo Hirayama and Rogers.D.W.O, *The EGS-4 code system*. Report SLAC-265 (1985).
[14] Rogers.D.W.O, Kawrakow.I, Seuntjens.J.P, Walters.B.R.B and Mainegra-Hing.E NRC user codes for EGSnrc, *NRCC Report PIRS-702,* Rev.B (2003).
[15] Haridas.G, Nayak.M.K, Thakkar.K.K, Krishnamachari.G, Anilkumar.S, Kale.M., Nayak.A.R, Sharma.D.N, Abani.M.C, Photon spectrum measurement experiments at Indus-1 Synchrotron Radiation Source, *BARC Report-BARC/2003/I/001* (2003).
[16] Bakshi.A.K, Nayak.M.K, Haridas.G, Chatterjee, Kher.R.K, Estimation of bremsstrahlung photon energy in the environment of high energy electron accelerator using $CaSO_4$:Dy based TL dosimeter. *Radiation Protection Dosimetry* (In Press).

A. Journal Articles

1. Arora P., Chattopadhyay M.K., Roy S.B.
Magnetocaloric effect in MnSi
Applied Physics Letters **91**, 062508-1-3 (2007)

2. Aziz F.*, Chari R., Oak S.M.
Experimental demonstration of fiber differential spectral technique for monitoring small fluctuations in ultrashort laser pulses
Optical Engineering **46**, 073601-1-6 (2007)

3. Babu S. S.*, Babu P.*, Jayasankar C.K.*, Joshi A.S., Speghini A.*, Bettinelli M.*
Laser transition characteristics of Nd^{3+}-doped fluorophosphates laser glasses
J. Non-Cryst. Solids **353**, 1402 (2007)

4. Banerjee Arup
Collective oscillations of a Bose-Fermi mixture: effect of unequal masses of Bose and Fermi particles
Physical Review A **76**, 023611-1-7 (2007)

5. Banerjee Arup, Chakrabarti A., Ghanty T.K.*
Time-dependent density functional theory calculation of Van der Waals coefficient of sodium clusters
J. Chemical Physics **127**, 134103-1-7 (2007)

6. Banerjee Arup, Harbola M.K.*
Comparison of Van der Waals coefficient C_6 of sodium clusters obtained via spherical jellium background model and all electron ab initio method
J. Computational Methods in Science and Engineering **5-6** (2007)

7. Barman S.R.*, Banik S.*, Shukla A.K.*, Kamal C., Chakrabarti A.
Martensitic transition, ferrimagnetism and Fermi surface nesting in Mn_2NiGa
Europhysics Letters **80**, 57002 (2007)

8. Bartwal K.S., Kar S., Kaithwas N.*, Deshmukh M.*, Dave M.*, Lalla N.P.*, Ryu H.*
Synthesis and characterization of $Y_3Al_5O_{12}$ nanocrystals
Advanced Materials Research **26-28**, 667-670 (2007)

9. Chatterjee S., Kumar P.Y.
Simple technique for the fabrication of Penta prism with high accuracy right angle deviation
Applied Optics **46**, 6520-6525 (2007)

10. Chaubey S., Joshi P., Kumar M., Arya R., Nath A.K., Kher S.
Development of long period grating sensors for temperature monitoring
Sadhana **32**, 513519 (2007)

11. Choubey R.K.*, Khattak B.Q., Kar S., Ramshankar P., Sen P.*, Bartwal K.S.
Influence of doping on OH absorption in $LiNbO_3$ crystals
Crystals Res. Technology **42**, 718-722 (2007)

12. Dasgupta, R., Ahlawat, S., Gupta, P.K.
Trapping of micron-sized objects at a liquid-air interface
J. Optics A: Pure and Applied Optics **9**, 189-95 (2007)

13. Delerue N.*, Dixit S. et al
A laser-wire system for the international linear collider
Pramana **69**, 1147-1150 (2007)

14. Ganeev R.A.*, Singhal H., Naik P.A., Chakravarty U., Arora V., Chakera J.A., Raghuramaiah M., Khan R.A., Kumbhare S.R., Kushwaha R.P., Gupta P.D.
Generation of high order harmonics of femtosecond radiation from the surface of various media
Optics & Spectroscopy **103**, 795 (2007)

15. Ganeev R.A.*, Naik P.A., Singhal H., Chakravarty U., Arora V., Chakera J.A., Khan R.A., Raghuramaiah M., Kumbhare S.R., Kushwaha R.P., Gupta P.D.
Generation of high harmonic laser plasma formed on the surface of a silver target
Optics and Spectroscopy **103**, 831 (2007)

16. Ganeev R.A.*, Singhal H., Naik P.A., Gupta P.D.
Single harmonic enhancement at high harmonic generation in GaAs plasma
Quantum Electronics **37**, 827 (2007)

17. Ganguli T., Porwal S., Sharma T., Ingale A., Kumar S., Tiwari P., Balamurugan A.K.*, Rajagopalan S.*, Tyagi A.K.*, Chandrasekaran K.S.*, Arora B.M.*, Rustagi K.C.*
Growth of strained ZnSe layers on GaAs substrates by pulsed laser deposition carried out in an off-axis deposition geometry
Thin Solid Films **515**, 7834-7842 (2007)

18. George, J., Mehandale, S.C., Sigh, B.P.*, Nathan, T.P.S.*
A study of the effect of axial mode spacing on the single longitudinal mode performance in end pumped solid-state lasers
Optics & Laser Technology **39**, 1193-8 (2007)

19. Ghosh H.
Excited state nonlinear optics of quasi-one-dimensional Mott-Hubbard insulators
Phys. Rev. B **75**, 235127- (2007)

20. Gupta P.K., Kush P.K., Tiwari A.*
Second law analysis of counter flow cryogenic heat exchangers in presence of ambient heat-in-leak and longitudinal conduction
***International J. Heat and Mass Transfer* 50**, 4754476 (2007)

21. Gupta, S.K., Niranjan, M.S.*, Kak A.
A study on the effect of brazing time on element diffusion silver diffusion into the base metal was examined for different brazing times
***Welding Journal* 86**, 47-50 (2007)

22. Jayabalan J., Singh A., Chari R., Oak S.M.
Ultrafast third-order nonlinearity of silver nanospheres and nanodiscs
***Nanotechnology* 18**, 315704-1-6 (2007)

23. Jejurikar S.M.*, Koinkar P.M.*, More M.A.*, Joag D.S.*, Adhi K.P.*, Kukreja L.M.
Field emission studies of nano structured c-axis oriented GaN film on SiO_x/Si(100) by pulsed laser deposition
***Solid State Comm.* 144**, 296-299 (2007)

24. Jejurikar S.M.*, Banpurkar A.G.*, Bankar D.N.*, Adhi K.P.*, Kukreja L.M., Sathe V.G.
Growth temperature and N_2 ambient pressure dependent crystalline orientations and band-gaps of pulsed laser deposited AlN / (0001) sapphire thin films
***J. Crystal Growth* 304**, 257-267 (2007)

25. Joshi P., Sharma R.K., Kishore J., Kher S.
Fabrication of photonic crystal fibre
***Current Science* 93**, 1214-1215 (2007)

26. Kadir A.*, Ganguli T., Kumar R., Gokhale M.R.*, Shah A.P.*, Ghosh S.*, Arora B.M.*, Bhattacharya A.*
The role of hydrostatic stress in determining the bandgap of InN epilayers
***Applied Physics Letters* 91**, 111913-1-3 (2007)

27. Kaithwas N.*, Deshmukh M.*, Kar S., Dave M.*, Lalla N.P.*, Ryu H.*, Bartwal K.S.
Preparation of $Y_3Al_5O_{12}$ nanocrystals by low temperature glycol route
***Crystal Res. Technology* 42**, 991-994 (2007)

28. Kamal C., Chakrabarti A.
Comparison of electronic and geometric structures of nanotubes with subnanometer diameters: a density functional theory study
***Physical Review B* 76**, 075113 (2007)

29. Kar S., Bartwal K.S.
Growth optimization of $Li_2B_4O_7$ crystals and their characterization
***Crystal Growth & Design* 7**, 2522-2525 (2007)

30. Karmakar S.*, Kulkarni N.V.*, Sathe V.G.*, Srivastava A.K., Shinde M.D.*, Bhoraskar S.V.* Das A.K.*
A new approach towards improving the quality and yield of arc-generated carbon nanotubes
***J. Physics D: Applied Physics* 40**, 4829-4835 (2007)

31. Kher S., Joshi P., Sharma R.K.
Radiation effects on pure silica core multimode fibres: radiation hardness issues for fibre optic sensors for particle accelerators and nuclear power stations
***Nuclear Instruments & Methods in Physics Research: Section A* 378**, 345-347 (2007)

32. Kheraj V.*, Panchal C.J.*, Patel P.K.*, Arora B.M.* Sharma T.K.
Optimization of facet coating for highly strained InGaAs quantum lasers operating at 1200nm
***Optics & Laser Technol.* 39**, 1395-1399 (2007)

33. Kim Kwang-Je* , Kumar V.
Electron beam requirements for a three-dimensional Smith-Purcell backward-wave oscillator for intense terahertz radiation
***Physical Review Special Topics - Accelerators and Beams* 10**, 080702-1-8 (2007)

34. Late D.J.*, More M.A.*, Misra P., Singh B.N., Kukreja L.M., Joag D.S.*
Field emission studies of pulsed laser deposited LaB_6 films on W and Re
***Ultramicroscopy* 107**, 825-832 (2007)

35. Lim H-H*, Prakash O., Kim B-J*, Pandiyan K.*, Cha M.*, Rhee B.K.*
Ultra-broadband optical parametric generation and simultaneous RGB generation in periodically poled lithium niobate
***Optics Express* 15**, 18294-18299 (2007)

36. Manekar M., Mukherjee C., Roy S.B.
Imaging of time evolution of the first-order magneto-structural transition in Fe-Rh alloy using magnetic force microscopy
***Europhysics Letters* 80**, 17004-1-8 (2007)

37. Markna J.H.*, Parmar R.N.*, Vachhani P.S.*, Kuberkar D.G.*, Misra P., Singh B.N., Kukreja L.M.
Enhancement of electronic transport and magnetoresistance of Al_2O_3 impregnated $(La_{0.5}Pr_{0.2})Sr_{0.3}MnO_3$ thin films
***Europhysics Letters,* 79,** 17005: 1-5 (2007)

38. Mishra S.*, Ingale A., Roy U.N.*, Gupta A.*
Study of annealing-induced changes in CdS thin films using x-ray diffraction and Raman spectroscopy
Thin Solid Films **516**, 91 (2007)

39. Mishra S.R., Tiwari S.K., Ram, S.P., Mehendale S.C.
Generation of hollow conic beams using a metal axicon mirror
Optical Engineering **46**, 084002-1-5 (2007)

40. Misra P., Ranganathan K., Muthukumaran N., Nathan T.P.S.*
Edge-pumped, folded zig-zag Nd:YAG slab laser
Optics & Laser Technol. **39**, 1269-1272 (2007)

41. Misra P., Sharma T.K., Kukreja L.M.
Temperature dependent photoluminescence from ZnO/MgZnO multiple quantum wells grown by pulsed laser deposition
Superlattices & Microstructures **42**, 212-217 (2007)

42. Mohanty S.K*., Gupta P.K., Verma R.S.
Self-rotation of an assembly of two or more cylindrical objects in optical tweezers: a simple approach for realization of optically driven micromotors
Current Science **93**, 695-698 (2007)

43. Patro P.K.*, Kulkarni A.R.*, Gupta S.M., Harendranath C.S.*
Improved microstructure, dielectric and ferroelectric properties of microwave-sintered $Sr_{0.5}Ba_{0.5}Nb_2O_6$
Physica B: Cond. Matter **400**, 237-242 (2007)

44. Prakash O., Mahakud R., Biswal R., Shrikanth G., Vora H.S., Dixit S.K.
Study on the quality of interference fringes from a pulsed UV source for application in a biprism based fiber Bragg grating writing
Applied Optics **46,** 6210-1-8 (2007)

45. Rajendiran P., Parihar Y. S., Deshpande A.U.
Automated bibliographic record capturing from web OPAC and online bibliographic database for library cataloguing in LibSys
Annals of Library and Information Studies **54**, 140-145 (2007)

46. Rao B.S., Naik P.A., Arora V., Khan R.A., Gupta P.D.
Angular distribution and dose measurements of hard x-ray emission from intense laser-plasma interaction
J. Applied Physics **102**, 063307-1-4 (2007)

47. Rawat A., Vyavahare P.D.*, Ramani A.K.*
Enhanced DSR for MANET with improved secured route discovery and QoS
International J. on Network Security **5,** 158-166 (2007)

48. Roy S. B., Chattopadhyay M. K.
Low temperature magnetic response of MnSi: Thermomagnetic history effects, metamagnetic transition and the kinetic arrest of the reverse transition.
Europhysics Letters **79,** 47007 (2007)

49. Sailaja R. *, Bisht P.B.*, Singh C.P., Bindra K.S., Oak S.M.
Influence of multiphoton events in measurement of two-photon absorption cross-sections and optical nonlinear parameters under femtosecond pumping
Optics Communications **277**, 433-39 (2007)

50. Selvamani R., Bhattacharyya S., Gupta S.M.
Dielectric properties and ac-conductivity analysis of $Bi_{3.25}La_{0.75}Ti_3O_{12}$ ceramic using impedance spectroscopy
J. Chem. & Physics of Solids **10**, 1016-(2007)

51. Sharma S., Jajoo A., Dube A.
5-Aminolevulinic acid-induced protoporphyrin-IX accumulation and associated phototoxicity in macrophages and oral cancer cell lines.
J. Photochemistry and *Photobiology B: Biology* **88,** 156162 (2007)

52. Sharma V. K., Chattopadhyay M. K., Kumar R., Ganguli T. Tiwari P., Roy S. B.
Magnetocaloric effect in Heusler alloys $Ni_{50}Mn_{34}In_{16}$ and $Ni_{50}Mn_{34}Sn_{16}$
J. Phys.: Condensed Matter **19,** 496207-(2007)

53. Sharma V. K., Chattopadhyay M. K., Roy S.B.
Kinetic arrest of the first order austenite to martensite phase transition in $Ni_{50}Mn_{34}In_{16}$: dc magnetization studies
Physical Review B **76**, 140401 (R) (2007)

54. Singh N.
Single mode operation of a narrow bandwidth dye laser using a single prism, grazing incidence grating long cavity
Optics & Laser Technol. **39**, 1140-1143 (2007)

55. Singh Rashmi., Khardekar R.K., Kumar A., Kohli D.K.
Preparation and characterization of nanocrystalline Nd-YAG powder
Materials Letters **61**, 921-924 (2007)

56. Sridhar R., Shukla S.K.
Design of the vacuum system for the LHC beam dump lines
Bulletin of Indian Vacuum Society **10**, 15-18 (2007)

57. Srikanth G.
Measurement of period of interference patterns with sub-micron period
Optics & Laser Technology **39**, 918-921 (2007)

58. Srivastava A., Patel H.S., Gupta P.K.
A view-based approach for the reconstruction of optical properties of turbid media
Current Science **93**, 359-65 (2007)

59. Srivastava H., Tiwari P., Srivastava A.K., Nandedkar R.V.
Growth and characterization of a-Fe_2O_3 nanowires
J. Applied Physics **102**, 054303-1-5 (2007)

60. Sundar R., Ranganathan K., Nath A.K.
Performance studies of diode-side-pumped CW Nd:YAG laser in copper coated optical pump cavity
Optics & Laser Technol. **39**, 1426-1431 (2007)

61. Tiwari A.K., Poddar D.R.*, Das B.N.*
On the equivalent radius of a radiating slot in impedance calculations
Progress in Electromagnetics Research **74**, 47-56 (2007)

62. Upadhyaya B.N., Chakravarty U., Kuruvilla A., Thyagarajan K., Shenoy M.R., Oak S.M.
Mechanisms of generation of multi-peak and mode-locked resembling pulses in Q-switched Yb-doped fiber lasers
Optics Express **15**, 11576-11588 (2007)

63. Verma Y., Rao K.D., Mohanty S.K.*, Gupta P.K.
Optical coherence tomography using a tapered single mode fiber tip
Laser Physics Letters **4**, 686-689 (2007)

B. Invited Talks

1. Banerjee Arup
Collective oscillation of Bose-Einstien condensates
Theoretical Physics Seminar Circuit, Chandigarh, October 2007

2. Ganesamoorthy S.
Growth of relaxor ferroelectric single crystals and their characterization
12th National Seminar on Crystal Growth, Kalpakkam, 21-23 Dec. 2007

3. Gupta P.D.
Laser wake field electron acceleration using intense ultrashort laser pulses
National Laser Symposium -7, Vadodara, Dec. 2007

4. Gupta P.K.
Biomedical applications of lasers
Indo-French Workshop Lasers, Quantum Optics and Biophysics, France, 29 Oct.-2 Nov. 2007

5. Gupta P.K.
Biomedical applications of lasers
Indo-Japanese Workshop on Recent Developments in Optics and Photonics, New Delhi, 14 Dec. 2007

6. Gupta P.K.
Laser manipulation of microscopic objects some recent developments
3rd Asian and Pacific Rim Symposium on Biophotonics in conjunction with ***Biophotonics Downunder***, Cairns, 9 - 11 July 2007

7. Gupta P.K.
Nano science and technology: activities at RRCAT
IBSA (India, Brazil & South Africa) Nanotechnology Meeting, Pretoria, 20-22 Nov. 2007

8. Gupta P.K.
Optical techniques for biomedical imaging and diagnosis
International workshop on Physics in Biology: a synergy, Hyderabad, 12-14 Dec. 2007

9. Joshi M.P.
Optoelectronic properties of photo-oxidized and photodegraded aromatic diamine TPD dye
IUMRS International Conference on Advanced Materials, Bangalore, Oct. 2007

10. Kukreja L.M.
Pulsed laser growth of nanostructured materials: some recent experiments
DAE-BRNS 4th National Symposium on Pulsed Laser Deposition of Thin Films and Nanostructured Materials, Rajkot, Oct. 2007

11. Kukreja L.M.
Conduction electrons in ZnO
National Conference on New Horizons in Theoretical and Experimental Physics, Cochin, Oct. 8 - 10, 2007

12. Kukreja L.M.
Annealed ZnO films: some mysteries
Sonderforschungsbereiche lectures, Ulm, Nov. 27, 2007

13. Kukreja L.M.
Electrical properties of ZnO films annealed at different temperatures
Applied Physics Seminars, Karlsruhe, Nov. 2007

14. Moorti A.
Cathode plasma jet pinching, intense x-ray emission, and fast ion generation in laser-triggered vacuum discharge
22nd National Symposium on Plasma Science & Technology, Ahmedabad, Dec. 8, 2007

15. Naik P.A.
High order harmonic generation and other ultrashort pulse laser-plasma interaction studies at RRCAT
Asia Pacific Plasma Theory Conference, Gandhinagar, Dec. 12, 2007

16. Naik P.A.
Laser-plasma based electron acceleration
22nd National Symposium on Plasma Science & Technology, Ahmedabad, Dec. 11, 2007

17. Raja S.S.
Laser based instruments for the nuclear fuel cycle
National Laser Symposium -7, Vadodara, Dec. 2007

18. Shinde R.S.
Recent trends in microwave ferrite technology for high power applications in research and industries
AICTE Sponsored Winter School on Ferroic Ceramics, Kharagpur, 5-16 Nov. 2007

19. Shinde R.S.
Challenging scenario in design of magnetic ceramics-ferrites & its measurement techniques in magnetic ceramic
AICTE Sponsored Winter School on Ferroic Ceramics, Kharagpur, 5-16 Nov. 2007

C. Seminars / Conference Presentations

C1. DAE-BRNS National Laser Symposium, Vadodara, Dec. 16-20, 2007

1. Agnihotri V., Ranganathan K., Hedaoo P., Misra P., Kumar M., Arya R., Oak S.M.
Diode-end-pumped, A-O q-switched Nd:YVO_4 laser for marking applications

2. Alimardani M.*, Paul C.P., Toyserkani E.*
Effects of the geometrical and temporal thermal variations on the stress fields formed in automated laser fabrication process

3. Ansari M.S., Singh B., Chandra R., Navathe C.P.
Development of pulse forming network for large size disk amplifiers in Nd:glass laser chain

4. Arora V., Singhal H., Naik P.A., Khan R.A., Gupta P.D.
Experimental study of K-shell line emission from magnesium plasma produced by ultrashort laser pulses

5. Arora V., Singhal H., Naik P.A., Kumbhare S.R., Gupta P.D.
Optimization of the K_α radiation produced by interaction of high intensity femtosecond laser pulses with thick titanium foils

6. Ashok P.C., Dasgupta R., Gupta P.K.
Measurement of axial position spectrum of trapped microspheres using image correlation technique

7. Bhandare R., Dave I., Raja S.S.
USB: a better choice for automation and control of tabletop instruments for physics based experiments

8. Bhatnagar P., Benerji N.S., Shrivastava B.B., Mittal J.K.
A generalized diffraction filtered resonator with a KrF excimer laser

9. Biswal R., Agrawal P.K., Dixit S.K., Mittal J.K.
On the production and use of fractionally distilled HBr gas to improve Cu:HyBrID performance

10. Chakravarty U., Upadhyaya B.N., Kuruvilla A., Oak S.M.
A high-power superfluorescent fiber source using Yb-doped double-clad fiber

11. Chakravarty U., Naik P.A., Khan R.A., Gupta P.D.
A novel method of intense keV x-ray generation from *in situ* produced silver clusters using Ti:sapphire laser pulses

12. Choubey A., Agrawal D.K., Vishwakarma S.C., Upadhyaya B.N., Ali S., Jain R.K., Sah S.K., Arya R., Joseph J.*, Kashi V. K.V.*, Oak S.M.
Laser cutting of fast breeder test reactor fuel subassembly in hot cell

13. Choubey A., Jain R.K., Agrawal D.K., Vishwakarma S.C., Upadhyaya B.N., Oak S.M.
Effect of pulse duration and spot overlap on laser cleaning with Nd:YAG laser

14. Daulatabad S.R., Subramanyam V.V., Chakraborty A., Singh B.
CAT-EYE resonator for high power copper vapour laser

15. Dubey V.K., Singh I.J., Jain R., Saxena P., Vora H.S., Mittal J.K.
A 6 channel nanosecond programmable time delay generation unit for a CVL MOPA system

16. George M.*, Munnera C.I.*, Singh C.P., Bindra K.S., Oak S.M.
Nonlinear optical studies in neutral red dye under nanosecond laser pulse excitation

17. George J., Oak S.M.
Effect of first oscillating mode location drift on single longitudinal mode performance

18. George J., Oak S.M.
Effect of pump spectra on single longitudinal mode performance

19. Jain L., Palod S., Bhanage V.P., Bhujle A.G., Navathe C.P.
Control system for experiments with laser cold atoms

20. Joshi M.J., Deshpande P.P., Navathe C.P.
Control system for laser marking system

21. Jayabalan J., Singh A., Chari R., Mukhopadhaya P.K., Srivastava H., Oak S.M.
Nanosecond laser induced de-aggregation of silver nanoprism aggregates

22. Kar S., Verma S., Patoliya N.*, Bartwal K.S.
Growth and characterization of pure and Mn doped $Li_2B_4O_7$ single crystals

23. Khan S., Jayabalan J., Chari R., Pal S., Porwal S., Sharma T.K., Oak S.M.
Transient reflectivity in GaAsP/AlGaAs quantum wells

24. Kumar A., Upadhyaya B.N., Oak S.M.
Real time analysis of laser weld pool characteristics

25. Kumar P.*, Moorthy Babu S.*, Ganesamoorthy S., Bhaumik I., Karnal A.K., Kanjilal D.*
Effect of H^+ ion implantation on the surface and structural properties of lithium niobate for optical waveguide application.

26. Mahakud R., Prakash O., Dixit S.K.
Analysis of the fiber Bragg grating written using second harmonic of copper vapor laser

27. Malik A., Sundar S.S., Raja S.S.
Alignment tolerancing in pre-aligned sealed nitrogen laser tube

28. Mendhe G., Rao B.T., Tiwari P., Kaul R., Shenoy N.M., Nakhe S.V., Oak S.M.
Experimental study on laser marking and micro-drilling with copper vapor laser

29. Mishra S.K., Aneesh K., Nigam S., Navathe C.P.
An air-core differentiating Rogowski coil for measuring fast high current in capillary discharge plasma experiment

30. Mishra S.R., Ram S.P., Tiwari S.K., Mehendale S.C.
Use of a hollow laser beam to improve atom transfer in a double-MOT system

31. Mokhariwale A., Bahadur R., Nakeh S.V.
Development of a capacitor charging power supply for excimer laser

32. Mukherjee C., Rajiv K., Mittal J.K.
Effect of moisture on thin film Fabry-Perot filter

33. Nakhe S.V., Mishra R.K., Tiwari G.N., Mittal J.K., Sinha A.K., Bhatt S.*, Vohra R.S.*, Jawale S.B.*, Sutha R.L.*, Singh S.*, Paramjit*, Mishra S.K.*, Gantayet L.M.
Development of 40W copper vapour laser operating at 9 kHz pulse repetition rate

34. Nayak I., Mishra R.K., Tiwari G.N., Nakhe S.V., Mittal J.K.
Development of 4 watt sealed off copper bromide laser

35. Nigam S., Mishra S.K., Prasad Y.B.S.R., Tripathi P.K., Aneesh K., Kushwaha R.P., Navathe C.P., Naik P.A., Gupta P.D.
Development of a high current fast capillary discharge plasma system

36. Palod S., Deshpande P.P., Bhanage V.P., Navathe C.P.
Virtual instrumentation for automating laser based experiments

37. Pathak A.K., Oak S.M.
Data acquisition software for laser material processing

38. Patidar R.K., Sharma A.K., Raghuramaiah M., Joshi R.A., Naik P.A., Gupta P.D.
Development of an Nd:phosphate glass laser system delivering 1J/1ns laser pulses for prototype study of optical parametric amplification of chirped pulses

39. Rajan C., Malik A., Dobale A.R.*, Sundar S.S.
Amplifier circuit for pulsed photo-acoustic spectroscopy system

40. Ram S.P., Mishra S.R., Tiwari S.K.
Generation of optical pulses with a variable delay from a single beam using AOMs in tandem: application to temperature measurement of cold atoms

41. Ram S.P., Tiwari S.K, Jayabalan J., Mishra S.R.
Measurement of a narrow spot-size by scanning of single pixel of a CCD camera

42. Ranganathan K., Sundar R., Hedaoo P., Oak S.M.
Thermal characteristics of flashlamp-pumped Nd:YAG laser : Heat-capacity mode of operation

43. Rao B.T., Singh J.*, Nath A.K.*, Oak S.M.
Effect of CO_2 laser pulse parameters on cut edge quality of mild steel

44. Rao B.T., Singh C.H.P., Kaul R., Nath A.K., Oak S.M.
Characteristics of laser cut stainless steel edges produced by pulsed mode CO_2 Laser

45. Samuel P.*, Senthil K. A. *, Moorthy Babu S.*, Ganesamoorthy S., Karnal A.K., Bhaumik I., Palanisamy P.K.*
Growth and characterization of Nd:KGW laser material.

46. Saxena P., Sharangpani K.K., Jain R., Talwar S., Dubey V.K., Singh I.J., Vora H.S.
SSV a real time integrated control electronics for automation of a CVL MOPA system

47. Sharma A., Arya R., Oak S.M.
Energy meter circuit for quasi-CW lasers

48. Sharma A.K., Patidar R.K., Raghuramaiah M., Naik P.A., Gupta P.D.
A new and simple method of temporal shaping of laser pulses

49. Sharma S.K., Singh A.J.*, Mukhopadhyay P.K., Ranganathan K., Oak S.M.
Reduction of fall time of intracavity frequency doubled AO q-switched green laser pulses

50. Sharma S.K., Singh Y.
In-situ investigation of saturation temperature of KDP solution for bulk crystal growth

51. Sharma T.K, Rawat P.*, Dixit V.K., Ganguli T., Jangir R., Pal S., Porwal S., Kumar R., Khakha A., Kheraj V.*, Singh S.D., Oak S.M.
Development of red laser diodes utilizing MOVPE grown InGaP quantum wells

52. Shenoy N.M., Sharangapani K.K., Tiwari G.N., Nakhe S.V., Mittal J.K.
Precision marking on metal surfaces using 8 W Cu-Br laser

53. Sheth S.S., Joshi O.P., Oak S.M.
DSP based embedded PMDC motor drive for laser material processing

54. Shukla S.*, Verma Y., Sahu K., Rao D.K., Dube A., Gupta P.K.
Effect of He-Ne laser irradiation on hair follicle growth in testosterone treated mice investigated with optical coherence tomography and histology

55. Singh A.J.*, Sharma S.K., Mukhopadhyay P.K., Ranganathan K., Oak S.M.
Efficient and high power green beam generation using water cooled non gray track resistant KTP crystal

56. Singh B., Subramanyam V.V., Daulatabad S.R., Chakraborty A.
Development of near 100 watt copper vapour lasers (KE-CVLs)

57. Singh B., Subramaniam V.V., Daulatabad S.R., Chakraborty A.
Output characteristics of a 77 W kinetically enhanced copper vapour laser

58. Singhal H., Chakravarty U., Rao B.S., Arora V., Naik P.A., Gupta P.D.
Dependence of high order harmonic intensity on the length of plasma plume : phase matching and absorption effects

59. Shukla P., Mishra G.K., Saxena P., Srivastava V.K., Talwar S., Khare R.
A novel confocal scheme for temporal stretching of laser pulses

60. Shukla S.*, Verma Y., Sahu K., Rao D.K., Dube A., Gupta P.K.
Effect of He-Ne laser irradiation on hair follicle growth in testosterone treated mice investigated with optical coherence tomography and histology

61. Shukla V., Bindra K.S.
Synthesis of Si nano-particles by laser ablation and optical limiting studies

62. Sudagar R.*, Chari R.
Ultrashort pulse diagnostics using a single mode fibre

63. Sundar R., Ranganathan K., Oak S.M.
Flat top beams from Gaussian mirrors: an experimental study

64. Sundar S.S.*, Rajan C., Raja S.S.
Alternative excitation sources for fluorescence based trace detection of uranium

65. Tiwari S.K., Ram S.P., Mishra S.R., Mehendale S.C.
Generation of a narrow non-diffracting beam using a metal axicon mirror

66. Tiwari V.B., Singh S., Rawat H.S., Singh M.P., Mehendale S.C.
Cold atomic pulses from a magneto-optical trap

67. Upadhyaya B.N., Vishwakarma S.C., Ali S., Bhawsar V., Sah S.K., Arya R., Agrawal D.K., Jain R.K.,

Choubey A., Oak S.M.
Development of an efficient 880 W CW Nd:YAG laser

68. Upadhyay J., Joshi M., Deshpande P.P., Sharma M.L., Navathe C.P.
A programmable high voltage variable slope ramp generator

69. Vachhani D.M., Arya R., Oak S.M.
Constant current capacitor charging power supply based on high-frequency, zero-voltage switched LCL-T resonant converter

70. Verma R.S., Swami M.K., Manhas S., Gupta P.K.
Mueller matrix based optimization of reflective type twisted nematic liquid crystal spatial light modulator for phase only modulation

71. Verma S.
Development and application of optical diagnostics for imaging crystal growth from solution (Ph.D. thesis summary)

72. Verma S., Depty E.*
Influence of pH on the growth rate and morphology of KDP crystals

73. Vishwakarma S.C., Jain R.K., Upadhyay B.N., Choubey A., Agrawal D.K., Oak S.M.
Development of in-situ laser based cutting technique for shock absorber rear nut in pressurized heavy water reactors

74. Vishwakarma S.C., Jain R.K., Upadhyaya B.N., Choubey A., Agrawal D.K., Oak S.M.
Development of in-situ laser based cutting technique for shock absorber rear nut in pressurized heavy water reactors

C.2 52nd DAE Solid State Physics Symposium
Mysore, 27-31 December 2007

1. Arora P., Chattopadhyay M.K., Roy S.B.
Magnetocaloric effect in MnSi : magnetization and heat capacity

2 Kamal C., Banerjee A., Chakrabarti A.
Time-dependent density functional theory calculation of van der Waals coefficients of small sodium and carbon clusters and C_{60}

3. Kumar P.*, Moorthy Babu S.*, Ganesamoorthy S., Bhaumik I., Karnal A.K., Kanjilal D.*
Development of proton implanted optical waveguides in lithium niobate.

4. Mondal P., Manekar M., Kumar R., Ganguli T., Roy S. B.
Structural and superconducting properties of as-cast Nb_3Al

5. Samuel P.*, Senthil K. A. *, Moorthy Babu S.*, Ganesamoorthy S., Karnal A.K.
Growth and characterization of Nd and Yb doped $KGd(WO_4)_2$ single crystals.

6. Sharma V. K., Chattopadhyay M. K., Chouhan A., Arora P., Kumar R., Ganguli T., Roy S. B.
Effect of annealing on the martensitic transition in $Ni_{50}Mn_{34}In_{16}$ alloy

7. Sharma V. K., Chattopadhyay M. K., Chouhan A., Arora P., Roy S. B.
Field induced martensite to austenite transition in $Ni_{50}Mn_{34}In_{16}$ alloy

8. Sokhey K. J. S., Manekar M., Chouhan A., Choudhary R.J.*, Gupta P., Phase D. M.*, Lodha G. S., Roy S. B.
Electrical transport study of laser ablated Co_2TiSn thin films

9. Verma S., Depty E., and Gupta P.K.
Strength of free convection during KDP growth and its relation to crystal quality

C.3 Other Seminars / Conference Presentations

1. Adhi K.P.*, Jejurikar S.M.*, Koinkar P.M.*, More M.A.*, Joag D.S.*, Kukreja L.M.
Nanostructured GaN and InN films for field emission devices
Proc. IUMRS-ICAM 2007, Bangalore, Oct. 2007

2. Agrawal S.*, Borage M., Tiwari S., Saxena R.*
Issues in the application of lossless turn-off snubber in high-power, high-frequency applications
National Systems Conference, Dec. 2007

3. Bansod T.*, Shukla S.K., Kumar KVANPS, Kotaiah S.
Study of initial dynamic pressure rise behaviour in Indus-2
International Symposium on Vacuum Science & Technology, Mumbai, 28-30 November 2007

4. Bhardwaj S.*, Borage M., Tiwari S.
Simplified loss analysis and comparison of full-bridge, full-range-ZVS, DC-DC converters
National Power Electronics Conference, December 2007

5. Chakrabarti A., Kratzer P.*, Liu K.K.*, Scheer M.*
Evidence of shape transition of InAs quantum dots on

$In_{0.5}Ga_{0.5}As/InP$ (001) from theoretical study
IUMRS-ICAM 2007, Bangalore, October 2007

6. Das A.K.*, Singh B.N., Misra P., Kukreja L.M.
Studies on Si doped ZnO thin films grown by sequential pulsed laser deposition
4th National Symposium on Pulsed Laser Deposition of Thin Films and Nanostructured Materials, Rajkot, 3-5 Oct. 2007

7. Dev V., Haridas P., Nayak M.K., Verma D., Haridas G.
Response check of ambient synchrotron radiation monitors
National Symposium on Radiation Protection, Kolkata, Nov. 2007

8. Dev V., Nayak M.K., Kumar V., Sahani P.K., Verma D., Haridas G., Thakkar K.K., Sarkar P.K., Sharma D.N.
Effect of storage ring shutdown on radiation level around Indus-1 synchrotron radiation source
National Symposium on Radiation Protection, Kolkata, Nov. 2007

9. Dixit V.K, Ganguli T., Sharma T.K., Singh S.D., Kumar R., Porwal S., Tiwari P., Ingale A., Oak S.M.
Two step growth process of GaP epitaxial layer grown on n-type Si (001) using MOVPE
IUMRS-ICAM 2007, Bangalore, October 2007

10. Dixit V.K., Singh S.D., Sharma T.K., Ganguli T., Jangir R., Pal S., Khattak B.Q., Srivastava A.K., Srivastava H., Oak S.M.
Studies on GaAs/AlGaAs based (p and n-type) quantum well infrared photodetector structures grown using metal organic vapour phase epitaxy
XIV International Workshop on Physics of Semiconductor Devices, Mumbai, Dec. 2007

11. Ganguli T., Kadir A.*, Gokhale M.*, Kumar R., Shah A.P.*, Arora B.M.*, Bhattacharya A.*
Study of the microstructure in MOVPE grown InN epitaxial layers by high resolution X-ray diffraction
XIV International Workshop on Physics of Semiconductor Devices, Mumbai, 17-20 December 2007

12. Gilankar S.G., Kush P.K.
Experimental verification of capture coefficients for a cylindrical cryopanel of closed cycle refrigerator based cryopump
International Symposium on Vacuum Science & Technology, Mumbai, 28-30 November 2007

13. Haridas G., Nayak M.K., Dev V., Thakkar K.K., Sarkar P.K., Sharma D.N.
Electron depth dose a tool for radiation safety programme in high energy electron accelerators
National Symposium on Radiation Protection, Kolkata, November 2007

14. Joshi P., Chaubey S., Kher S.
Influence of boron co-doping on temperature sensitivity of long period gratings in optical fibre
ICMAT 2007, Singapore, July 2007

15. Kamal C., Chakrabarti A.
Interesting trends in electronic structure of ultra-small carbon nanotubes: a first principles study
IUMRS-ICAM 2007, Bangalore, October 2007

16. Kher S., Joshi P., Chaube S., Oak S.M.
Design and development of compact sensing head based on single long period fiber grating for simultaneous temperature and strain measurements
National Conference on "Advances in Sensors for Aerospace Applications, Hyderabad 14-15 December 2007

17. Krishnan S.R.*, Bindra K.S., Oak S.M.
Development of sensitive photo diode based high dynamic range laser power meter using microcontroller
National Symposium on Instrumentation, Tiruchengode, 24-26 October 2007

18. Kumar A., Senecha V.K., Kotaiah S.
Cusp magnetic field configuration and heat removal system design studies for the H- ion plasma chamber
DAE-BRNS-PSI Symposium on Ion Beam Technology and Applications (SIBTA07),, Mumbai, Sept. 2007

19. Misra P.*, Sharma T.K.*, Prinz G.M.*, Thokne K.*, Kukreja L.M.
Photoluminescence from ultra-thin ZnO/ZnMgo quantum wells
Proc. IUMRS-ICAM 2007, Bangalore, Oct. 2007

20. Misra P., Sharma T.K., Kukreja L.M.
Basic photoluminescence processes at different temperatures in ZnO / (0001) sapphire thin films grown by pulsed laser deposition
4th National Symposium on Pulsed Laser Deposition of Thin Films and Nanostructured Materials, Rajkot, 3-5 October 2007

21. Moorti A., Naik P.A., Gupta P.D.
Experimental study of high-energy ion generation in a vacuum discharge triggered by multi-ps laser pulses
22nd National Symposium on Plasma Science & Technology, Ahmedabad, Dec. 6-10, 2007

22. Moorti A., Naik P.A., Gupta P.D., Bhat R.K.
Intense x-ray emission from plasma pinching in a

multi-ps laser-triggered vacuum discharge in non-coaxial geometry
22nd National Symposium on Plasma Science & Technology Ahmedabad, Dec. 6-10, 2007

23. Nayak M.K., Verma D., Dev V., Kumar V., Sahani P.K., Haridas G., Thakkar K.K., Kumar M.*, Prasad L.C.*, Sarkar P.K.*, Sharma D.N.*
Radiation energy estimation during Ti-sapphire laser plasma experiments at RRCAT, Indore
National Symposium on Radiation Protection, Kolkata, November 2007

24. Pal S., Ingale A., Dixit V.K., Sharma T.K., Porwal S., Mukharjee C., Oak S.M.
Comparative studies on as-grown and nanotextured GaN:Mg epilayer
XIV International Workshop on Physics of Semiconductor Devices, Mumbai, 17-20 Dec. 2007

25. Petwal V.C., Rao J.N., Bapna S.C., Subbaiah K.V.*
Dose profiles for EB radiation processing: comparing Monte Carlo simulation and experimental data
17th National Symposium on Radiation Physics, Kolkata, 16-18 November 2007

26. Prasad Y.B.S.R., Nigam S., Mishra S.K., Aneesh K., Tripathi P.K., Kushwaha R.P., Naik P.A., Navathe C.P., Gupta P.D.
Initial results from the high voltage capillary discharge experiment
22nd National Symposium on Plasma Science & Technology, Ahmedabad, Dec. 6-10, 2007

27. Rao B.S., Arora V., Naik P.A., Khan R.A., Gupta P.D.
Energy spectrum measurement of fast electrons produced in ultra-intense laser-plasma interaction
22nd National Symposium on Plasma Science & Technology, Ahmedabad, Dec. 6-10, 2007

28. Rao B.S., Naik P.A., Singhal H., Arora V., Chakravarty U., Khan R.A., Gupta P.D., Nakajima K.*, Kameshima T.*
Initial experiments on laser based electron acceleration at RRCAT, Indore
Laser and Plasma Accelerators Workshop 2007, Azores, Portugal, 9-13 July, 2007

29. Rathore S.S.*, Das A.K.*, Singh B.N., Misra P., Kukreja L.M.
Studies on CoZnO thin films grown by pulsed laser deposition,
4th National Symposium on Pulsed Laser Deposition of Thin Films and Nanostructured Materials, Rajkot, 3-5 October 2007

30. Ratnakala K.C., Tiwari S.K., Shukla S.K., Kotaiah S.
Out gassing rate measurement of copper plated stainless steel
International Symposium on Vacuum Science & Technology), Mumbai, 28-30 November 2007

31. Rawat A., Gupta A.*, Gupta S.*
Evaluation of Sybil attack prevention in SRP for MANETs
International Conference on Sensor and Related Networks 2007, Vellore, Dec.2007

32. Rawat A., Vyavahare P.D.*, Ramani A.K.*
Improved system components for secure data communication in MANETs using secured DSR
IEEE Third International Conference on Wireless Communications and Sensor Networks, Allahabad,13-15 December 2007.

33. Rawat A., Vyavahare P.D.*, Ramani A.K.*
Implications of proactive route discovery in MANET's on-demand routing protocols
International Conference on Sensor and Related Networks 2007, Vellore, Dec. 2007

34. Sahu K., Rai R., Sharma M., Bansal H., Gupta P.K.
Effect of methylene blue photosensitization on antibiotic resistance of E. coli
International conference on frontiers of Radiation Biology, 175-176, Kottayam, February 8-11, 2007

35. Sahu K., Sharma M., Gupta P.K.
Effect of incubation time on photodynamic inactivation of human colon adenocarcinoma cells due to endogenously synthesized protoporphyrin IX induced by delta-aminolevulinic acid methyl ester
International Symposium on Light and Life -2007, 50, Hyderabad, August 29- 31,2007

36. Saxena M. K., Joshi P., Kishore J., Kher S., Oak S.M.
Microcontroller and LabVIEW based automated set-up for calibration of fiber grating based strain sensors
National Symposium on Instrumentation, Tiruchengode, October 2007

37. Singh B.N., Misra P., Das A.K.*, Kumar R.*, Kailath B.J.*, Mishra M.*, Phase D.M.*, DasGupta A.*, DasGupta N.*, Kukreja L.M.
DC-Discharge assisted pulsed laser growth of ultra-thin silicon oxynitride films
4th National Symposium on Pulsed Laser Deposition of Thin Films and Nanostructured Materials, Rajkot, 3-5 October 2007

38. Singh B.N., Misra P., Das A.K.*, Kumar R.*, Kailath B.J.*, Mishra M.*, Phase D.M.*, DasGupta A.*, DasGupta N.*, Kukreja L.M.

Growth of ultra-thin silicon-oxinitride films using DC-discharge assisted pulsed laser annealing of silicon
Proc. IUMRS-ICAM 2007, Bangalore, October 2007

39. Singh S.D., Sharma T.K., Mukherjee C., Oak S.M.
Impact of growth parameters on the structural properties of InP/GaAs type-II quantum dots grown by metal-organic vapour phase epitaxy
XIV International Workshop on Physics of Semiconductor Devices, Mumbai, 17-20 December 2007

40. Sridhar R., Ratnakala K.C., Sindal B.K., Tiwari S.K., Malviya K.K., Bhatnagar P., Shukla S.K., Kotaiah S.
Ultra high vacuum testing of the new RF cavity of Indus-1
International Symposium on Vacuum Science & Technology), Mumbai, 28-30 November 2007

41. Suhane S.K., Nayak M.K., Bhatnagar V., Chouksey S., Kotaiah S.
Design and development of 700 MeV electron beam shutter for transfer line-3 of Indus-2 SRS
17th National Symposium on Radiation Physics, Kolkata, 14-16 November, 2007

42. Thota S.*, Misra P., Kukreja L.M., Kumar J.
Characteristics of pulsed laser deposited $Zn_{1-x}Ni_xO$/ZnO bi-layer thin films
4th National Symposium on Pulsed Laser Deposition of Thin Films and Nanostructured Materials, Rajkot, 3-5 October 2007

43. Upadhyay A., Patel K.*, Naik P.A., Gupta P.D., Gantayat L.M.*
3D-PIC simulations of laser plasma based acceleration schemes
22nd National Symposium on Plasma Science & Technology, Ahmedabad, Dec. 6-10, 2007

44. Vadjikar R.M., Senecha V.K., Kumar A., Hannurkar P.R., Kotaiah S.
Simulation of beam extraction from ion source
DAE-BRNS-PSI Symposium on Ion Beam Technology and Applications (SIBTA07), Mumbai, 19-21 September 2007

45. Verma D., Nayak M.K., Dev V., Kumar V., Sahani P.K., Haridas G., Thakkar K.K., Sarkar P.K.*, Sharma D.N.*
Radiological status during Indus-2 SRS commissioning
National Symposium on Radiation Protection, Kolkata, November 2007

46. Yadav D.P., Shiroman R., Shukla S.K., Kotaiah S.
Development of UHV compatible machined diamond profile gaskets for Indus-2
International Symposium on Vacuum Science & Technology, Mumbai, 28-30 November 2007

47. Yedle K., Singh Rajvir, Jain A.K.
Successful vacuum brazing
International Symposium on Vacuum Science & Technology, Mumbai, Nov. 28-30, 2007

Note: '' indicates author affiliation other than RRCAT, Indore.*

Best Poster Awards

Two papers from RRCAT presented in the DAE-BRNS National Laser Symposium-2007 at Vadodara (Dec. 2007) received the *"Best Poster Award"* of the Indian Laser Association for the year 2007. Each paper received a cash price of Rs. 1,500 and a certificate.

The award winning papers are :

1) A novel method of intense keV x-ray generation from *in situ* produced silver clusters using Ti:sapphire laser pulses.
Chakravarty U., Naik P.A., Khan R.A., Gupta P.D.

2) Effect of He-Ne laser irradiation on hair follicle growth in testosterone treated mice investigated with optical coherence tomography and histology.
Shukla S.*, Verma Y., Sahu K., Rao D.K., Dube A., Gupta P.K.

N.1 Agreement signed between RRCAT and CERN on TL-2 of CTF-3

An agreement was signed between RRCAT, Indore and CERN, Switzerland under Novel Accelerator Technology Programme (NAT) for Compact Linear Collider (CLIC) Test Facility3 (CTF-3). This agreement was signed on October 19, 2007 at CERN by Dr. V.C. Sahni, Director, RRCAT and Dr. R. Aymar, Director General, CERN.

Dr. V.C. Sahni, Director, RRCAT and Dr. R. Aymar, Director General, CERN, signing the agreement.

Under this agreement, for CTF-3, complete physics design of transfer line-2 (TL-2), mechanical design of components, fabrication, vacuum testing, and supply to CERN will be responsibilities of RRCAT. Physics (optics) design of TL-2 has already been completed and approved by CERN.

TL-2 will consist of five dipole magnets (two will be long magnets and three will be short). Mechanical design of magnets has already been completed. Magnets are under various stages of construction. Five dipole vacuum chambers and 56 straight vacuum chambers (both, cylindrical and racetrack profile) will be fabricated. All vacuum chambers will be made from aluminium alloy 6061-T6. Design of vacuum chambers has been completed and are under fabrication.

RRCAT delegation with CERN counterparts at the time of signing the agreement.

N.2 Director RRCAT signs MOU with SLAC, U.S.A.

Dr. V.C. Sahni, Director, RRCAT visited Stanford Linear Accelerator Centre (SLAC), U.S.A., with Fermilab's Dr. Shekhar Mishra and signed an agreement with SLAC Director Dr. Persis Drell.

The agreement is an addendum to a pre-existing Memorandum of Understanding between U.S. and Indian universities and accelerator centers that specifies collaborative activities on accelerator R&D and high energy physics projects. As a result of the addendum, SLAC and Indian institutions will work together to further develop a beam dump design and prototypes for the International Linear Collider (ILC). Additionally, Indian institutions will work with both SLAC and Fermilab to develop an ILC radio frequency unit.

The addendum specifies collaborative activities between SLAC and four Indian R&D centres : Raja Ramanna Center of Advanced Technology (RRCAT), Indore, Bhabha Atomic Research Centre (BARC), Mumbai, Variable Energy Cyclotron Centre (VECC), Kolkata and Inter University Accelerator Centre (IUAC), New Delhi.

Dr. V.C. Sahni, Director, RRCAT, signs an agreement with Dr. Persis Drell, Director, SLAC.

N.3 Activities of the Women's Cell in RRCAT

Women's Cell of RRCAT has been actively engaged in the empowerment of women in the Centre. It has been organizing Women's Day function for last three years, as mark of celebration and for enhancing the communication amongst women employees of the Centre. Further in this direction, special efforts are being made to open an intranet / e-mail route of communication for women within RRCAT, as a confidence building measure.

The Cell organized a special lecture by Ms. Smita Gate, IAS officer of the 1992 batch, the then Chairperson, Finance Corporation of M.P., on 24th Aug. 2007. Ms. Gate delivered a scintillating lecture on the topic "My experiences of bureaucracy". As the Cell members felt that empowerment of women cannot be achieved without participation of the men, this lecture was kept open to all.

Ms. Gate described her experiences of implementing the water shade management project, which she had executed for the rural women for the villages in Shujalpur of M.P. in the capacity of SDM. It was heartening to hear how a single person can inflict confidence in so many to achieve the nearly impossible. She emphasized the fact that although society does not welcome changes, they are necessary for the progress of the society. She also noted that learning goes a long way and can be achieved at any age. Her experience in controlling of the mob gave a fine example of courage and importance of timely measures in achieving success. She and her project got a special award from the President of India for its successful implementation. It was a success story against all odds and gave an account of how women can empower themselves with the help of other men and women.

Communicated by:
A. Ingale (alka@cat.ernet.in)

N.4 राजा रामन्ना प्रगत प्रौद्योगिकी केन्द्र द्वारा जुलाई 2007 से आयोजित हिन्दी की विभिन्न गतिविधियाँ

राजा रामन्ना प्रगत प्रौद्योगिकी केन्द्र, इन्दौर में राजभाषा हिंदी के प्रचार-प्रसार के क्षेत्र में भी संवैधानिक अपेक्षाओं के अनुरूप प्रभावी कदम उठाए गए हैं। केंद्र की राजभाषा कार्यान्वयन समिति ने केंद्र में कार्यरत अधिकारियों/कर्मचारियों के सहयोग से हिंदी की लोकप्रियता में संवृद्धि एवं प्रशासन में राजभाषा के उपयोग को बढ़ाने के क्षेत्र में ठोस कारवाई की। इस दिशा में किए गए कार्यों तथा प्रमुख उपलब्धियों का ब्यौरा निम्नानुसार है :-

इस केन्द्र के मुख्य सभागृह में दिनांक 14 सितंबर 2007 को हिन्दी दिवस मनाया गया जिसमें भारत सरकार के माननीय गृहमंत्री श्री शिवराज पाटील तथा परमाणु ऊर्जा आयोग के अध्यक्ष माननीय डॉ. अनिल काकोडकर द्वारा हिन्दी दिवस पर जारी संदेशों का वाचन किया गया तथा केन्द्र के उच्च स्तरीय कवियों द्वारा कविता पाठ किया गया, जो अत्यंत सराहनीय रहा।

प्रशासनिक एवं विज्ञान लेखन कार्य की आवश्यकता एवं सहजता नामक विषय पर 24 सितंबर, 2007 को एक राजभाषा वार्ता का आयोजन किया गया जिसमें भूजल विभाग, जोधपुर, राजस्थान के डॉ. डी. डी. ओझा मुख्य वार्ताकार थे। इस अवसर पर मुख्य अतिथि डॉ. विनोद चन्द्र साहनी, निदेशक, आरआरकेट, अध्यक्ष, राभाकास श्री एस.के. शुक्ला, मुख्य प्रशासनिक अधिकारी एवं विशिष्ट अतिथि श्री टी. एन. नायर तथा राजभाषा वार्ता की अध्यक्ष, संयुक्त नियंत्रक (वित्त एवं लेखा) श्रीमती रेखा रायकर कुमार ने भी अपने-अपने सूचनाप्रद एवं ज्ञान वर्धक विचार व्यक्त किए।

प्रशासनिक एवं विज्ञान लेखन कार्य की आवश्यकता एवं सहजता : वार्ताकार डॉ. डी. डी. ओझा, भूजल विभाग, जोधपुर, राजस्थान।

उक्त अवधि के दौरान इंदौर स्थित केंद्र सरकार के कार्यालयों की नगर राजभाषा कार्यान्वयन समिति की बैठक का सफलतापूर्वक आयोजन दिनांक 16 अगस्त, 2007 को आरआरकेट के निदेशक की अध्यक्षता में सी.जी.ओ. काम्प्लेक्स स्थित पत्र सूचना कार्यालय में किया गया। आकाशवाणी, इंदौर द्वारा प्रकाशित गृह पत्रिका ''मालववाणी'' को सर्वश्रेष्ठ गृह पत्रिका के लिए राजभाषा शील्ड समिति के अध्यक्ष माननीय डॉ. विनोद चन्द्र साहनी, निदेशक, आरआरकेट ने प्रदान की। इस अवसर पर केन्द्रीय उत्पाद शुल्क एवं सेवाकर आयुक्तालय के पूर्व सहायक निदेशक (राजभाषा) एवं नराकास के पूर्व सचिव श्री राज केसरवानी, की सेवानिवृत्ति पर उन्हें शॉल श्रीफल तथा प्रशस्ति-पत्र से सम्मानित किया गया।

प्रथम विश्व हिन्दी दिवस समारोह : अध्यक्ष, राभाकास श्री एस.के.शुक्ला, संयुक्त नियंत्रक (वित्त एवं लेखा) श्रीमती रेखा रायकर कुमार, भापअकें की अनुसंधान वैज्ञानिक श्रीमती डेजी जोसफ, श्री प्रभु जोशी, कार्यक्रम प्रभारी, दूरदर्शन केन्द्र, इन्दौर, मुख्य प्रशानिक अधिकारी श्री टी.एन. नायर तथा जय नारायण सोनी, सहायक निदेशक (राजभाषा)।

परमाणु ऊर्जा विभाग के निदेशानुसार हर वर्ष 10 जनवरी को विश्व हिन्दी दिवस मनाया जाएगा। तद्नुसार इस केन्द्र में दिनांक 10 जनवरी, 2008 को प्रथम विश्व हिन्दी दिवस के उपलक्ष्य में भाषा और भूमंडलीकरण विषय पर साहित्यिक व्याख्यान के लिए श्री प्रभु जोशी, कार्यक्रम प्रभारी, दूरदर्शन केन्द्र तथा आहार में सूक्ष्म मात्रिक तत्व तथा मनुष्यों में इनका महत्व विषय पर वैज्ञानिक व्याख्यान के लिए भापअकें की अनुसंधान वैज्ञानिक श्रीमती डेजी जोसफ को आमंत्रित किया गया, जिन्होंने बहुत ही रोचक ढंग से व्याख्यान देकर दर्शकों का मन जीत लिया।

केंद्र में हिन्दी का कार्यसाधक ज्ञान रखने वाले कर्मचारियों के विभिन्न वर्गों के लिए उपरोक्त अवधि के दौरान कुल 2 एक पूर्ण दिवसीय हिन्दी कार्यशालाएं क्रमश :

दिनांक 28.09.2007 तथा 18.12.2007 को आयोजित की गई। इन कार्यशालाओं में लगभग 47 अधिकारियों/कर्मचारियों को सरकार की राजभाषा नीति, पेंशन एवं लेखा से संबधित विभिन्न मुद्दें, हिन्दी साफ्टवेयर आईएसएम, सेवा पंजी, जी पी एफ, छुट्टी नियमावली, परमाणु ऊर्जा विभाग की विभिन्न प्रोत्साहन योजनाएं, विभिन्न हिन्दी पत्राचार, पारिभाषिक शब्दावली आदि विषयों की पर्याप्त जानकारी दी गई।

इस वर्ष दिनांक 17 सितंबर से 25 सितंबर, 2007 तक हिंदी निबंध, टिप्पणी/आलेखन, वर्ग पहेली, कल्पना शक्ति, कहानी, हिन्दी टंकण तथा अनुवाद प्रतियोगिताओं का आयोजन तथा 23 अक्टूबर से 30 अक्टूबर 2007 तक विभिन्न हिन्दी प्रतियोगिताएं यथा आशुभाषण, वाद-विवाद, खुला प्रश्नमंच, सुगम संगीत तथा प्रश्न मंच आदि का आयोजन किया गया।

पिछले वर्ष के दौरान कुल 14,209/- रूपए की हिन्दी पुस्तकें खरीदी गई तथा वर्ष 2008 के दौरान कुल 50 हजार रूपए की साहित्यिक एवं वैज्ञानिक पुस्तकें खरीदी जा रही हैं। परमाणु ऊर्जा विभाग की इस केंद्र में दिनांक 15.07.07 से लागू नई हिंदी प्रोत्साहन योजना के अंतर्गत टिप्पणी/आलेखन में कुल 6 तथा हिन्दी टंकण में दो कर्मचारियों को पुरस्कृत किया गया।

उपर्युक्त के अलावा प्रशासन एवं लेखा प्रभाग के सहयोग से तनाव प्रबंधन, लेखा से संबंधित मुद्दें, आत्मबल, विकिरण स्वास्थ्य एवं समाज आदि विभिन्न विषयों पर भी हिन्दी में वार्ताओं का आयोजन किया गया।

प्रस्तुति

जय नारायण सोनी (jsoni@cat.ernet.in)

N.5 Largest Rose Garden Award - 2008 for RRCAT

RRCAT has bagged 1st prize for *Largest Rose Garden* for the year 2008, together with 25 prizes under different cut rose flower entries under Institutional category, in the "26th All India Rose Convention and Rose Show" organised by the "Malwa Rose Society", Indore from 19th to 21st Jan 2008 at Gandhi Hall.

The trophy and the certificate.

The prize consists of a trophy and certificate of appreciation which was given jointly by Shri. Kantilal Bhuriya, Hon. Minister of State for Agriculture and Smt. Sumitra Mahajan, Lok Sabha MP from Indore.

A photograph of the prize-winning rose garden.

On behalf of RRCAT, the prize was received by Mr. R.V. Joshi Head, Horticulture Cell on 20th January 2008.

Communicated by:
R.V. Joshi (rjoshi@cat.ernet.in)

N.6 RRCAT scientists bag the "Best Thesis Award" of the Indian Laser Association

Two young laser scientists from RRCAT received the *"Best Thesis Award"* of the Indian Laser Association for the year 2007. Each of them received a cash price of Rs. 2,500 and a certificate.

Dr. Jogy George of Solid State Laser Division of RRCAT got the award for his Ph.D. thesis entitled *"A study of diode pumped solid state lasers"*. He received Ph.D. degree from I.I.T. Bombay and the thesis work was carried out under the supervision of Prof. B. P. Singh (Dept. of Physics, I.I.T. Bombay) and Prof. S. C. Mehendale (Head, Laser Physics Applications Division, RRCAT).

Dr. Sunil Verma of Laser Materials Development & Devices Division won the award for his Ph.D. thesis entitled "*Development and application of optical diagnostics for imaging crystal growth from solution*". He got his Ph.D. from I.I.T. Kanpur under the supervision of Prof. K. Muralidhar, (Head, Department of Nuclear & Mechanical Engg, I.I.T. Kanpur), and Dr. V. K. Wadhawan (Ex-Head, LMDDD, RRCAT, currently "Raja Ramanna Fellow" at Bhabha Atomic Research Centre, Mumbai).

Invitation to pursue Ph.D Programme in specialized areas of Physics & Chemistry at the Raja Ramanna Centre for Advanced Technology, Indore

Raja Ramanna Centre for Advanced Technology (RRCAT) (formerly called Centre for Advanced Technology (CAT)), Indore, was founded in 1984 by the Department of Atomic Energy (DAE) for dedicated pursuit of R&D in the areas of Accelerators, Cryogenics, Lasers, Plasma Physics, Vacuum Technology etc. Since then, the Centre has set up two Synchrotron Radiation Sources Indus-1 & Indus-2, which are National Research Facilities, and many smaller accelerators for radiation processing applications. The Centre has excellent cryogenic facilities as well as state-of-the-art equipments for low temperature physics measurements. Variety of laser systems, particularly high power lasers have been built and are being used for a wide range of applications. These include gas lasers (like copper vapour lasers, CO2 lasers) solid state lasers (like diode pumped solid state lasers, semiconductor lasers). They have been deployed for the studies in the areas like biomedical applications of lasers, and laser-plasma interaction. The Centre also has long standing programme in the areas of RF-superconductivity, low-temperature physics, material science, cold atom physics, non-linear optics, opto-electronics, nano-science etc.

RRCAT is a Constituent Institute of the Homi Bhabha National Institute (HBNI, http://www.hbni.ac.in), a Deemed University, and invites students with appropriate qualifications to pursue Ph.D programme in various specialized areas of physics and chemistry listed above. As per the rules of HBNI, the Ph.D. programme consists of course work of one year duration and research work of up to 4 years duration. The Ph.D. programme will commence in September 2008. DAE Junior Research Fellowships will be offered to those selected for the pursuit of Ph.D. programme. The fellowship amount is Rs. 12000 per month for the first two years and Rs. 14000 per month for the next three years subject to satisfactory progress.

Persons having M.Sc. degree in Physics/Chemistry with minimum 60% marks and who have cleared one of the national level screening tests listed in the 'Selection Process' described at http://www.cat.ernet.in/hrd/advt/phdad.html, are eligible to apply. The applicants should have also scored minimum 60% marks in B.Sc. Those applicants whose final results of M.Sc. degree are awaited can also apply. In the event of selection, mark sheet of the final result would have to be submitted by November 1, 2008. Continuation in the programme will be subject to the candidate obtaining minimum 60% marks.

Please visit above mentioned URL for further details related to Eligibility Criteria, Application Procedure, Selection Process etc.

The last date for receiving applications at RRCAT by post : April 15, 2008.

Application complete in all respects should be sent to:
Assistant Personnel Officer (Recruitment),
Raja Ramanna Centre for Advanced Technology,
P.O. : RRCAT, Indore - 452 013 (M.P.)

RRCAT Newsletter is a publication of
Raja Ramanna Centre for Advanced Technology,
P.O. : RRCAT, Indore - 452 013, M.P., India

Website: www.cat.gov.in/newsletter/NL
Printed at : Naidunia Printery
Indore, Ph.: 0731-276-3121